FLOW CONTROL DEVICES IN SAGD COMPLETION DESIGN: ENHANCED HEAVY OIL/BITUMEN RECOVERY THROUGH IMPROVED THERMAL EFFICIENCIES

A Dissertation

by

SUDIPTYA BANERJEE

Submitted to the Office of Graduate and Professional Studies of
Texas A&M University
in partial fulfillment of the requirements for the degree of

DOCTOR OF PHILOSOPHY

Chair of Committee,	Berna Hascakir
Committee Members,	Hadi Nasrabadi
	Jerome J. Schubert
	Yuefeng Sun
Head of Department,	A. Daniel Hill

December 2016

Major Subject: Petroleum Engineering

ABSTRACT

The volume of heavy oil/bitumen recoverable worldwide is vast in quantity but difficult and energy intensive to extract due to the high in-situ oil viscosity of these unconventional plays. One method of thermal recovery, steam-assisted gravity drainage (SAGD), has proven a commercial success in heavy oil/bitumen production by using steam to raise the temperature of heavy oil/bitumen in the reservoir with a resulting lower hydrocarbon viscosity, shifting the relative mobility of reservoir oil to one favorable for extraction via horizontal wells.

However, geological and reservoir heterogeneity often complicate this task resulting in uneven production rates, higher operational costs, and stranded heavy oil/bitumen. This work theorizes that SAGD recovery is improved using flow control devices (FCDs) to force conformance in SAGD laterals. To test this theory, a novel protocol and test flow loop was developed to measure pressure drop across an autonomous hybrid FCD while flowing multiphase mixtures containing steam. This laboratory data was used to qualify existing pressure drop correlations and determine if nitrogen gas, a common test gas to describe FCD pressure drop response, creates suitable data for modeling steam systems. Finally, the flow loop was used to induce a steam “flash”, a transition of water at saturation temperature to vapor due to a suddenly decreased pressure environment, within the FCD to determine if steam flashing changes expected pressure drops.

Using linear regression, a correlation of expected pressure drop across the autonomous hybrid FCD for mixtures of heavy oil/bitumen, water, and steam was generated. Existing correlations proved inadequate for mixtures containing steam, consistently underestimating pressure drop across the FCD. However, the empirical correlation of this research highly matched laboratory data with an R-squared value of 0.94. A secondary linear model captured modifications in FCD behavior due to steam flashing. This second model also exhibited a strong goodness-of-fit with an R-squared value of 0.96. For both empirical correlations, p-values less than 0.05 were easily obtained, inferring the statistical significance of each correlation.

Correlations generated in this research were added to the REVEAL™ reservoir simulation package to accurately forecast FCD impact on SAGD well pair performance. Simulating a four year production period for SAGD well pairs in Albertan reservoirs consistently show that FCD usage improved bitumen recovery by 50% or more while simultaneously decreasing cumulative steam/oil ratios (cSOR) by 1-2 m^3/m^3. The mechanism of action for this change was due largely to improved steam chamber conformance and by eliminating steam breakthrough events in the producer. Net Present Value (NPV) analysis of improvements with the additional cost of FCD completion tools unfailingly showed a strong economic argument for the use of FCDs to improve thermal efficiency.

ACKNOWLEDGEMENTS

Famed scientist Isaac Newton once wrote, “If I have seen further it is by standing on the shoulders of Giants”, an acknowledgment that even his groundbreaking discoveries built upon the hard work of those who came before him. I must, in turn, credit any accomplishments of mine to my parents, Dr. Sukumar and Mrs. Anita Bandopadhyay. I don’t have the words to express how grateful I am for their sacrifice, but their decisions to leave both home and family for a better life in America has shaped me and the opportunities I have enjoyed in life. I would also like to thank my committee members for their time and feedback throughout the course of this research.

Let me also extend my gratitude to the Society of Petroleum Engineers, whose STAR Fellowship provided the financial support to make a return to academia possible for me. Thanks are also due Texas A&M University and their support of the Ramey Thermal Recovery Laboratory and the members of the Heavy Oil, Oil Shales, Oil Sands, & Carbonate Analysis and Recovery Methods (HOCAM) Research Team.

Finally, thanks to Sara Jean Gencur, who started this chapter of my life as my dearest friend and will end it as my beloved wife. She, and the loving dogs who fill our home, have given me the best family anyone could ever hope for.

SYMBOLS, ABBREVIATIONS, AND NOMENCLATURE

AIC	Akaike's Information Criteria
AIC_c	Corrected Akaike's Information Criteria
AWR	Above Well Region
BIC	Bayesian Information Criteria
cDOR	Calendar day rate
cSOR	Cumulative Steam-Oil Ratio
FCD	Flow Control Device
FRR	Fluid Resistance Rating
GHG	Greenhouse Gases
HO-B	Heavy Oil/Bitumen
ICD	Inflow Control Device. Alternatively, injection control device.
NPV	Net Present Value
NWR	Near Well Region
OCD	Outflow Control Device
PI	Productivity Index
RF	Recovery Factor
SAGD	Steam-Assisted Gravity Drainage
SSSV	Subsurface Safety Valve
TWGP	Troll West Gas Province
TWOP	Troll West Oil Province

A_c = Vena Contracta cross-sectional area, m^2

B_o = Oil formation volume factor, reservoir bbl/STB

C_d = Discharge coefficient, Dimensionless

D = Pipe diameter, ft or m

d = Restriction diameter, m

d_h = Hydraulic diameter, ft

Eu = Euler Number, Dimensionless

f = Fanning friction factor, Dimensionless

F_a = Thermal expansion coefficient, Dimensionless

F_g = Reservoir geometric factor, Dimensionless

$ff_{mixture}$ = Friction factor term, Dimensionless

g = Acceleration due to gravity, 9.8 m/s^2

g_c = Gravitational conversion factor, 32.17 lb_m-ft/lb_f-s^2

h = Reservoir thickness, ft

h_{fg} = Latent heat of evaporation, kJ/kg

h_{fi} = Specific enthalpy of a saturated liquid at position *i*, kJ/kg

h_s = Height of the steam chamber, m

I_{ani} = Index of anisotrophy, Dimensionless

k = Reservoir permeability, mD

k_i = Effective permeability of fluid *i*, mD

L = Length of fluid travel, ft

L_w = Wellbore length, ft or m

$l_{channel}$ = Length of channel, ft

M = Mobility ratio, Dimensionless

N_H = Horizontal Well Number, Dimensionless

N_{Re} = Reynolds Number, Dimensionless

O = Orientation, degrees

p_e = Pressure at the reservoir boundary, psi

p_{wf} = Bottomhole flowing pressure, psi

q = Volumetric flow rate, STB/day

q_o = Oil volumetric rate, m^3/day

r_w = Wellbore radius, ft

S = Slip ratio, Dimensionless

s = Completion/damage/stimulation skin, Dimensionless

s_R = Partial penetration skin, Dimensionless

T = Temperature, °C

u = Fluid velocity in the wellbore, ft/s

v = Average fluid velocity, ft/s or m/s

v_b = Distance from the well to the drainage boundary in the horizontal direction perpendicular to the well, ft

v_{exp} = Two-phase specific volume of steam, ft^3/lb_m

v_f = Specific volume of saturated liquid, ft^3/lb_m

v_{fg} = Specific volume of vaporization, ft^3/lb_m

v_s = Kinematic viscosity of oil at steam temperature, °C-m^2/s

w =	Steam volumetric rate, lb_m/hr
x =	Fluid “quality”, Dimensionless
x_b =	One-half of the reservoir extent in the direction of the well, ft
Y_2 =	Vapor expansion coefficient, Dimensionless
y_b =	Distance to the drainage boundary in the y-direction, ft
α =	Thermal diffusivity of the reservoir, m^2/s
Δp =	Pressure drop, psi or Pa
Δp_{FCD} =	Pressure drop across the FCD, psi
Δp_r =	Reservoir pressure drop, psi
Δp_{sp} =	Orifice pressure drop for a single-phase fluid, Pa
Δp_{steam} =	Pressure drop for a steam flow, psi
Δp_w =	Wellbore pressure drop, psi
ΔS_o =	Difference between initial and residual oil saturation, Dimensionless
ϵ =	Pipe roughness, ft
λ_i =	Mobility of fluid *i*, mD/cP
μ_i =	Viscosity of fluid *i*, cP
ρ =	Fluid density, lb_m/ft^3 or kg/m^3
ρ_g =	Gas density, kg/m3
ρ_l =	Liquid density, kg/m3
σ =	Flow area ratio, Dimensionless
σ_c =	Contraction coefficient, Dimensionless

σ_p =	Flow profile coefficient, Dimensionless
σ_v =	Viscosity coefficient, Dimensionless
ϕ =	Porosity, Dimensionless
ϕ_{lo}^2 =	Two-phase correction multiplier, Dimensionless
χ_{steam} =	Mass fraction of saturated liquid that is converted to steam, Dimensionless

TABLE OF CONTENTS

Page

LIST OF FIGURES

Page

LIST OF TABLES

Page

1. INTRODUCTION*

Starting in the 1980s, advances in drilling technology made horizontal and multilateral wells a primary well design type to economically develop challenging reservoirs, particularly reservoirs with unconventional resources. Horizontal wells have been widely used to increase wellbore contact with the reservoir, increase flowing area, and thus increase well productivity (Babu and Odeh 1989; Joshi 2003). Horizontal wells are particularly attractive in thin reservoirs where the well orientation allows for greater reservoir contact than a vertical alternative. In achieving larger contact, horizontal wells allow for lower drawdowns at comparable rates of oil and gas production, reducing coning tendencies, mitigating the risk of sand production, and generally lowering drawdown-

---

* Reprinted with permission from "Flow Performance of Horizontal Wells with Inflow Control Devices" by C. Atkinson, F. Monmont, and A.F. Zazovsky, 2004. European Journal of Applied Mathematics, Vol. 15, No. 4, Copyright 2004 by Cambridge University Press.

* Reprinted with permission from "Understanding the Heat-Transfer Mechanism in the Steam-Assisted Gravity Drainage (SAGD) Process and Comparing the Conduction and Convection Flux in Bitumen Reservoirs" by M. Irani and S. Ghannadi, 2013. SPE Journal, Vol. 18, No. 1, Copyright 2013 by Society of Petroleum Engineers.

* Reprinted with permission from "Two-Phase Pressure Drop in Multiple Thick- and Thin-Orifice Plates" by G. Kojasoy, F. Landis, P. Kwame-Mensah, and C.T. Chang, 1997. Experimental Thermal and Fluid Science, Vol. 15, No. 4, Copyright 1997 by Elsevier Publishing

* Reprinted with permission from "Screen-Inflow-Design Considerations with Inflow Control Devices in Heavy Oil" by O. Oyeka, F. Felten, and B. Least, 2014. Proceedings from the SPE Heavy Oil Conference-Canada, Calgary, Alberta, Canada. Copyright 2014 by Society of Petroleum Engineers.

* Reprinted with permission from "The Theory of a Fluidic Diode Autonomous Inflow Control Device", by M. Fripp, L. Zhao, and B. Least, 2016. Proceedings from the SPE Middle East Intelligent Energy Conference and Exhibition, Manama, Bahrain. Copyright 2016 by Society of Petroleum Engineers.

* Reprinted with Permission from "Enhanced Oil Recovery on Troll Field by Implementing Autonomous Inflow Control Devices" by M. Halvorsen, M. Madsen, and M. Vikoren Mo, 2016. Proceedings from SPE Annual Technical Conference and Exhibition, San Antonio, Texas, USA. Copyright 2016 by Society of Petroleum Engineers.

related production problems (Dikken 1990; Ihara et al. 2013). Horizontal wells may additionally enhance production by contact with naturally occurring fractures or by connecting disconnected drainage areas (Novy 1995). Horizontal wells accomplish these production enhancements through a drainage pattern that deviates from that for a vertical well. The flow geometry in the near wellbore region is typically radial but transitions to a linear flow pattern farther away from the well. Wells that are horizontally oriented are strongly influenced by the anisotropy of horizontal to vertical permeability, forcing analytical models of flow to consider these differences from conventional vertical wells (Economides 2013; Joshi 2003). Fluid flow for horizontal wells is largely one-dimensional (**Figure 1**). However, once flow moves converges on the lateral itself, the flow is forced into a two-dimensional radial arrangement to traverse the pressure gradient created wellbore itself.

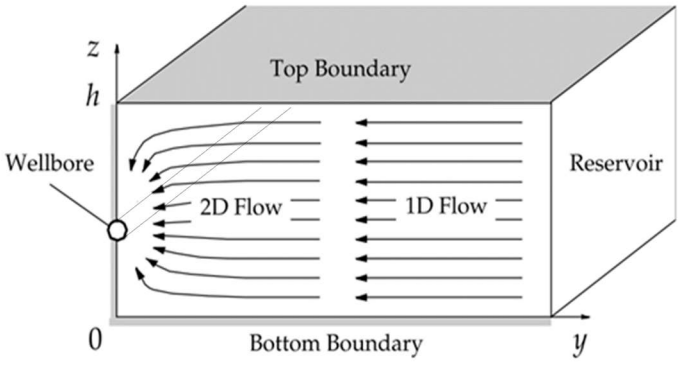

Figure 1: Schematic representation of the 1D flow to 2D flow near the horizontal wellbore. (Atkinson et al. 2004)

Unlike vertical wells, flow within the horizontal wellbore is interdependent with flow in the reservoir. **Figure 2** provides an example of this, with frictional pressure drop within the horizontal lateral affecting the moving front of the oil-water contact and the gas-oil contact over time. The name "heel-to-toe effect" is applied to this behavior, characterizing how high drawdown at the heel contributes to early breakthrough and how high pressure drops along the wellbore creates a situation of tubing limited production (Li et al. 2013; Li and Zhu 2010; Moen and Asheim 2008; Sagatun 2010). This coning behavior undermines the economic value of a horizontal well as the most productive zones are now producing an unwanted fluid (water, gas) while oil reserves are ineffectively recovered from other points along the reservoir.

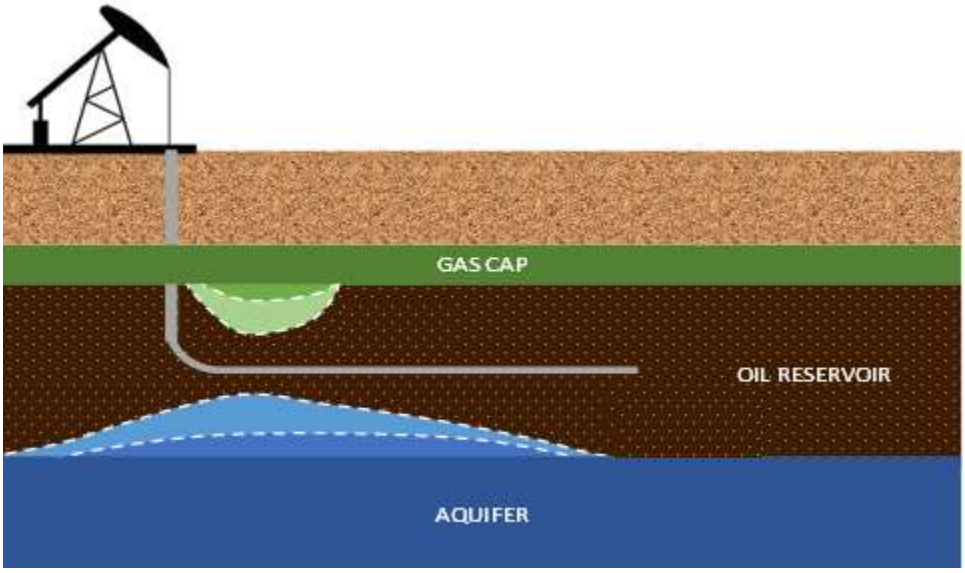

Figure 2: Simplified representation of gas and water coning at the heel of a horizontal well design over time. Adapted from Bitto (2013).

Even when the magnitude of wellbore pressure drop is insignificant relative to reservoir pressure drop, non-conformance of the injection/production fluid front may still be observed. In these cases, an uneven profile is generated by heterogeneities in fluid properties, geological factors, or reservoir properties along the length of the wellbore. No reservoir is completely homogenous and the degree of heterogeneity can vary significantly, even within the same field. Common root causes of irregular production/injection fluid fronts along a horizontal lateral include, but are not limited to: horizontal and/or vertical permeability distribution (Al-Khelaiwi et al. 2010; Baker et al. 2008; Nasr et al. 2000; Yang and Butler 1992), variations in porosity (Llaguno et al. 2002), water saturation heterogeneity/characteristics (Baker et al. 2008), variations in the distance between the wellbore(s) and fluid contacts (Al-Khelaiwi et al. 2010; Baker et al. 2008; Edmunds and Chhina 2001), variations in localized reservoir pressure (Al-Khelaiwi et al. 2010; Tabatabaei and Ghalambor 2011), changes in capillary pressure and relative permeability along the wellbore (Wang and Leung 2015), localized skin damage or fractures (Furui et al. 2003; Tam et al. 2013), changes in mineralogy or wettability (Ipek et al. 2008; Le Ravalec et al. 2009; Pooladi-Darvish and Mattar 2002), changes in temperature (Bois and Mainguy 2011; Irani and Cokar 2016), changes in fluid density, viscosity, or both (Gates et al. 2008; Larter et al. 2008), or the presence or absence of in-situ emulsifiers that blend reservoir and/or introduced fluids into something novel (Ezeuko et al. 2013).

With the exception of geospatial heterogeneity, like variations in the distance between wellbore(s) and fluid contacts, these root causes fundamentally change the local

mobility ratio. Mobility ratio is defined as in **Equation 1**, where $\lambda_{displacing}$ [mD/cP] is the mobility of the displacing fluid and $\lambda_{displaced}$ [mD/cP] is the mobility of the displaced fluid. Each mobility (λ) for a given fluid is in turn the ratio of the effective permeability (k, [mD]) over the fluid viscosity (μ, [cP]) (Green and Willhite 1998).

$$M = \frac{\lambda_{displacing}}{\lambda_{displaced}} = \frac{k_{displacing} / \mu_{displacing}}{k_{displaced} / \mu_{displaced}} \quad \text{...} \quad \textbf{(Eq. 1)}$$

When the local mobility ratio deviates strongly from the average mobility ratio along the wellbore, coning of the gas cap/aquifer, sand production, and/or uneven production/injection profiles will follow.

Fluid flow in a horizontal well is commonly calculated by assuming either a constant wellbore pressure or infinite conductivity and thus is not influenced by pressure drop in the well (Anklam and Wiggins 2005; Penmatcha et al. 1999; Wu et al. 2011). For steady-state flow to a partially penetrating horizontal wellbore, one such model proposed by Furui et. al (2003) is show in **Equation 2**:

$$q = \frac{2kx_b(p_e - p_{wf})}{141.2\mu B_o \left(\ln\left[\frac{hI_{ani}}{r_w(I_{ani}+1)}\right] + \frac{\pi y_b}{hI_{ani}} - 1.224 + s + s_R \right)} \quad \text{...} \quad \textbf{(Eq. 2)}$$

Here, q is the volumetric flow rate [bbl/day], k is reservoir permeability [mD], x_b [ft] is one-half the reservoir extent in the direction of the well, p_e [psi] is the pressure at the drainage boundary, p_{wf} [psi] is the bottomhole flowing pressure, μ [cP] is the fluid viscosity, B_o [res. Bbl/STB] is the oil formation volume factor, h [ft] is reservoir thickness, r_w [ft] is wellbore radius, y_b is the distance to the drainage boundary in the y-direction [ft], y_b [ft] is the distance from the well to the drainage boundary in the horizontal direction

perpendicular to the well, I_{ani} [dimensionless] is the index of anisotropy, s [dimensionless] is the skin accounting for completion and damage, and s_R [dimensionless] is the partial-penetration skin factor. The partial-penetrating skin factor may be calculated with the method of Babu and Odeh (1989). **Equation 2** may be re-arranged to express the overall pressure drop as shown below in **Equation 3**:

$$p_e - p_{wf} = \frac{70.6qB_o\mu}{kx_b}\left(\ln\left[\frac{0.249hI_{ani}}{r_w(I_{ani}+1)}\right] + \frac{\pi y_b}{hI_{ani}} + s + s_R\right) \quad \textbf{...} \quad \textbf{(Eq. 3)}$$

Models that assume uniform flow or infinite conductivity, however, oversimplify fluid physics by ignoring frictional losses in the wellbore. In cases with long wells or high flow rates, the magnitude of wellbore pressure losses can be comparable to the drawdown in the reservoir and thus negatively impact the productivity index (PI) of the well in addition to modifying reservoir conformance (Dikken 1990; Furui et al. 2005; Hill and Zhu 2008; Novy 1995; Ozkan et al. 1995; Penmatcha et al. 1999; Penmatcha and Aziz 1999). Several investigators have developed methods to calculate the pressure drop in a horizontal wellbore and determine the significance of this pressure drop to production profiles. Dikken (1990) was one of the first to formulate the effects of frictional wellbore pressure losses on horizontal wells. The Dikken model established behavior for single phase, non-transient, turbulent flow. Novy (1995) built upon this foundation, generalizing the Dikken model and including non-Darcy effects. Penmatcha and Aziz (1999) continued this work for early transient and pseudo-steady state conditions and established that non-uniformity was greater during transient conditions than during pseudo-steady state or steady state conditions. The common consensus of this body of research is that wellbore pressure drop is important if it is significant relative to reservoir pressure drop (Hill and Zhu 2008).

Here, significant wellbore pressure drop is considered to be 10-15% of reservoir pressure drop (Novy 1995).

If a well is perfectly horizontal, the pressure drop along a distance can be expressed for a single-phase fluid as (Archer and Agbongiator 2005; Economides 2013; Hill and Zhu 2008):

$$\Delta p = \frac{2 f \rho u^2 L}{g_c D} \quad \text{...} \quad \textbf{(Eq. 4)}$$

Here, Δp [psi] is the pressure drop along a length of pipe, f [dimensionless] is the fanning friction factor, ρ [lb_m/ft^3] is fluid density, u [ft/s] is the velocity in the wellbore, L [ft] is the distance the fluid travels, g_c [lb_m-ft/lb_f-s^2] is the gravitational constant, and D [ft] is the pipe diameter. The definition of Fanning friction factor is provided below (Churchill 1977):

$$f = 2\left(\left(\frac{8}{N_{Re}}\right)^{12} + \left(\left(2.457 \ln\left(\left(\left(\frac{7}{N_{Re}}\right)^{0.9} + 0.27\frac{\epsilon}{D}\right)^{-1}\right)\right)^{16} + \left(\frac{37530}{N_{Re}}\right)^{16}\right)^{-1.5}\right)^{1/12} \quad \text{...} \quad \textbf{(Eq. 5)}$$

For **Equation 5**, ϵ [ft] is the roughness of the inner surface of the pipe, D [ft] is pipe diameter, and N_{Re} is the dimensionless Reynolds number. The formulation of **Equation 5** is appropriate for both laminar and turbulent fluid flow. To determine if the pressure drop in the wellbore is significant relative to the rservoir pressure drop, a ratio of **Equation 4** to **Equation 3** is considered with consistent units as in **Equation 6**:

$$\frac{\Delta p_w}{\Delta p_r} = \frac{\frac{2f\rho u^2 L_w}{D}}{\frac{q\mu}{4\pi k x_b}\left(\ln\left[\frac{0.249hI_{ani}}{r_w(I_{ani}+1)}\right] + \frac{\pi y_b}{hI_{ani}} + s + s_R\right)} \quad \text{...} \quad \textbf{(Eq. 6)}$$

The new terms in this equation are wellbore pressure drop, Δp_w [psi], and reservoir pressure drop, Δp_r [psi]. L [ft], the length term in **Equation 4**, has been replaced by the length of the horizontal wellbore, L_w [ft]. To further simplify **Equation 6**, a reservoir geometric factor is constructed by grouping together terms as follows:

$$F_g = \ln\left[\frac{0.249hI_{ani}}{r_w(I_{ani}+1)}\right] + \frac{\pi y_b}{hI_{ani}} + s + s_R \quad \text{...} \quad \textbf{(Eq. 7)}$$

This reservoir geometric factor captures multiple items: radial/elliptical flow occurring in the near wellbore ($\ln\left[\frac{0.249h\ ani}{r_w(I_{ani}+1)}\right]$), linear flow occurring from the reservoir boundary to the radial flow region ($\frac{\pi y_b}{hI_{ani}}$), near-well and completion skin (s), and partial penetration and convergence skin (s_R). Using this reservoir geometric factor, the pressure drop ratio of **Equation 6** can be rearranged as follows:

$$\frac{\Delta p_w}{\Delta p_r} = \frac{\frac{8f\rho q^2 L_w}{\pi^2 D^5}}{\frac{q\mu F_g}{4\pi k x_b}} = 8f\left(\frac{4q\rho}{\pi D\mu}\right)\left(\frac{kL_w x_b}{D^4 F_g}\right) \quad \text{...} \quad \textbf{(Eq. 8)}$$

In the first parentheses on the far right side of **Equation 8** is the dimensionless Reynolds number for pipe flow, N_{Re}, and in the second parentheses is a new dimensionless number that Hill and Zhu (2008) label the Horizontal Well Number (N_H). The friction factor is, of course, already dimensionless. Thus, the ratio of the pressure drop in the wellbore to the pressure drop in the reservoir of **Equation 8** may be rewritten as **Equation 9**:

$$\frac{\Delta p_w}{\Delta p_r} = 8 f_f N_{Re} N_H \quad \cdots \quad \textbf{(Eq. 9)}$$

From **Equation 9**, certain behavior can be deduced. The pressure drop in the wellbore becomes significant for high Reynolds number (N_{RE}) and for high Horizontal Well Number (N_H). High Reynolds number can be expected when the wellbore flow rate (q, [ft^3/s]) is high, when wellbore diameter (D, [ft]) is small, or when the produced/injected fluid density (ρ, [lb_m/ft^3]) is large or the viscosity (μ, [cP]) is small. High Horizontal Well Numbers will correspond to high permeability reservoirs (k, [mD]), longer well laterals (L_w, [ft]), and reservoirs where the pressure drop (Δp, [psi]) in the reservoir is relatively small (Economides 2013; Hill and Zhu 2008).

During "heel to toe effect" (**Figure 2**), the contribution to the total well production rate is disproportionately large at the heel of the lateral in the absence of mitigating reservoir or fluid heterogeneities (Atkinson et al. 2004; Tabatabaei and Ghalambor 2011). Over time, as the in-situ oil vacates the region near the heel more rapidly than at the toe, any existing gas cap or aquifer is seen as advancing towards the wellbore in this regions more quickly than at points along the wellbore with lower flux.

To control or regulate fluid velocity or fluid flow rate within a horizontal well, flow control devices (FCDs) are implemented (Foster et al. 1987). The larger family of flow control devices accomplish this task in a multitude of roles, inclusive but not limited to subsurface safety valves (SSSVs), wellhead chokes, flow metering valves, valves downstream of the well within the process chain (surface safety valves), and downhole throttles on reservoir flux. In this work, the focus is on the latter role as downhole throttling devices placed at the interface between well completion and reservoir to equalize a non-

conforming production or injection fluid profile (Denney 2015; Li et al. 2013). Used in this fashion, downhole FCDs are often referred to in industry as "inflow control devices" or "injection control devices" (ICDs), depending on the direction of reservoir flux (Banerjee and Hascakir 2015; Bybee 2008; Jain et al. 2013; Li et al. 2013). "Outflow control device" (OCD) is also often used in place of injection control device. In common parlance, the term FCD or ICD/OCD may be used interchangeably when discussing downhole applications.

1.1 Historical Application of Flow Control Devices (FCDs)

The first downhole field application of FCDs for the recovery of hydrocarbon is credited to Norsk Hydro and Baker Hughes in the early 1990s (Al-Khelaiwi and Davies 2007; Bybee 2008; Mikkelsen et al. 2005). In this first industrial trial, inflow control devices were applied to horizontal wells in the Troll field, a subsea giant gas field found on the Norwegian shelf of the North Sea. The Troll field is characterized by a thin oil column. In the Troll West oil province (TWOP), the thin oil layer measures between 22 and 26 meters while the oil layer in the Troll West gas province (TWGP) measures anywhere between 4 and 13 meters (Halvorsen et al. 2012; Henriksen et al. 2006). The main reservoir drive mechanism of this field is gas expansion so horizontal wells were selected and placed approximately 0.5 meters above the oil-water contact to maximize oil recovery despite initial water cuts typically being higher than 50% (Mikkelsen et al. 2005). In previous well tests, Norsk Hydro had established that gas breakthrough would occur almost immediately for a conventional horizontal well placed in TWGP and early in well

life for a well in TWOP. Coning of the gas cap broke through the thin oil layer and dominated total production for the remainder of well life and so the oil column was deemed to have no commercial value (Henriksen et al. 2006). However, by incorporating FCDs to regulate the production profile and drilling longer horizontal laterals, water/gas breakthrough was delayed, longer well life was observed, higher cumulative oil production was obtained, and net present value (NPV) was increased. FCDs are now a default choice for wells drilled to produce Troll oil (Henriksen et al. 2006).

Since that initial field trial, FCDs/ICDs have been extensively used across the globe to delay water/gas breakthrough in high production rate horizontal wells (Abdelfattah et al. 2012; Al-Khelaiwi and Davies 2007; Jain et al. 2013; Karim et al. 2010; Li et al. 2013). Multiple differing FCD geometries have been commercialized to accomplish the goal of equalizing reservoir flux along the wellbore. All FCD geometries function in a similar manner: rather than allowing fluid flow between the reservoir and completion to seek the pathway of least resistance, FCDs induce an additional pressure drop along the length of the well to equalize the total sum of pressure drops for any given fluid flow path (Atkinson et al. 2004). As variance in flow path resistance is minimized, fluid conformance to the lateral is maximized. However, the mechanism by which this pressure drop is created can vary wildly between geometries, resulting in drastically different long-term injection/production behavior as reservoir and operational conditions change (Carpenter 2015; Denney 2015).

In late 2008, FCDs were proposed for use in a steam-assisted gravity drainage (SAGD) well pair. Multiple conformance issues were identified to exist in SAGD

horizontal wells with similarities to the problems encountered with gas coning control in light-oil applications (Stalder 2013). The working theory was that completion design for a SAGD horizontal well pair could be simplified through use of FCDs while the overall economics could be improved through improved steam chamber growth and better steam-trap control. A field trial on Surmont 102-06 was started in late 2009 to assess the validity of these theories with positive results (Stalder 2013; Vachon et al. 2015).

1.2 The Effects of Non-Conformance on SAGD Economics

A more complicated application of horizontal well configuration is seen for steam-assisted gravity drainage (SAGD) where heat and mass transfer concepts must be considered together to define fluid flow. In current practice, the two horizontal well configuration used in the SAGD process have typical lateral length ranging from 500 to 1500 meters with laterals arranged parallel to each other in a vertical plane a few meters from the bottom of the pay zone (Butler and Stephens 1981; Wilson 2015). Interwell spacing vertically is typically 5 meters, though drilling tolerances may cause this distance to vary anywhere between 3 and 10 meters (Irani 2013). These horizontal wells are surrounded by heavy oil/bitumen reserves (HO-B), a low value product that is economically unrecoverable at native viscosity and temperature (Edmunds and Gittins 1993). In-situ bitumen in the reservoir exhibits viscosity in excess of 1 million cP and initial reservoir temperatures on the order of 10° C (Gates and Leskiw 2010).

To initiate a steam chamber, steam is circulated in both wellbores for a period of up to three months through tubing and out of the annulus (**Figure 3A)** (Chen et al. 2008;

Gates and Chakrabarty 2006). Thermal energy moves via conduction between the two wellbores (Irani and Cokar 2016). Once thermal and hydraulic communication between the two wellbores is established (**Figure 3B**), true SAGD begins. The upper well in the pair no longer circulates steam but injects it into the reservoir (**Figure 3C**).

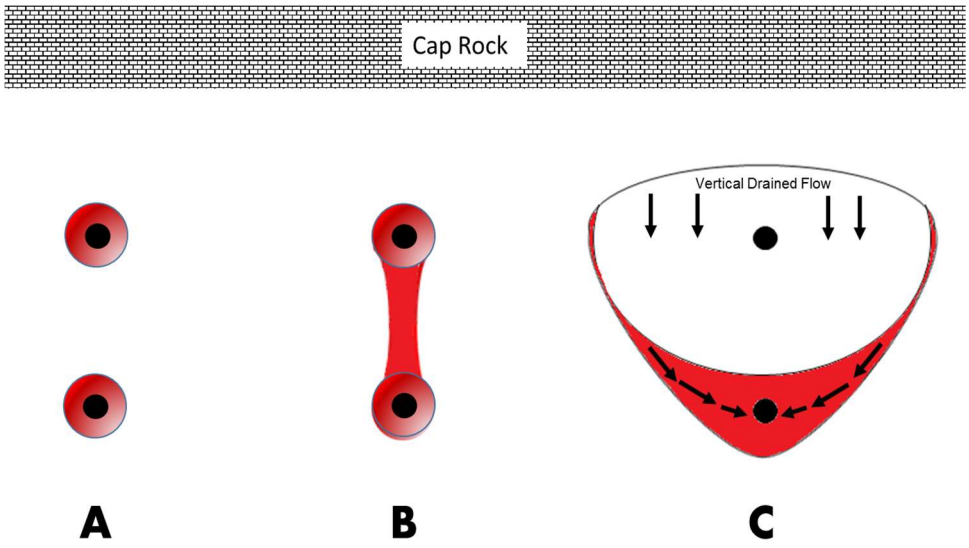

Figure 3: (A) Cross-section of the SAGD process during circulation, (B) the establishment of hydraulic communication, and (C) "true" SAGD. Adapted from Irani and Ghannadi (2013).

Two types of flow exist during the steam chamber growth process: one is ceiling drainage, as heated bitumen at the top of the steam chamber is immediately mobilized downwards to the production well and is in turn impeded by steam rise, and the other is slope drainage, where condensate and bitumen are mobilized by conduction from the

steam chamber and allowed to run down the edges of the steam chamber to the production well (Edmunds 2013; Sharma and Gates 2011).

In the SAGD process, oil flows at the edge of a steam chamber of changing volume in which steam condenses (Butler 1985; Butler 1987; Butler and Kanakia 1994; Butler et al. 1981; Butler and Stephens 1981; Butler and Yee 2002; Chow and Butler 1996). Butler proposed a semi-analytical numerical solution to predict oil-drainage rate to a horizontal well. Assuming that only steam flows in the steam chamber, oil drains along the vertical steam-chamber boundary, the steam pressure is constant in the steam chamber, oil saturation is residual, and heat transfer ahead of the steam chamber to cold oil occurs by conduction only, Butler formulated the following relationship (**Equation 10**):

$$q_o = L_w \sqrt{\frac{1.5\phi \Delta S_o k_o g \alpha h_s}{m v_s}} \quad \text{...} \quad \textbf{(Eq. 10)}$$

Where L_w [m] is the length of the horizontal well, ϕ [dimensionless] is the porosity of the formation, ΔS_o [dimensionless] is the difference between initial and residual oil saturation to steam, k_o [m^2] is the effective permeability for the flow of oil, g [m/s^2] is the acceleration due to gravity, α [m^2/s] is the thermal diffusivity of the reservoir, h_s [m] is the steam chamber height, m [dimensionless] is a constant between 3 and 4 (dependent on the oil viscosity vs. temperature relationship), and v_s [°C-m^2/s] is the kinematic viscosity of oil at steam temperature (Butler 1985; Butler and Stephens 1981; Chen et al. 2008). The consequences of this model are that steam chamber growth is necessary for oil production in the SAGD method and that the rate of drainage is a function of the height and, critically, the homogeneous permeability of the steam chamber. Over time, other researchers have

modified the Butler gravity-drainage model to better match observed experimental oil rates which, while on the same order as the Butler model forecasts, proved lower than the model predicted. Reis (1992) introduced an empirical dimensionless temperature coefficient and a maximum fluid velocity to substitute for local interface velocity to represent more realistically the experimental data reported in literature. Akin (2013) also attempted to modify the model to better fit experimental data by establishing viscosity as a function of asphaltene content. Nasr et al. (2000) included counter-current "ceiling drainage" to the Butler model. These studies, however, were generally performed for homogeneous and isotropic reservoirs (Chen et al. 2008). If the assumption of a homogeneous formation holds true, then issues of non-conformance in the SAGD process would be dependent solely on wellbore pressure drop, as outlined earlier. For this case, operators might realistically manage any non-conformance issues by simply varying tubing diameter or well length.

By all accounts, the presumption of homogeneity does not hold for Albertan bitumen formations. Gates (2008) and Larter (2008) have written extensively on the large spatial variations in fluid viscosity in heavy oil and bitumen fields (Larter et al. 2008). Oil phase viscosity can change by orders of magnitude in less than 30 meters in the vertical direction in some Albertan reservoirs with temperature-viscosity responses varying on a similar scale (Gates et al. 2008). The presence of thin shale layers and with horizontal layers of different permeability is also significant in impact on fluid flow to horizontal wells (Yang and Butler 1992). Shale distributed in the near well region (NWR) might impact the SAGD process differently than shale distributed in the above well region

(AWR) (Chen et al. 2008). Pooladi-Darvish (2002) constructed a series of 2D layered models on the basis of underground test facility field data to study the effects of shale continuity in the vertical direction on SAGD operations in the presence of gas cap and top water. Ipek et al. (2008) incorporated the effects of geomechanics in SAGD operations for a series of reservoirs with varying degrees of shale content. Kumar et al. (2013) studied the effects of thermal conductivity and permeability heterogeneity introduced by the presence of shale lenses on SAGD performance. The consensus of these differing works is that variations in permeability affected steam chamber development more prominently than variations in thermal conductivity. While shale layers hindered fluid drainage within the near wellbore region and the expansion of the steam chamber in the above-well region, SAGD performance was adversely affected only when shale lenses were present in the near well region or if the above well region contained long and continuous shale (Wang and Leung 2015). A thorough literature review clearly indicates that homogeneity is not a reasonable assumption for Albertan heavy oil fields and that non-conformance is a reasonable expectation due to variations in fluid properties and reservoir characteristics along normal wellbore lengths, non-conformance that is readily seen in reported field behavior.

As mobilization of bitumen is dependent on delivering thermal energy via steam, it is unsurprising that the economics of SAGD are controlled by the costs of generating steam and waste water treatment/recycling of the produced condensate (Yang et al. 2009). Additionally, the SAGD method is often criticized for its environmental footprint; in spite of its viability as a bitumen extraction technique, SAGD generates considerable

greenhouse gas (GHG) emissions in the process of generating the quantities of steam necessary for the process (Al-Murayri et al. 2011; Brandt 2012; Kovscek 2012; Morrow et al. 2014; Welch 2011). Based on field data, between 2 and 5 tons of steam are injected into the reservoir to produce each ton of bitumen (Gates and Leskiw 2010). This illustrates how critical energy maintenance is to the SAGD process, with an optimal process delivering injected energy solely to producible bitumen. In evaluating SAGD performance, the most economic projects generally demonstrate low cumulative steam-oil ratio (cSOR), a high recovery factor (RF), and a high calendar day oil rate (cDOR) over the project life.

Cumulative steam-oil ratio is critical to the economic viability of a SAGD project and easily undermined by thermal inefficiencies. A major operational concern is injected steam bypassing immobile bitumen reserves and traveling directly from injection to production well. To prevent this, the rate that the producer removes condensate and emulsion from the reservoir is balanced against the rate at which gravity feeds liquids to the production well to ensure a steady liquid level above the production well and below the injection well (Yuan and Nugent 2013). This liquid pool, being denser than steam, is not easily displaced by the steam phase and prevents live steam from flowing directly into the producer. The maintenance of this liquid pool is called steam trap control (Gates and Leskiw 2010).

In field practice, the liquid level cannot be directly measured from surface. Instead, temperature gauges are installed along the length of the producer well to measure the temperature difference between the fluid exiting the upper injector and entering the lower

producer. This temperature difference is referred to as subcool and serves as a surrogate variable for liquid level height (Wilson 2015). The smaller the interwell subcool difference, the closer the produced liquids are to the steam temperature, and thus the smaller the height of the liquid pool (Gotawala and Gates 2012). However, subcool is not constant along the length of the production lateral; there is localized variability in subcool. Moreover, flow capacity of the wellbore is large compared to that of the reservoir in the same direction, making compensating steam movement in the reservoir difficult (Vander Valk and Yang 2007). Furthermore, local liquid levels cannot effectively drain parallel to the well due to the very low drainage angles (Edmunds 2013).

Operational risk comes with steam trap maintenance. Too low an average subcool and steam breakthrough will occur at points along the producing lateral, negatively impacting cSOR, thermal efficiency, and the economics of the project. Too large an average subcool and liquid occupies a significant fraction of the steam chamber, preventing the free movement of steam to the chamber boundaries and potentially flooding the injector well itself (Banerjee et al. 2013b; Carpenter 2015; Gotawala and Gates 2012). Inflow control devices (ICDs), a subset of Flow Control Devices (FCDs), are used to overcome problems with uneven steam trap height, allowing for more aggressive production rates and less manipulation of subcool. The mechanism of ICD/FCD action are discussed in detail in the following section.

1.3 Overview of Available Flow Control Devices

There are multiple flow control device (FCD) geometries commercially available with varied focus on specific operational risks or methods of generating a favorable pressure drop (Fripp and Dykstra 2013; Fripp et al. 2015; Garcia et al. 2009; Loretz and Hosatte 2007; Russell et al. 2013a; Russell et al. 2013b). All FCDs may be sorted into three broad categories: channel-style FCDs, restriction-style FCDs, and autonomous FCDs (Al-Khelaiwi and Davies 2007; Banerjee et al. 2013a; Lauritzen et al. 2011). **Table 1** summarizes the operational strengths and weakness of these geometry categories to the SAGD process prior to the thorough explanation within the relevant design subsections. As autonomous FCDs are not a homogenous group, **Table 2** expands upon autonomous FCD sub-types with details again provided in the relevant subsection.

Table 1: Summary of Commercially Available FCD Designs

Geometry	***Mechanism of Action***	***Strengths for SAGD Applications***	***Weakness for SAGD Applications***
Channel-style FCD	Frictional Drag	Low risk of plugging or erosion May control steam flashing No moving parts	Sensitive to flowing fluid viscosity
Restriction-style FCD	Bernoulli Principle	Inexpensive No moving parts	Significant risk of plugging or erosion May cause steam flashing
Autonomous FCD	Varied	Additional steam trap control	Varied

Table 2: Comparison of Commercially Available Autonomous FCDs

Autonomous FCD Type	*Mechanism(s) of Action*	*Strengths for SAGD Applications*	*Weakness for SAGD Applications*
Hybrid	Frictional drag, Bernoulli principle, Momentum effects	Low risk of plugging or erosion May control steam flashing Insensitive to fluid viscosity No moving parts	Smallest autonomous response
Fluidic Diode	Momentum effects	No moving parts	Risk of plugging or erosion May cause steam flashing
Rate-Control Valve	Variable-size restriction	Additional steam trap control Strongest autonomous response	Risk of plugging or erosion Moving parts Limited throughput May cause steam flashing

1.3.1 Channel-Style Flow Control Devices

Channel-style flow control devices (FCDs) are one of the earliest geometries of FCD used downhole in the oil and gas industry (Banerjee et al. 2013b; Li et al. 2013). It is the first type of FCD used to equalize production on a horizontal producer (Al-Khelaiwi and Davies 2007; Henriksen et al. 2006; Mikkelsen et al. 2005) as well as the first geometry used in a SAGD production well (Stalder 2013). Common geometries include helical channels wrapped around a base pipe and labyrinth pathways (**Figure 4).** In **Figure 4**, fluid moves from the reservoir through a sand control screen or debris filter to remove solid materials from the produced fluid. The fluid phase then moves in a microannulus between the screen/debris filter and base pipe into the FCD subassembly where it must pass through one or more constant area channels set in parallel. Upon exiting the helical channels, the produced fluid passes through perforations into the production tubing (Qudaihy et al. 2005).

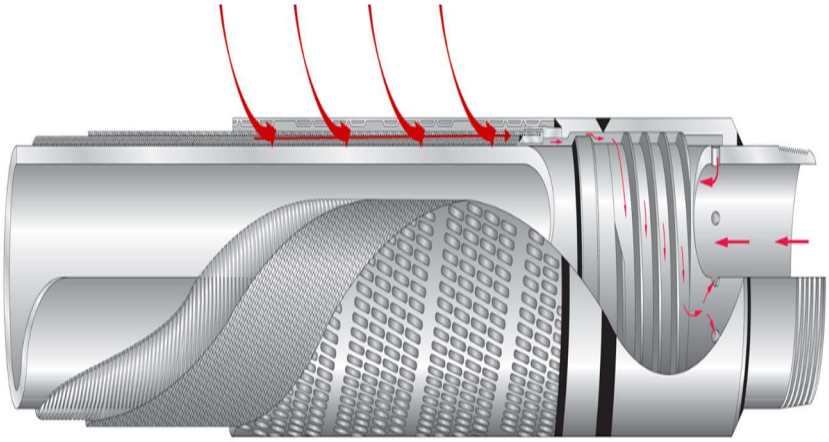

Figure 4: Exploded view of flow in a helical geometry, channel-style FCD. Adapted from Bitto (2005)

Pressure drop across channel-style FCDs occur due to viscous and inertial forces acting upon the fluid. Viscous forces consist largely of fluid drag along the channel walls while inertial forces refers to shear forces within the fluid that resist changes in direction or velocity (Lauritzen and Martiniussen 2011). This geometry induces pressure drop over a longer interval compared to restriction-style FCDs, creating an advantageous condition where erosion or plugging of the FCD can be avoided (Al-Khelaiwi and Davies 2007; Visosky et al. 2007). However, this device style's dependence on friction to generate the majority of its pressure drop makes it highly sensitive to the viscosity of the flowing fluid.

Predicting multiphase flow performance through a channel has been well established in fluid flow mechanics. For fully developed flow in a horizontal pipe, the pressure drop may be expressed as (Lauritzen and Martiniussen 2011; Lee et al. 2013):

$$\Delta p_{channel} = f\left(\frac{L}{D}\right)\left(\frac{v^2}{g_c}\right) \quad \textbf{...} \quad \textbf{(Eq. 11)}$$

In this equation, L [ft] is the length of the channel, D [ft] is the diameter of the channel, v is the fluid average velocity [ft/s], and g_c [lb_m-ft/lb_f-s^2] is a conversion factor. The friction factor, f [dimensionless], is a function of the dimensionless Reynolds number (N_{Re}) and is calculated as follows (Lee et al. 2013):

$$N_{Re}488 = 1\frac{d_h \rho v}{\mu} \quad \textbf{...} \quad \textbf{(Eq. 12)}$$

$$f = a_2 {N_{Re}}^{b_2} + \frac{a_2 {N_{Re}}^{b_2} + a_1 {N_{Re}}^{b_1}}{\left(1 + \left(\frac{N_{Re}}{t}\right)^c\right)^d} \quad \textbf{...} \quad \textbf{(Eq. 13)}$$

Where d_h [ft] is the hydraulic diameter, ρ [lb_m/ft^3] is the density, v [ft/s] is the fluid velocity, μ [cP] is the viscosity, and a_1, a_2, b_1, b_2, c, d, and t are empirically determined dimensionless constants intended to force a fit of the model to experimental data.

1.3.2 Restriction-Style FCDs

For multiple industries, it is a common practice to flow liquid and gas mixtures through restriction-style chokes (Ajienka et al. 1994; Alimonti et al. 2010; Almeida 2013; Campos et al. 2014; Elgibaly and Nashawi 1998; Grose 1985; Kojasoy et al. 1997; Perkins 1993; Schüller et al. 2003; Zhang and Cai 1999). Specifically within the oil and gas

industry, restriction-style FCDs are heavily used as wellhead chokes to control production from wells, as a critical part of single or multiphase flow measurement valves, and within gas lift valves (Ajienka et al. 1994; Al-Attar 2013; Almeida 2013; Surbey et al. 2013). In SAGD operations, restriction-style FCDs have been used in injection wells as a "steam splitter", a tool to both mechanically divert steam down the wellbore, add additional points of steam injection, and control the rate of injection into particular reservoir zones to equalize steam delivery along the lateral length (Ghesmat and Zhao 2015; Medina 2015).

Figure 5 portrays a restriction-style FCD arranged for a production well (Oyeka et al. 2014). Here, an optional sand control screen is illustrated around a production base pipe. Fluid produced from the reservoir is filtered of solid material by the sand control media before being channeled into a micro-annulus between the screen and base pipe. This annular gap is adjusted by wire stand-offs which separate the annulus into several sections evenly distributed around the circumference of the base pipe, providing the dominant flow path (Atkinson et al. 2004). When the fluid reaches the end of the pipe, it encounters the FCD subassembly where it encounters a sudden restriction in its flow path, oriented axially in this illustration.

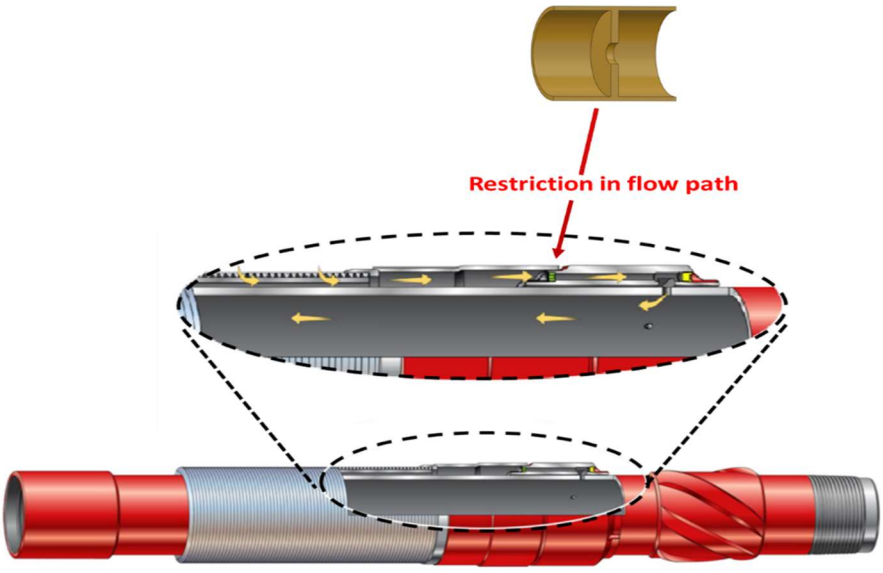

Figure 5: Exploded view of a restriction-style FCD in a production joint Adapted from Oyeka et al. (2014).

This constriction to flow creates a differential pressure drop across the restriction, in line with Bernoulli's principle for incompressible flow (Darby 2001; Van Ness and Abbott 2008). Fluids, once downstream of the FCD, encounter perforations to allow entrance into the production base pipe (Banerjee et al. 2013a). If the restriction-style FCD is oriented radially, the FCD also serves as the entrance into the production base pipe (Al-Khelaiwi and Davies 2007). The particular type of restriction may vary with common styles including thin and thick orifice chokes, nozzles, short tubes, and venturi restrictions (Abdelfattah et al. 2012; Atkinson et al. 2004; Banerjee et al. 2013a; Banerjee and Hascakir 2015; Banerjee et al. 2013b; Bybee 2008).

Significant effort has gone into characterizing flow behavior across restriction-style chokes by numerous researchers. Published models fall into either empirical or

theoretical models (Alsafran and Kelkar 2013; Elgibaly and Nashawi 1998). Empirical models largely follow the form of Gilbert (1954), and include proposed models by Ros (1960), Achong (1961), Ashford and Pierce (1975), and Osman and Dokla (1992). These models were developed on specific ranges of data and should not be used to extrapolate beyond those ranges (Alsafran and Kelkar 2013; Elgibaly and Nashawi 1998).

The second category, theoretical models, attempts to derive pressure drop relationships from mass, momentum, and energy balances. Models within this group are more often used by industry due to their ability to model both critical and subcritical flow, adding to a perception of greater accuracy (Alsafran and Kelkar 2013). To clarify the previous statement, critical flow occurs when fluid velocity across the restriction is equal to the speed of sound in that medium. Conversely, subcritical flow is when fluid velocity is less than the speed of sound in the fluid medium. If the flow is subcritical, the flow rate is related to the pressure drop across the restriction. However, if the flow is critical, the pressure drop is related only to upstream pressure as reduction in downstream pressure cannot be communicated upstream (Darby 2001; Janssen 1967; Ramamurthi and Nandakumar 1999; Roul and Dash 2012). To optimize a restriction-based FCD, understanding the critical/subcritical boundary and the fluid flow pattern across the restriction is of absolute importance. Prominent theory-based restriction models used by industry include those proposed by Sachdeva (1986), Perkins (1993), Fortunati (1972), and Alsafran (2013) as these models are able to simulate the physical phenomena in both subcritical and critical regimes.

In single phase fluid flow, the theoretical analysis to evaluate pressure drop caused by abrupt contraction of the flow area is accomplished with one-dimensional analysis. We begin by considering the orifice restriction case: as a fluid stream passes through a sharp edge "thin" orifice restriction, the flow contracts to an area smaller than that of the orifice itself. This smaller area, A_c, is called the vena contracta (ASME 2006; Van Ness and Abbott 2008). As fluid converges towards the opening of an orifice, it builds up considerable inward radial momentum that causes the flow stream to continue to flow "inwards" for a distance downstream of the restriction (Darby 2001; Sahin and Ceyhan 1996). As the flow stream continues downstream of the vena contracta the flow expands in an irreversible process to the pipe cross-sectional area, A. Correspondingly, the pressure of the flow stream decreases across the restriction and continues to decrease to the point of the vena contracta, with some recovery of pressure occurring as the flow stream expands outwards to the pipe cross-sectional area. **Figure 6** is an illustration of the converging and diverging flow streams and the corresponding pressure profile upstream, across, and downstream of an orifice flow meter. This behavior is unique to orifice restrictions; a vena contracta does not occur with variant restrictions such as nozzles or venturi restrictions where the maximum pressure drop occurs across the restriction itself (Almeida 2013; Banerjee and Hascakir 2015; Darby 2001).

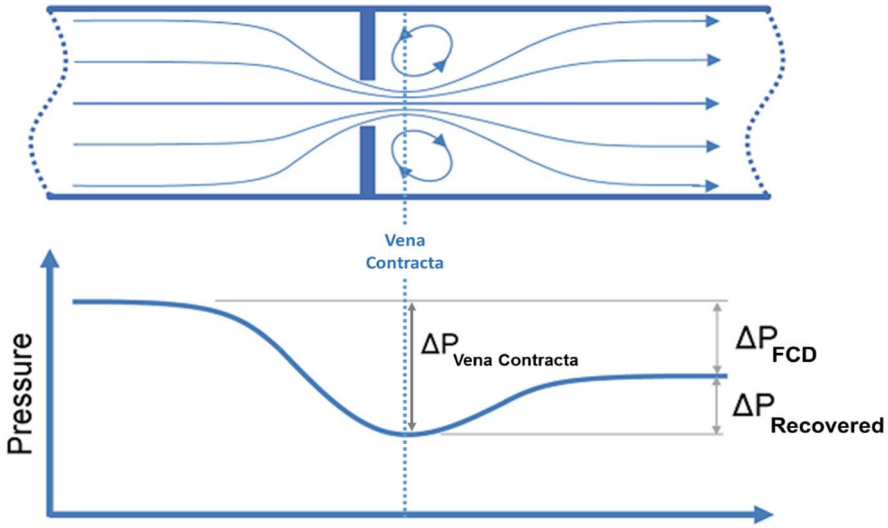

Figure 6: Pressure profile upstream, across, and downstream of an orifice restriction (Darby 2001). $\Delta P_{vena\ contracta}$ is the measured pressure drop at the point of the vena contracta while ΔP_{FCD} is the ultimate, unrecovered pressure loss across the restriction. $\Delta P_{Recovered}$ is the difference between these two values.

If the orifice is "thick", then an expansion after the vena contracta occurs within the geometry of the orifice itself with a second expansion occurring as the fluid stream exits the thick orifice (Fossa and Guglielmini 2002). Per Chisholm (1983), the thick orifice behavior occurs when the depth of the orifice (s) is greater than half of the orifice diameter (d). As such, FCD geometries relying on short tubes for pressure drops would be considered analogous to the "thick" orifice case while longer tube FCDs would be analogous to a channel-style FCD. **Figure 7** illustrates the contraction and expansion behavior of the flow stream through a thin and thick orifice geometry.

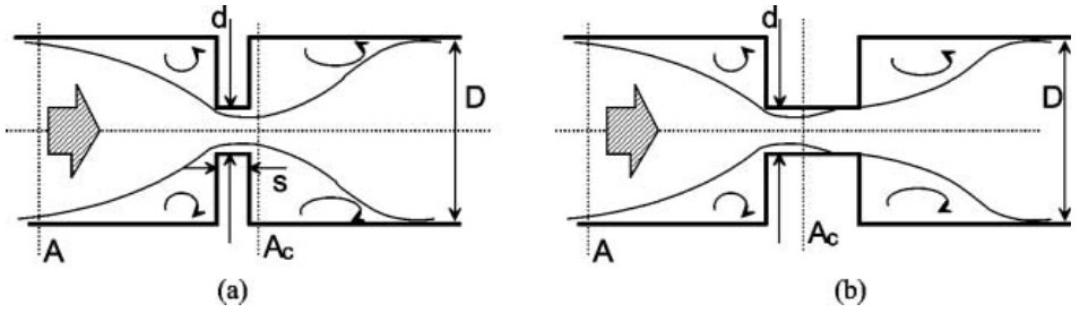

Figure 7: Single-phase flow across a thin (a) and thick (b) orifice (Kojasoy et al. 1997). In this illustration, D is the full pipe diameter, d is the diameter of the restriction, A is the cross-sectional area of the pipe, A_c is the interfacial area at the vena contracta, and s is depth of the restriction.

Assuming incompressible flow and that each expansion occurs irreversibly, the single-phase pressure drop (Δp_{sp}, [Pa]) for a thin orifice can be expressed as in **Equation 14** (Alimonti et al. 2010; Fossa and Guglielmini 2002):

$$\Delta p_{sp} = \frac{\rho v^2}{2}\left[\frac{1}{\sigma\sigma_c} - 1\right]^2 \quad \text{... (Eq. 14)}$$

$$where\ \sigma = \left(\frac{d}{D}\right)^2 \quad \text{... (Eq. 15)}$$

$$and\ \sigma_c = \frac{A_c}{A\sigma} \quad \text{... (Eq. 16)}$$

In **Equation 14**, ρ [kg/m^3] is fluid density, v [m/s] is mean fluid velocity across the restriction, σ [dimensionless] is the flow area ratio (**Equation 15**), d [m] is the restriction diameter, D [m] is the pipe diameter, σ_c [dimensionless] is the contraction coefficient (**Equation 16**), and A_c [m^2] is the previously defined vena contracta area. The pressure drop behavior predicted by **Equation 14** is for an ideal case and deviates from

experimental data (Ajienka et al. 1994). As a result, the pressure drop from **Equation 14** is corrected by three independent dimensionless coefficients termed the contraction coefficient (σ_c), the viscosity coefficient (σ_v) and the flow profile coefficient (σ_p). The viscosity coefficient, σ_v, corrects the theoretical equation for streamwise viscosity effects and is dominant at extremely low Reynolds numbers. The contraction coefficient, σ_c, corrects the theoretical equation for convergence of flow as it exits the restriction and is dominant at very high Reynolds numbers. The profile coefficient, σ_p, corrects the theoretical model for wall-induced viscous effects and is the dominant coefficient for flow through nozzle and venturi variants of restriction-style FCDs (Grose 1985). In practice, most models use a single coefficient known as the discharge coefficient (C_d, [dimensionless]) which is the product of these three terms, as outlined in **Equation 17**.

$$C_d = \sigma_c \sigma_p \sigma_v \quad \textbf{...} \quad \textbf{(Eq. 17)}$$

The orifice discharge coefficient is defined as the ratio of the actual flow rate through a restriction to that predicted by an equation derived from one-dimensional inviscid flow theory (Darby 2001; Grose 1985; Lin 1982; Van Ness and Abbott 2008). Thus the discharge coefficient functions to estimate dissipation and vena contracta effects upon the ideal model (Campos et al. 2014). Using this discharge coefficient, **Equation 14** is corrected to provide a realistic local pressure drop for a thin orifice as in **Equation 18**:

$$\Delta p_{sp} = \frac{\rho v^2}{2}\left[\left(\frac{1}{\sigma}\right)^2 - 1\right]\frac{1}{C_d^2} \quad \textbf{...} \quad \textbf{(Eq. 18)}$$

If the restriction behaves as a thick orifice, a double expansion is responsible for the loss of mechanical energy. For these conditions, the ideal pressure drop is expressed as **Equation 19**:

$$\Delta p_{sp} = \frac{\rho v^2}{2}\left[\left(\frac{1}{\sigma\sigma_c}\right)^2 - 1 - \frac{2}{\sigma^2}\left(\frac{1}{\sigma_c} - 1\right) - 2\left(\frac{1}{\sigma} - 1\right)\right] \quad \text{...} \quad \textbf{(Eq. 19)}$$

By manipulating **Equation 14** and **18** as well as **Equation 14** and **19**, σ_c can be written as:

$$\sigma_{c,thin} = \frac{1}{\sigma + \frac{\sqrt{1-\sigma^2}}{C_d}} \quad \text{...} \quad \textbf{(Eq. 20)}$$

$$\sigma_{c,thick} = \frac{1}{1 + \sqrt{\frac{(1-\sigma^2)}{{C_d}^2} - 1 + 2\sigma - \sigma^2}} \quad \text{...} \quad \textbf{(Eq. 21)}$$

Expressing the contraction coefficient solely in terms of the flow area ratio is convenient as the size of the vena contracta is very rarely known during the design process for restriction-style FCDs.

Establishing the correct discharge coefficient is also challenging. For single-phase flow, the discharge coefficient is a function of Reynolds number and the flow area ratio. The dependence on Reynolds number is very weak, except for low Reynolds numbers, and close to unity for venturi or nozzle flow meters (Campos et al. 2014; Kiljański 1993; Mayer et al. 2014; Rahman et al. 2009; Ramamurthi and Nandakumar 1999). For these variants of restriction-style FCDs, dissipation effects are almost negligible which in turn is reflected in the discharge coefficient. For an orifice restriction conforming to ISO 5167,

the discharge coefficient can be determined using the correlation in **Equation 22** (Urner 1997):

$$C_D = 0.5959 + 0.0312\sigma^{2.1} - 0.184\sigma^8 + 0.0029\sigma^{2.5}\left(\frac{10^6}{N_{Re}}\right)^{0.75} + 0.09\left(\frac{L_1}{D}\right)\left(\frac{\sigma^4}{1-\sigma^4}\right) - 0.0337\left(\frac{L_2}{D}\right)\sigma^3 \quad \text{... (Eq. 22)}$$

For **Equation 22**, L_1=L_2=0.0254 meters, σ [dimensionless] is the flow area ratio previously defined, D [m] is the unrestricted pipe diameter, and N_{Re} is the dimensionless Reynolds number. This relationship is unwieldy and only applies to restrictions conforming to the ISO standard, so a simplification proposed by Morrison (2003) is used. In the work of Morrison, the discharge coefficient for a restriction-style FCD is not a function of Reynolds number but instead a function of the Euler dimensionless number (Eu). The Euler number is defined as:

$$Eu = \frac{\Delta P}{0.5\rho v^2} \quad \text{... (Eq. 23)}$$

Here ρ [kg/m^3] is density, v [m/s] is mean fluid velocity, and ΔP [Pa] is the pressure drop. Morrison found that using the Euler number as a rough equivalent for $(1/C_d)^2$ proved as accurate as using a discharge coefficient calculated from the Reynolds number. Morrison's exact correlation for discharge coefficient as a function of Euler number is provided in **Equation 24**:

$$C_d = \frac{1}{\sqrt{Eu}}\left(\frac{1-\sigma^4}{\sigma^4}\right) \quad \text{... (Eq. 24)}$$

The Morrison method has the benefit of eliminating viscosity from the calculation of pressure drop across a restriction. Thus, the calculation of C_d is simplified and the pressure

drop calculation is improved as uncertainty in the fluid viscosity term can no longer influence the results (Jain et al. 2014; Morrison 2003).

However, in multiphase fluid flow, the calculation of pressure drop due to gas-liquid two-phase flow through a restriction is yet to be solved in current engineering practice (Roul and Dash 2012). There is no assurance that a non-homogenous two-phase flow follows the behavior outlined for single phase flow (Kojasoy et al. 1997). As a comprehensive unifying equation for multiphase pressure drop across a restriction has yet to be developed, most multiphase models compensate by introducing a correction factor, known as the two-phase multiplier, to the single phase pressure drop formula (Schüller et al. 2003). The two-phase multiplier is defined as the ratio of the two-phase pressure drop through the restriction to the single-phase pressure drop obtained at liquid mass flux equal to the overall two-phase mass flux (Roul and Dash 2012). Models to predict the two-phase multiplier have been proposed by many prominent researchers. Chisholm (1983) developed the expression:

$$Two - Phase\ Multiplier = \Phi_{lo}^2 = 1 + \left(\frac{\rho_l}{\rho_g} - 1\right)[Bx(1-x) + x^2] \quad \textbf{...} \quad \textbf{(Eq. 25)}$$

Where ρ_l [kg/m^3] is the density of the liquid phase, ρ_g [kg/m^3] is the density of the gas/vapor phase, B is a dimensionless constant assumed to be 0.5 for thin orifices and 1.5 for thick ones, and x [dimensionless] is the ratio of mass flux of gas to the total mass flux of mixture, also known as the "quality".

The Morris equation applies to thin orifices and gate valves and can be expressed as (Morris and Garimella 1998):

$$\Phi_{lo}^2 = \left[x\frac{\rho_l}{\rho_g} + S(1-x)\right]\left[x + \left(\frac{1-x}{S}\right)\left(1 + \frac{(S-1)^2}{\left(\frac{\rho_l}{\rho_g}\right)^{0.5} - 1}\right)\right] \quad \text{...} \quad \textbf{(Eq. 26)}$$

$$where\ S = slip\ ratio = \sqrt{1 + x\left(\frac{\rho_l}{\rho_g} - 1\right)} \quad \text{...} \quad \textbf{(Eq. 27)}$$

Simpson et al. (1981) proposed a model where the slip correlation was independent of the quality of the mixture:

$$\Phi_{lo}^2 = [1 + x(S-1)][1 + x(S^5 - 1)] \quad \text{...} \quad \textbf{(Eq. 28)}$$

$$where\ S = \left(\frac{\rho_l}{\rho_g}\right)^{1/6} \quad \text{...} \quad \textbf{(Eq. 29)}$$

As establishing the pressure drop across a restriction-style FCD is not an analytical exercise, optimizing usage for the production lateral in a SAGD completion is difficult. Establishing single-phase flow behavior for emulsions of bitumen and condensate is a daunting enough task, given the variability with phase externality and temperature. To then run multiple laboratory trials with steam in order to obtain an empirical fit and appropriate two-phase multiplier correction factor borders on impossible when cost and effort are considered. Yet restriction-style FCDs can be optimized and analytically modelled for the pseudo-multiphase fluid that passes through the injector in SAGD well pairs. High-quality steam is used for injection in SAGD projects, which means that the injected steam behaves as a multiphase mixture of liquid and vapor (Medina 2015). However, this two-phase flow behavior is not as complicated as others (Steven and Hall

2009). Thermal EOR operations use wet steam, a mixture of saturated liquid and saturated vapor, which mixtures homogenously and maintains equilibrium conditions (Chien and Schrodt 1995). The thermodynamic properties of steam are also well known and available in published steam tables (Griston and Cire 1989). The rate of steam injection and steam quality are all controllable factors. As a result, the general orifice flow equation may be adapted for wet steam as follows (Chien and Schrodt 1995):

$$\Delta p_{steam} = \left(\frac{w\sqrt{1-\sigma^4}}{13.115 C_d F_a Y_2 d^2} \right)^2 v_{exp} \quad \text{...} \quad \textbf{(Eq. 30)}$$

Where w [lb_m/hr] is the steam flow rate, σ [dimensionless] is the ratio of restriction diameter to pipe diameter, C_d [dimensionless] is the discharge coefficient, d is the restriction diameter [ft], F_a [dimensionless] is the thermal expansion coefficient, and Y_2 [dimensionless] is the vapor expansion coefficient. These last two coefficients are calculated according to Miller (1996). The last term, v_{exp} [ft^3/lb_m] is the two-phase specific volume of the steam as it flows through the restriction. James (1965) offers **Equation 31** as a means of calculation of v_{exp}:

$$v_{exp} = A(v_{fg}) \left(\frac{x}{100} \right)^B + v_f \quad \text{...} \quad \textbf{(Eq. 31)}$$

Here, x [dimensionless] is the steam quality, v_{fg} [ft^3/lb_m] is the specific volume of vaporization, and v_f [ft^3/lb_m] is the specific volume of the saturated liquid. A and B are dimensionless constants that are experimentally determined for a specific range of steam pressure and temperature. Using **Equation 30**, inexpensive restriction-style FCDs can be optimized and easily modelled for SAGD injector wells where steam trap control/FCD

autonomy isn't a necessary feature for establishing fluid conformance.

1.3.3 Autonomous Hybrid FCDs

A fundamental problem that exists with most passive FCDs is how they respond to breakthrough of unwanted fluids. Though restriction-style and frictional-style FCDs delay breakthrough of unwanted water/gas/steam, when unwanted fluid break-through occurs, these FCD geometries exhibit lower pressure drop for the unwanted fluids than they do for the oleic hydrocarbons. As a result, that segment will see an increase in flow rate and in water/gas cut compared to other segments of the lateral, potentially creating a new non-conforming fluid profile later in well life (**Figure 8A**). The class of FCDs known as "autonomous" FCDs reverses this behavioral trend. Instead of a reduced pressure drop for unwanted fluid, autonomous FCDs increase the pressure drop for unwanted fluid. Now, if an unwanted breakthrough event happens, the segment in contact with the unwanted fluid exhibits a decrease in flow rate compared to other segments in the lateral, correcting the conformance profile along the lateral over time (**Figure 8B**).

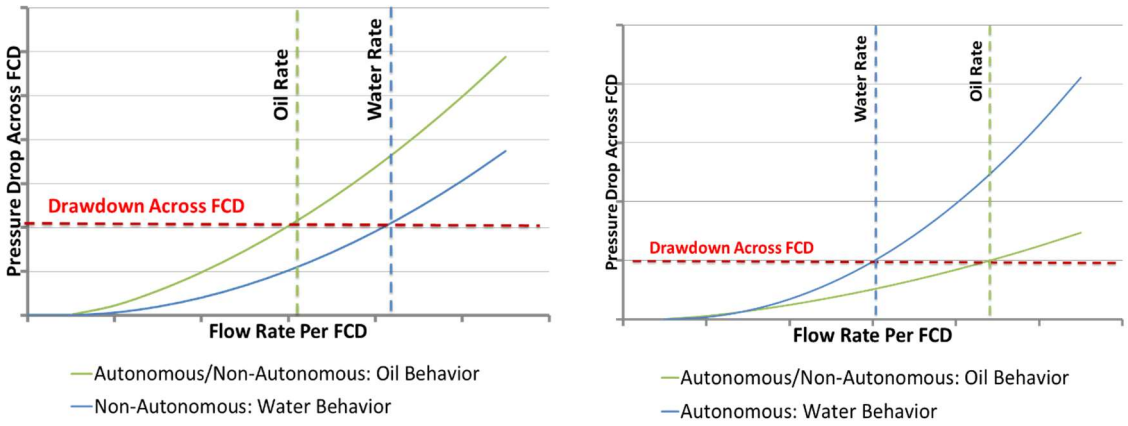

(A) Breakthrough Event for Non-Autonomous FCD

(B) Breakthrough Event for Autonomous FCD

Figure 8: Comparison of Pressure Drop Response for Autonomous and Non-Autonomous FCDs to Unwanted Fluids

It is important to distinguish "autonomous" FCDs from "active" FCDs; autonomous FCDs exhibit control over unwanted fluids passively and without operator intervention, relying on properties intrinsic to the fluid or fluid regime to trigger changing behavior. By contrast, active FCDs (such as intelligent control valves, FCDs with sliding sleeves, etc.), require oversight by operators and direct intervention in order to modify performance behavior. Three commercial FCD geometries exhibit autonomous behavior: fluidic diodes, rate-controlled production valves, and hybrid FCDs. However, the manner by which each provides autonomy varies wildly from manufacturer to manufacturer and introduce new operational advantages and risks depending on the mechanism of action.

The fluidic diode FCD is a credit-card sized device that alters its restriction to fluid flow based on the spinning momentum of the fluid passing through the device (Least et al. 2014). Autonomous behavior is achieved by driving fluid flow through preferential

channels based on the fluid's inherent inertial and viscous forces with simplified internal FCD geometry described in **Figure 9**. If viscous forces are dominant, fluid is fairly evenly divided between the straight and divergent pathways of **Figure 9**, a typical response for most oils. However, fluids where inertial forces are significantly greater than viscous forces (e.g., gas and water) will favor the straight pathway and bypass the divergent pathway (Fripp et al. 2013). Viscous fluids moving through the divergent pathway are generally lower velocity, and therefore require little change in angular momentum to exit the FCD and exhibit minimal rotation in the vortex chamber. If moving through the straight pathway, fluids enter the vortex chamber tangentially and with higher angular momentum. This momentum must be dissipated and fluid velocity reduced by frictional drag while spinning within the vortex chamber before the fluid flow path can be directed to the FCD exit.

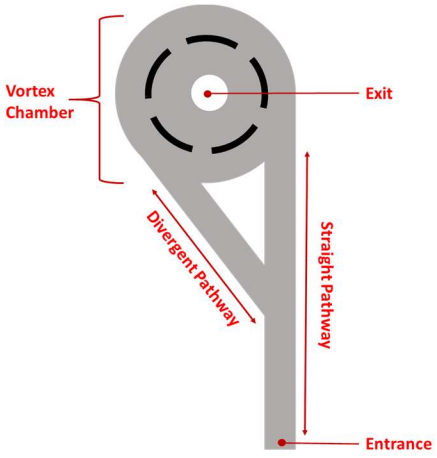

Figure 9: Simplified Internal Schematic of a Fluidic Diode FCD. Adapted from Fripp (2013)

Figure 10A is an external view of a fluidic diode device while **10B** illustrates the housing into which the fluidic diode FCD is secured to a production joint. Due to its reduced size, the pathway cross-sectional area is quite small compared to its commercial peers, leading to higher velocities for the same volumetric flowrates with potential operational risks due to channel plugging or erosion. Similar to frictional-style FCDs, fluidic diode performance is highly dependent on fluid viscosity. As such, it shares similar issues regarding changing performance as production fluid viscosity changes due to emulsification, temperature change, etc. Unlike frictional-style FCDs, the fluidic diode only provides a pressure drop in one direction, either injection or production, depending on installation. Thus, fluidic diodes will not equalize steam distribution during SAGD start-up and circulation, only production profiles during true SAGD. **Figure 11** provides an illustration of the flow path from the reservoir, through the fluidic diode FCD, and into the base pipe. An additional concern is that should a fluidic diode induce steam flashing, it is most likely to occur at the exit nozzle and thus jet uncontrolled steam into the production tubing.

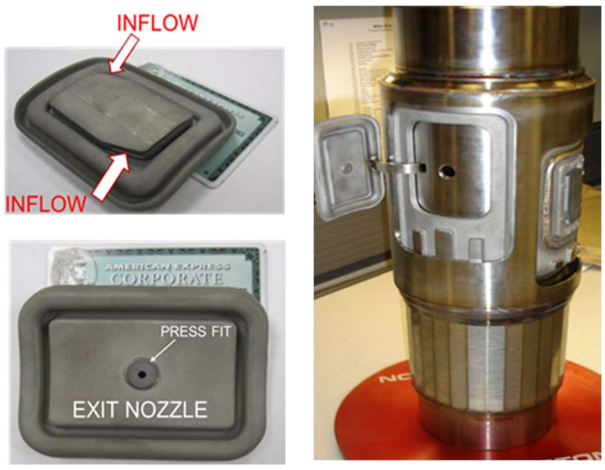

(A) (B)

Figure 10: (A) Photo of a fluidic diode unit with credit card for size reference and (B) the housing subassembly securing a fluidic diode unit to the production joint

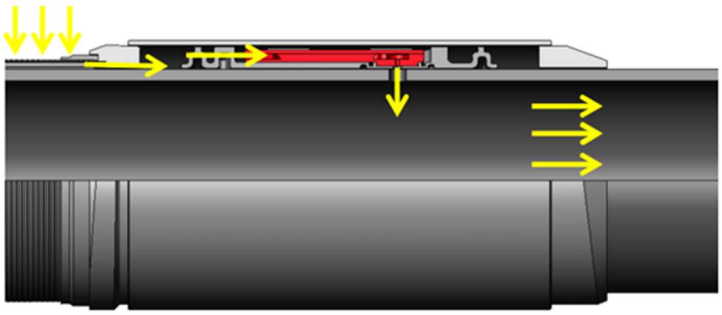

Figure 11: Fluid flow path (from reservoir to base pipe) through a fluidic diode FCD installed for production equalization

A second autonomous FCD geometry is that of the Rate-Controlled Production (RCP) valve. This FCD geometry modifies a more traditional restriction-style FCD by introducing a moving disc into the flow path. The position of this disc is dependent on the fluid properties and flow conditions within the RCP. For highly viscous and heavy oils,

the disc remains at the bottom of the FCD chamber and provides no obstruction to the restriction at the FCD exit. However for low viscous fluid (e.g., gas), the pressure on the flowing side of the disc is lower than the pressure on the back side of the disc due to the high velocity of the flowing fluid. In this case, the pressure imbalance pushes the disc upwards towards the disc seat and reduces the flow area of the exit orifice (Halvorsen et al. 2012). When reduction in flow area at the exit orifice occurs, there is a corresponding increases in pressure drop across the FCD. **Figure 12A** & **12B** illustrates the changing disc position for oil and gas flow while **Figure 12C** shows how the RCP valve is inset into the production joint.

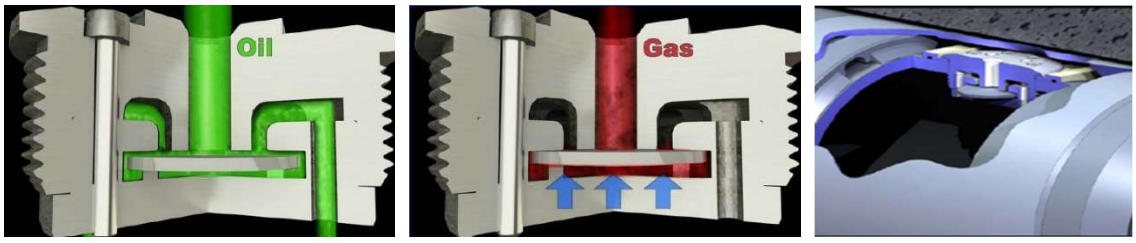

(A) (B) (C)

Figure 12: (A) Exploded view of the RCP with disc position under oil flow, (B) Exploded view of the RCP with disc position under gas flow, (C) Exploded view of the base pipe illustrating how the RCP is inset into a production joint (Halvorsen et al. 2016)

Though the RCP has the strongest autonomous response to unwanted gas flow of any commercial autonomous FCD, it brings with it a number of operational challenges that limit its suitability for field use. One immediate concern is FCD orientation; the RCP

must be installed in the well with gravity initially pulling the internal disc downwards else the FCD will not function as designed. Another major concern is in the operational reliability of the disc itself; dependent on a moving part, the FCD is subject to failure should the disc ever jam, deform, break, or have its range of motion compromised by foreign materials (Banerjee and Hascakir 2015). In contrast, no other FCD geometry introduces the additional risk of a moving part. Erosion and plugging continue to be an operational risk for the exit orifice just as it is for the RCP's non-autonomous counterpart. Finally, the throughput of the RCP is exceptionally low. To quantify this, a flow rate of 2.5 gallon/minute of water across the RCP would require a drawdown on the order of 450 psi, well beyond a desirable pressure drop for such a low production flowrate.

The final autonomous design available commercially is the hybrid FCD, a design that uses multiple restrictions in series placed in a labyrinth pathway. This design hybridizes restriction-style FCDs (by using multiple restrictions within the flow path) and frictional-style FCDs (by creating pressure losses through wall drag and tortuosity) while providing autonomous choking to steam. By distributing the pressure drop over multiple subcomponents, no one individual point of pressure loss is critical to overall function. Cross-sectional flow area through this geometry is 4-10 times larger than other autonomous FCDs, significantly lowering internal velocities and thus lowering the risk of both plugging and erosion (Banerjee et al. 2013b). The staggered restrictions within this geometry also serve to add a secondary control over steam flashing. Should steam flashing occur across the restriction of any given cell, the downstream cells serve to create a stronger choke to steam passage, controlling the rate at which it may enter the production

tubing. **Figure 13** provides a view of the interior of the hybrid FCD. **Figure 14** provides a close up view of one of the selectable flow paths; depending on which flow path is left unplugged, the pressure drop behavior across the hybrid FCD may be scaled up or down due to the number of cells in the flow path.

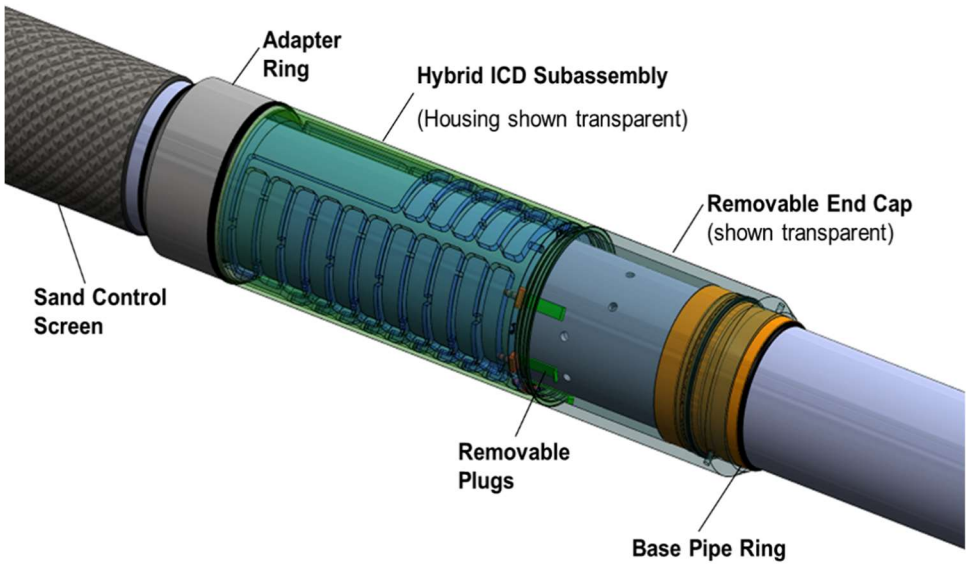

Figure 13: View of a Hybrid ICD assembly with transparent housing subassembly (Banerjee et al. 2013b)

Figure 14: One of multiple fluid pathways within a hybrid FCD subassembly (Banerjee and Hascakir 2015)

Unlike most other FCDs, multiphase testing has been done on the hybrid FCD by third-party laboratories. As a result, this geometry has one of the better characterized pressure drop response to a multiphase fluid. Lee et al. (2013) have suggested that multiphase performance may be accurately described by **Equation 32**, where the pressure drop across a hybrid FCD is dependent on a unique friction factor term ($ff_{mixture}$) that is a function of the dimensionless Reynolds number. This friction factor term is defined in **Equation 33**.

$$\Delta p_{FCD} = ff_{mixture} \frac{l_{channel}}{D_h} \rho_{mixture} \left(\frac{v^2}{24 g_c} \right) \quad \text{...} \quad \textbf{(Eq. 32)}$$

$$ff_{mixture} = a_2 N_{Re}^{b_2} + \frac{\left(a_2 N_{Re}^{b_2} + a_1 N_{Re}^{b_1} \right)}{\left(1 + \left(\frac{N_{Re}}{t} \right)^c \right)^d} \quad \text{...} \quad \textbf{(Eq. 33)}$$

Here $ff_{mixture}$ and N_{Re} are dimensionless numbers, $l_{channel}$ is the length of the FCD channel [ft], D_h is the hydraulic diameter [ft], $\rho_{mixture}$ is the mixture density [lb_m/ft^3], v is the mixture

velocity [ft/s], g_c is a conversion factor [lb_m-ft/lb_f-s^2], and a_1, a_2, b_1, b_2, c, d, and t are dimensionless constants used to fit the empirical laboratory data for multiphase flow.

Like the fluidic diode, the hybrid FCD has no moving parts to introduce additional operational risk. This geometry, unlike the fluidic diode, has demonstrated viscosity insensitivity up to 300 cP. It is also less prone to plugging or erosion due to the larger flow areas within its geometry. The redundancy of restrictive cells placed in series provide a theorized benefit in terms of controlling a steam flash event within the FCD. Finally, the hybrid FCD has the most extensive run history for both heavy oil and conventional FCD use. For this multitude of reasons, this hybrid FCD geometry is the focus of this work's laboratory testing and simulation work, offering the best balance of performance and operational reliability of all autonomous FCDs that might be applied to a SAGD producer. Descriptions of multiphase performance, previously provided in equations 32 and 33, may prove insufficient for modeling the autonomous hybrid FCD performance for SAGD conditions. This empirical regression to multiphase data is intended to capture the physics of water and gas coning, not the steam breakthrough events of SAGD production (Lee 2013). Furthermore, the data used to generate these empirical constructs relies on nitrogen gas to serve as the gas phase. While this is an understandable choice, as nitrogen is inert, nonflammable, and readily available, nitrogen is also not a saturated fluid at test conditions. As such, it cannot capture the reversible transition from liquid to vapor phase that occurs with water in SAGD production and thus multiphase correlations based on nitrogen test cases are unlikely to mimic the behavior of multiphase flow that occurs in a SAGD production well.

2. PROBLEM STATEMENT

Economic recovery of heavy-oil and bitumen has enabled Canada to become a significant player in the world energy market (National Energy Board 2016). Credit for this massive shift is due largely to the Steam Assisted Gravity Drainage (SAGD) process as this particular thermal recovery method has increased the country's proven reserves from roughly 7 billion barrels to 175 billion barrels in-situ (Banerjee et al. 2013b; Butler and Yee 2002). However, the SAGD process has been open to criticism; the steaming process is seen as wasteful of water and contributes to global greenhouse gas emissions while the economics of the process can be quickly undermined by the inability to produce enough steam from surface facilities or the on-going costs of steam generation (Kovscek 2012). The use of Flow Control Devices (FCDs) suggests a panacea to many of these criticisms. It is hypothesized that FCD usage improves steam conformance and prevents unwanted steam breakthrough, improving thermal efficiency in the SAGD process (Stalder 2013; Vachon et al. 2015). This would also have a corollary effect of reducing steam/water usage, the size required of steam surface facilities, on-going costs of generating steam, and the greenhouse gas emissions that come from steam generation.

While FCD performance has been reasonably well characterized for controlling water breakthrough, this research began when no data was available for FCD performance for fluids at or near saturation temperature as would exist in a SAGD process (Riel et al. 2014; Vachon et al. 2015). Limited information exists for FCD performance with any sort of gas-phase fluid (Coronado et al. 2009; Lauritzen and Martiniussen 2011; Lauritzen et al. 2011; Least et al. 2014; Least et al. 2013; Lee et al. 2013; Peterson et al. 2010).

Moreover, for a SAGD injector, steam splitters have a limited run history, but not in conjunction with any sort of production control and with little to no performance characterization (Kyanpour and Chen 2013; Medina 2015). As a result, it is not currently possible to accurately forecast the effect of an FCD completion upon steam chamber development or bitumen production in a SAGD well pair. The sole evidence available that FCDs provide a benefit to the SAGD process is a single field installation, the Surmont 102-06 well pair, with no other group having yet established repeatability of these results (Stalder 2013; Vachon et al. 2015).

This research will use closed-loop flow data measuring FCD pressure drop while flowing live steam and under steam flash conditions to create a statistically significant ($p=0.05$) pressure drop equation for multiphase steam flow through an autonomous hybrid FCD geometry. Akaike's Information Criterion (AIC) and Bayesian Information Criterion (BIC) selection methods will be used to establish the best prediction model for a steam-assisted gravity drainage conditions. Using the derived prediction model, representative simulations will be run to establish the quantitative benefit of FCDs to SAGD completions within Petroleum Expert's REVEAL™ software. Economic improvement will be measured using improvement in cSOR, NPV, and RF compared to a conventional SAGD completion.

3. MATERIAL AND METHODS*

3.1 Developing a Steam FCD Performance Model

To design SAGD completions that leverage FCD behavior effectively it is necessary to characterize FCDs under likely multiphase flow conditions. Commercial vendors of FCDs have provided some data to characterize the pressure drop performance of their offerings but these limited sets use a variety of different approaches, many of which are inappropriate for SAGD conditions (Lauritzen and Martiniussen 2011; Least et al. 2012; Least et al. 2014; Least et al. 2013; Lee et al. 2013; Wileman et al. 2013; Zhao et al. 2014). To effectively forecast FCD behavior, specific FCD completion geometries were installed into a high temperature multiphase flow loop capable of subjecting a given FCD geometry to representative SAGD conditions, including limited data collection on FCD performance under steam flash conditions. Reported results in this work focus on the autonomous hybrid flow control device. Developed previously by the author, it is believed that this geometry is the best available autonomous FCD for a SAGD producer by combining autonomy with operational benefits such as erosion and plugging resistance and large fluid throughput.

In establishing experimental design, only two responses were considered notable: the fluid pressure drop across the FCD geometry and the steam fraction of the fluid exiting the FCD. The first response, pressure drop across the FCD, is critical for sizing FCD

---

installations in completion design and for establishing the degree of autonomous behavior the FCD provides. The second response, exiting steam fraction, is valuable for establishing if the FCD might improve steam quality of wet steam when used in an injector role or if steam flashing might produce well damaging conditions in a producer role. **Figure 15** provides an overview of the experimental design method.

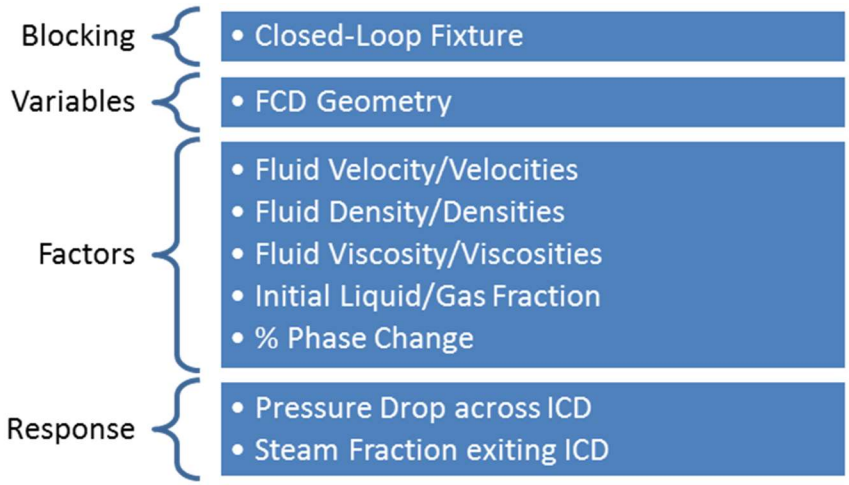

Figure 15: Summary of Experimental Design

The factors that were experimentally varied included fluid temperatures (ranged from 25° C to 300° C), FCD orientation (vertical or horizontal), liquid mass flow rate (ranged from 2 to 22 m^3/day), liquid viscosity (0.01 to 300 cP), liquid density (varying as a function of temperature and viscosity), water cut, gas-phase type (nitrogen or steam), gas-phase density (varying as a function of temperature and pressure), gas-phase viscosity (varying as a function of temperature and pressure), and finally gas-phase flow rates (0-5% by mass

of liquid). Fluid characteristics at the FCD outlet were also measured to capture any change in fluid temperature, composition, viscosity, or density. Performed tests are outlined in the matrix of **Table 3**.

Table 3: Test Matrix for FCD Closed-Loop Test (Inlet Conditions)

Base Fluid	***Pressure***	***Temperature, ° C***	***FCD Orientation, degree***	***Inlet Flowrate, m^3/d***	***Nitrogen Fraction***	***Steam Quality***
Water	Variable	25, 80, 220, 250, 270	0 and 90	3-20 (10 rates per orientation)	0%	0%
Water	Variable	25, 80, 220, 250, 270	0 and 90	5-20 (3 rates per orientation)	0.1-5%	0%
Oil	Variable	40, 80, 220, 250, 270	0	3-20 (10 rates per temperature)	0%	0%
40% Water/ 60% Oil	Variable	220, 250, 270	0	3-24 (8 rates per temperature)	0%	0%
70% Water /30% Oil	Variable	220, 250, 270	0	3-24 (8 rates per temperature	0%	0%
Water/Oil	Variable	220, 250, 270	0	5-20 (3 rates per temperature	0%	0-5%
Water/Oil	Variable	220, 250, 270	0	5-20 m^3/d (3 rates per temperature	0%	0-5%

A number of operational challenges were present in constructing the closed-flow loop testing setup, focused mostly around ensuring a consistent delivery of well-mixed liquid phase and gas/vapor phase fluids at a constant ratio to the inlet of the FCD fixture. Consequently, liquid was moved through the flow loop by a piston-style positive

displacement metering pump. A piston-style pump was deemed best to minimize oscillations in liquid flowrate or liquid pressure during the testing process, improving data collection. This pump was also deemed effective in mixing multi-component liquids (oil and water mixtures) allowing for assumptions of a homogenous, mixed liquid phase to hold. To ensure a controllable delivery of gas/vapor, the gas/vapor component was introduced into the liquid stream shortly before entering the FCD test fixture. This ensured minimal cooling of the vapor component within the flow loop, minimal absorption of the gas phase into the liquid phase, and avoided allowing the final mixture time to separate into distinct phases with subsequent phase slippage. If nitrogen was used in a trial, the inert gas was injected immediately upstream of the FCD into the liquid phase. Steam, however, was not externally added to the liquid phase but was generated from the liquid water component by manipulating an inlet control valve upstream of the FCD. By creating an instantaneous upstream pressure drop, the throttling valve served to generate a steady and measurable steam quality from the liquid phase at the inlet of the tested FCD geometry. However, any calculated values derived from the liquid flow rate must consider the loss of mass from the liquid stream corresponding to steam generation. **Figure 16** is a schematic of the closed loop flow assembly, marking both pressure/temperature gauges upstream and downstream of the FCD test fixture, the point of nitrogen gas injection into the flow loop, and the throttling valve upstream of the FCD used to induce steam flashing in the fluid mixture.

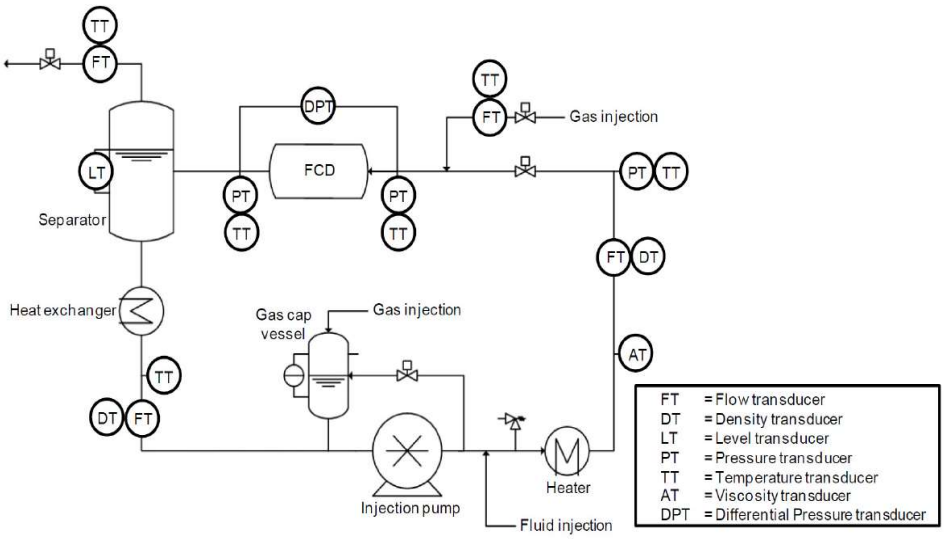

Figure 16: Schematic of the FCD Flow Loop (Vachon et al. 2015)

Initial trials, considering only single-phase oil/water or a single-phase liquid and nitrogen gas, were performed at ambient temperature and served to validate the setup of the constructed flow loop. This data set was directly compared against existing published performance models for the tested FCD geometry, such as that presented in **Equation 32** with the expectation of a high degree of agreement. This "validation" set of trials was also compared to an identical set with a non-horizontal orientation to establish whether FCD position influences pressure loss across the device. Again, the expectation is for a high degree of agreement between the two data sets and for orientation to be a negligible influence.

One critical area of interest is whether FCD usage in a SAGD producer will (a) induce steam flashing and (b) control steam flashing should it occur. All tested FCD geometries rely on a distributed pressure drop along a pathway length. Furthermore, fluid

is considered to be adiabatic as it moves through the FCD fixture. As a result, it is possible for liquid near saturation temperature to enter a lower pressure environment within or downstream of the FCD and maintain sufficient enthalpy that a fraction vaporizes to the steam state with both vapor and liquid now cooled to the saturation temperature of the liquid at the reduced pressure. If steam flashing should occur, the fluid within the device will take on significantly different characteristics from inlet conditions. Steam occupies significantly more volume for the same mass than water, so mixture density will drop, mixture velocity will increase by orders of magnitude, and mixture viscosity will likewise be reduced. Since all existing performance models rely on fluid conditions at the inlet and assume they remain static across the FCD, a flashing event may distort real pressure drops across an FCD from those predicted by existing theoretical models. **Equation 34** allows for the prediction of how much water will vaporize from the liquid phase to the steam phase for a given pressure drop within the FCD.

$$\chi_{steam} = \frac{h_{f1} - h_{f2}}{h_{fg}} \quad \textbf{...} \quad \textbf{(Eq. 34)}$$

Where χ_{steam} is the mass fraction of saturated liquid at that will be converted to vapor, h_{f1} is the specific enthalpy of the saturated liquid at the higher pressure [kJ/kg], h_{f2} is the specific enthalpy of the saturated liquid at the lower pressure [kJ/kg], h_{fg} is the latent heat of evaporation of the fluid at the lower pressure [kJ/kg]. A practical method of establishing a flashing event within the FCD geometry is to adjust the throttling valve upstream of the FCD until gauges indicate a steady-state steam flashing occurrence right at the outlet of the FCD. Then, continue adjusting the throttling valve until it induces a steady-state steam

flashing occurrence immediately at the inlet of the FCD. With these two choke settings now known, adjusting the upstream throttling valve to an average intermediate position should ensure that steam flashing occurs within the FCD geometry itself. With flashing occurring within the FCD geometry, empirical pressure losses during a steam flashing event may be compared to existing models that rely on static inlet conditions to predict FCD pressure loss. The advantage of this method is that fluid specific enthalpies need not be known as long as measurement gauges can indicate the flashing events and the exiting flow composition. Statistical regression allows for developing a correction factor to correct existing FCD performance models and produce a new, more realistic FCD performance model that is ideal for SAGD performance optimization.

3.2 Statistical Analysis

In this study, single-phase oil and water streams and multiphase mixtures of oil/water/steam or oil/water/nitrogen were flowed through an FCD fixture to measure fluid pressure loss across a given FCD geometry under different fluid conditions and levels of steam flashing. Using this data, an empirical expression for pressure drop across the FCD under known fluid/mixture density, viscosity, flow rate, and enthalpy was created through statistical analysis and linear regression tools. This empirical expression captures the effect of steam flashing within the FCD geometry itself.

Fitting regression models to data involving two or more predictors is one of the most widely used statistical procedures. In this work, an analysis of variance approach (ANOVA) was used to test whether a linear association exists between pressure loss across

an FCD and a subset/all of the expected predictors of this pressure loss. Based on the existing pressure loss models for restriction-style, frictional-style, and hybrid autonomous FCD, the predictors expected to influence pressure loss across a given FCD geometry are: maximum fluid velocity and/or velocity squared, fluid density, fluid viscosity, fluid temperature, FCD orientation, FCD hydraulic diameter, FCD pathway length, and gas/liquid fraction. Here, all predictors are continuous with the exception of FCD orientation which is a "dummy" variable where a change in orientation may only produce an additive change in pressure loss. All fluid properties are established at FCD inlet conditions. Thus, the initial "full" linear model used to describe FCD pressure loss for the autonomous hybrid geometry is that of **Equation 35**.

$$\Delta p_{FCD} = \beta_0 + \beta_1 v + \beta_2 v^2 + \beta_3 \rho + \beta_4 \mu + \beta_5 T + \beta_6 X + \beta_7 D_H + \beta_8 L + \beta_9 O + e \quad \textbf{...} \quad \textbf{(Eq. 35)}$$

For **Equation 35**, β_i (for i=0 to 9) are dimensionless regression coefficients, v is velocity [m/s], v^2 is velocity squared [m^2/s^2], ρ is fluid density [kg/m^3], μ is fluid viscosity [cP], T is temperature [°C], X is the liquid fraction [dimensionless], D_H is the hydraulic diameter [m], L is the FCD pathway length [m], and O is orientation [dimensionless] which is assigned a value of 1 for horizontal or 2 for vertical. This model is a construct based on the literature survey of critical predictors in FCD pressure drop. Density, for example, is a predictor that is featured in the pressure drop equation for a restriction-style FCD and allows for the model to capture the effects of inertial forces within the flow path. Viscosity, conversely, is a predictor known to greatly affect frictional-style FCDs and captures viscous effects in the fluid flow regime. Temperature directly effects the viscosity of the

liquid phase and reflects the enthalpy and saturation of the fluid, indicating how likely a steam flash event for the liquid phase. Similarly, the remaining predictors were selected because of an expectation that they may be significant in shaping the pressure drop relationship across the autonomous hybrid FCD. As this model contains variables of different orders (e.g., velocity and velocity squared) and high correlated variables (e.g., density and temperature), it is highly unlikely that this full variable set will meet the requirements for a valid linear model. The Box-Cox procedure will be used to transform the response variable, ΔP_{FCD}, and/or the predictor variables to overcome problems due to non-linearity. Box and Cox (1964) provide a general method for transforming a strictly positive response variable. The Box-Cox procedure aims to find a transformation that makes the transformed response variable close to normally distributed having taken into account the regression model under consideration.

To avoid overfitting the closed-loop flow test data, the full model will see insignificant and redundant variables removed to construct a useful prediction model containing only a subset of predictors. In general, the more predictor variables used in a valid model the lower the bias of the prediction, but the higher the variance. Including too many predictors in a regression model is commonly called over-fitting while the opposite is called under-fitting (Sheather 2008). Four criteria will be used to evaluate every possible combination of the predictor variables present in the full model: R^2-adjusted, Akaike's Information Criteria (AIC), Corrected AIC (AIC_c), and Baynesian Information Criteria (BIC). The R^2-adjusted criteria takes the well-known coefficient of determination (R^2) and modifies it by weighing it according to the number of predictors in the considered model.

The usual practice is to choose the subset of predictors with the highest value of R^2-adjusted (Stapleton 2009). AIC functions by balancing the goodness of fit of a reduced model against a penalty for model complexity. As such, the smaller the value of AIC, the better the model (Gelman and Hill 2007; Sheather 2008; Stapleton 2009). AIC_c is a bias-corrected version of AIC for use when the sample size is small or when the number of parameters estimated is a moderate to large fraction of the sample size. As sample size gets large, AIC_c converges to AIC (Gelman and Hill 2007; Sheather 2008). BIC is defined such that the smaller the value of BIC the better the model. BIC is similar to AIC except that the penalty term is replaced by the logarithm of sample size, thus the penalty in BIC is greater than the penalty in AIC for larger sample sizes (Gelman and Hill 2007; Sheather 2008; Stapleton 2009).

All possible subsets of predictor variables, and thus all possible simplified regression equations, are considered to establish which predictor variables are effective in determining pressure loss across a given FCD geometry. **Figure 17** from Sheather (2008) provides a flowchart of the model reduction decision process.

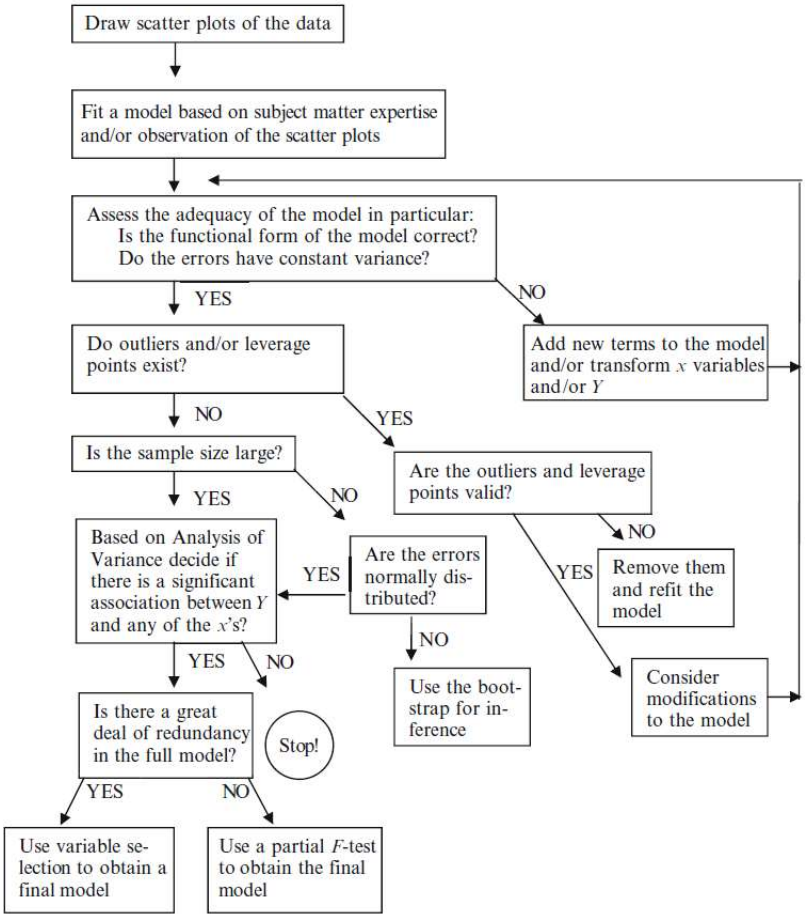

Figure 17: Flowchart of Steps Involved in a Multiple Linear Regression Analysis Reprinted with permission from *A Modern Approach to Regression with R* by Simon J. Sheather, 2008, Springer Texts in Statistics. New York, New York. © 2008 by Simon Sheather.

3.3 Numerical Modeling

Given the economic risk involved in deviating from proven completion design, as well as the long delay due to extended circulation/start-up periods in collecting meaningful field data, analysis of FCD performance through trial-and-error field installations is not a realistic outcome. Instead, numerical modeling within reservoir simulation software

becomes necessary to establish performance trends for new completion design. As such, FCD usage in numerous Albertan SAGD fields are considered within Petroleum Experts® software to quantify the benefit of FCD usage in the injector and/or producer of a SAGD pair. Petroleum Experts® software was chosen due to the familiarity of the software to the author, because it is an effective and proven commercial reservoir simulator that considers mass, momentum, and energy-balance equations in its predictions over time, and because the software handles the near-well bore dynamics of FCD performance extremely well and has been used for conventional FCD well design worldwide.

Reservoir heterogeneity is introduced by including randomly distributed, discontinuous shale lenses. The shale is characterized by low vertical permeability, typically in the range of 10^{-6} to 10^{-3} mD. For laterally oriented thin shale lenses, it is assumed that the occurrence of shale in sand reduces the vertical permeability of the sand block dramatically but has no effect on horizontal permeability. Therefore, a reduction factor of 10^{-5} is applied to the vertical permeability of the shaly-sand blocks in this study. Most reservoir properties, including horizontal permeability, vertical permeability, initial temperature, initial oil/water saturation, initial reservoir pressure, and porosity were initialized based on published data for the respective field and thus vary from model to model. For all simulations, the Stone II model is used to calculate relative permeability for three phase-flow (Stone 1973). Following the work of Sasaki et al. (2001), a temperature/viscosity dependency is approximated by the fit:

$$\mu_b = 205633\, T_o^{-3.512} \quad \ldots \quad \textbf{(Eq. 36)}$$

Where μ_b is bitumen viscosity [cP] and T_o is the oil temperature [°C]. This relationship between oil temperature and viscosity is presented visually in **Figure 18**.

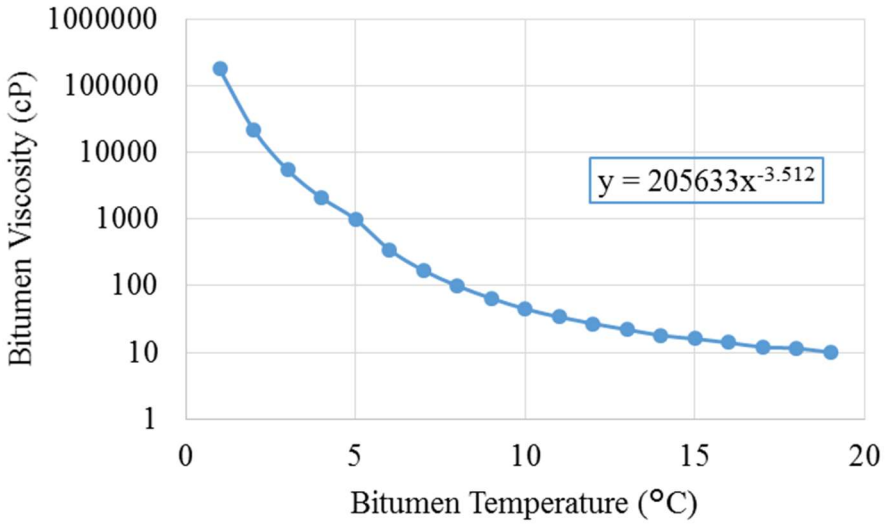

Figure 18: Bitumen Viscosity at Different Temperatures

The circulation phase was handled consistently for each run. Steam was circulated down the injection well and returns from the injection well were limited to 60 m^3/day. Simultaneously, 60 m^3/day of steam were also circulated down the production well, though return volumes were allowed to increase over time. This was continued until thermal and hydraulic communication between the two wells was established. During true SAGD, steam injection was based on 100% quality at the heel of the well. The model assumes 2,700 kPa of steam being available at surface to deliver to all strings in the injector well. An additional drawdown constraint of 500 psi (3447 kPa) was added to both

injector and producer. Reservoir parameters for a typical Surmont reservoir well pair, Christina Lake reservoir well pair, and McKay River well pair are presented in **Table 4** (Baker et al. 2010).

Table 4: Summary of Reservoir Properties Used in Simulation Models

Variable	***Surmont***	***Christina Lake***	***McKay River***
Porosity (ϕ), fraction	0.35	0.34	0.31
Horizontal Permeability (k_h), D	4-11	4-10	1.7-8.5
Ratio of Vertical to Horizontal Permeability (k_v/k_h), dimensionless	0.8-1	0.875-1	0.13-1
Initial Water Saturation (S_{wi}), fraction	8-40%	15-31%	16-25%
Initial Reservoir Temperature, °C	11	10	7
Initial Reservoir Pressure, kPa	2800	2500	400
Reservoir Depth, m	420	350	145
Injected Steam Temperature, °C	240	220	200

Three alternate cases were considered with each simulation model. The first serves as a control and as a baseline and models the performance of a typical SAGD well pair with dual points of steam delivery in the injector. This simulation model was run for a 4-year timespan and was operated with an optimal subcool of 20° C. Case two considers FCDs installed in the injector and producer from the point of well installation and also

was operated for a 4-year timespan and 20° C subcool. Case three modifies case two by operating more aggressively with the subcool reduced to 5° C.

3.4 Economic Evaluation

To optimize and compare SAGD performance, the net present value (NPV) over a period of four years was chosen as the economic performance indicator. The simulation results of daily oil production and steam injection are the base to calculate daily income. The cost of steam was estimated at $8/bbl of cold water equivalent. The price of produced oil was projected at $50/bbl, which corresponds to a WTI price of approximately $60/bbl (Yang et al. 2009). The interest rate (or discount rate) of 10% per annum was used to discount future cash flow to their present values. Taxation rates of 25% were assumed.

4. RESULTS

4.1 Statistical Analysis

As almost all published multiphase FCD testing has relied on nitrogen as a representative gas phase, an early concern was whether this test gas was suitable as a stand-in for steam to predict pressure drop across as FCD geometry. Unlike steam, nitrogen gas is not saturation temperature and will not fluctuate between a liquid and vapor phase. As a gas, its density is far less sensitive to temperature than steam, as is its measured viscosity. However, significant financial investment has been made in these testing protocols, so if existing performance descriptions were valid for steam it would simplify the simulation of FCD devices in SAGD wells and speed their adoption.

Using a pressure drop equation for the autonomous hybrid FCD published by Baker Hughes, the empirically measured FCD pressure drop for single-phase and multiphase fluids was compared against the predicted value from the Baker Hughes correlation. Consistently, the Baker Hughes model was found to under-predict the real pressure drop across the autonomous hybrid FCD for multiphase mixtures without steam (**Figure 19**). If steam was present in the fluid mixture, the Baker Hughes model proved adequate at low pressure drops but increasingly inaccurate with larger flow rates/target pressure drops, though the trend of this error is not as clear cut as with mixtures that do not contain steam.

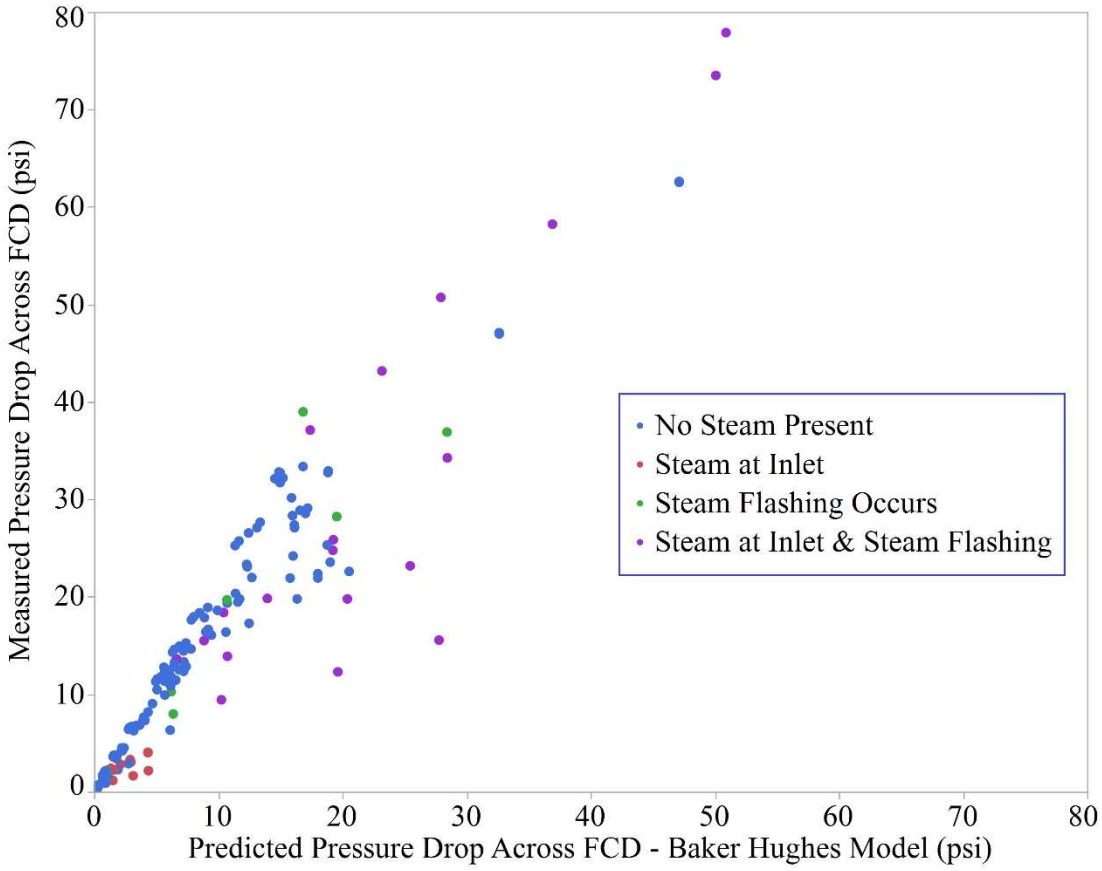

Figure 19: Comparison of Baker Hughes Pressure Drop Model to Empirical Data

With significant error in existing literature pressure drop models, it becomes an absolute necessity to create an accurate pressure drop relationship for the autonomous hybrid FCD to incorporate in a reservoir simulator. Based on theory and intuition, it is expected that pressure drop across any FCD geometry will be a dependent on properties of the fluid passing across it. Critical properties from the orifice pressure drop (**Equation 19**) and from previous characterizations of the autonomous hybrid FCD geometry (**Equation 32**, **Equation 33**) suggest that a place to start regression analysis and build a predictive function of pressure drop is with fluid properties such as fluid viscosity, fluid

density, fluid velocity (or fluid velocity squared) within the FCD, and the enthalpy of the vapor and liquid phase of the fluid upstream and downstream of the introduced pressure drop. The first three fluid properties (viscosity, density, velocity) feature prominently in the orifice pressure drop equation, the frictional channel pressure drop equation, and along with hydraulic diameter form the dimensionless Reynolds number that is the basis of the Garcia characterization of the autonomous hybrid FCD curve.

Certain assumptions were made in building the regression formula. The first assumption is that liquid and vapor phase experience sufficient turbulence entering the FCD that they may be considered a homogenous mixture. The second assumption, based on the homogeneity assumption, is that there is no phase slippage within the FCD. With these assumptions, fluid density is now a function of liquid density, vapor density, and mass fraction of liquid and gaseous components. Mixture viscosity likewise is a function of liquid and vapor density and their relative mass fractions. As only one FCD geometry is considered, hydraulic diameter is a constant; fluid velocity is used in place of volumetric flow rate. In order to consider phase change within the device, inlet fluid temperature is considered. The initial "full" linear model constructed to predict pressure drop across the FCD thus has the form of **Equation 37**.

$$\Delta p_{FCD} = \beta_0 + \beta_1 v + \beta_2 v^2 + \beta_3 \rho + \beta_4 \mu + \beta_5 T + \beta_6 X + \beta_7 D_H + \beta_8 L_{FCD} + \beta_9 O + e \quad \textbf{... (Eq. 37)}$$

Here, β_i (for i=0 to 9) are dimensionless regression coefficients, v is velocity [m/s], v^2 is velocity squared [m^2/s^2], ρ is fluid density [kg/m^3], μ is fluid viscosity [cP], T is temperature [°C], X is the liquid fraction [dimensionless], D_H is the hydraulic diameter

[m], L_{FCD} is the FCD pathway length [m], and O is orientation [dimensionless] which is assigned a value of 1 for horizontal or 2 for vertical.

Using the open source R statistical software, the full linear model of **Equation 37** was fit to the experimental data collected in the closed-loop flow test. Fitted values from this predictive model was then plotted against the experimental data (**Figure 18**) illustrating a strong fit to the analytical data. However, a strong linear fit alone does not validate the model being considered, as it must hold to the required underlying assumptions of normalcy, constant variance, etc. required for a linear model fit. **Figure 19** provides a visual depiction of common diagnostic plots. If the regression formula met the requirements of constant variance, then **Figure 20** would have a seemingly random distribution of error terms, each with a similar magnitude of deviance from the fitted values and without any discernable trend in distribution. However, residual error clearly trends upwards with increasing fitted values (**Figure 20, upper left**). To determine if a higher order variable term might correct this trend in residuals, a plot of standardized residuals versus fitted values (**Figure 20, lower left**) was also generated but resulted in the same conclusion. Graphical descriptions of residual normalcy (**Figure 20, upper right**) do not suggest regression error due to an overly small data set, as normalcy can be observed. Finally, errors in residual variance due to outliers can be ignored as no point demonstrates significant leverage over the final linear regression fit (**Figure 20, lower right**). It becomes apparent that the full model does not meet the requirements of constant variance, and so transformation of the predictor variables and/or the response variable is necessary in order to apply most linear regression techniques.

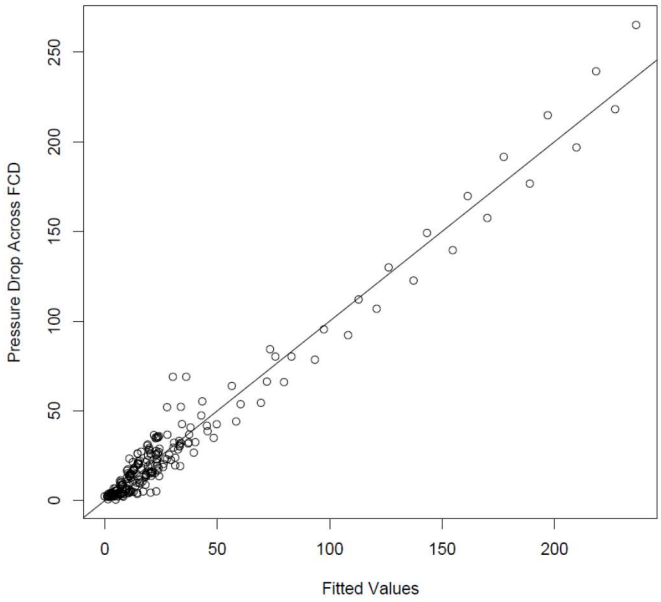

Figure 20: Fitted Values from the Predictive Model vs. Actual FCD Pressure Drop

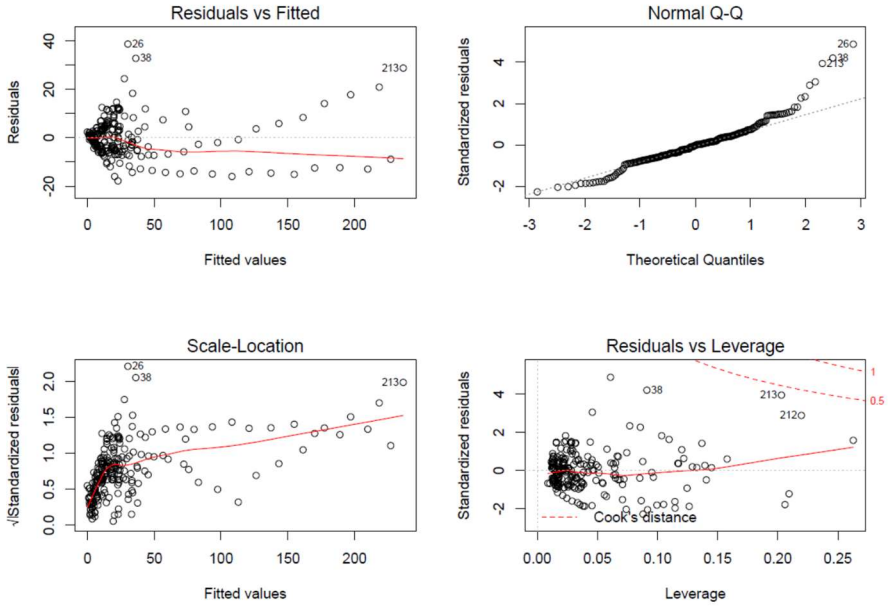

Figure 21: Diagnostic Plots of the Full Regression Model

To determine what transformation would be appropriate, a Box-Cox analysis was run on the data set. The statisticians George Box and David Cox developed a procedure to identify an appropriate exponent (Lambda = l) to use to transform data into a "normal shape." The Lambda value indicates the power to which all data should be raised. In order to do this, the Box-Cox power transformation searches from $\lambda = -5$ to $\lambda = +5$ until the best value is found. The Box-Cox power transformation is not a guarantee for normality. This is because it actually does not really check for normality; the method checks for the smallest standard deviation. The assumption is that among all transformations with Lambda values between -5 and +5, transformed data has the highest likelihood – but not a guarantee – to be normally distributed when standard deviation is the smallest. Therefore, it is absolutely necessary to always check the transformed data for normality using a probability plot. Using this statistical method with the gathered research data, the maximum log-likelihood occurs at a lambda value of roughly 0.45, suggesting either a logarithmic transformation or a square-root transformation of the predictor variable values. Based on the Box-Cox output, a logarithmic transformation of both predictor and response variables should be effective in normalizing the variance in error terms and provide a legitimate and statistically significant linear model.

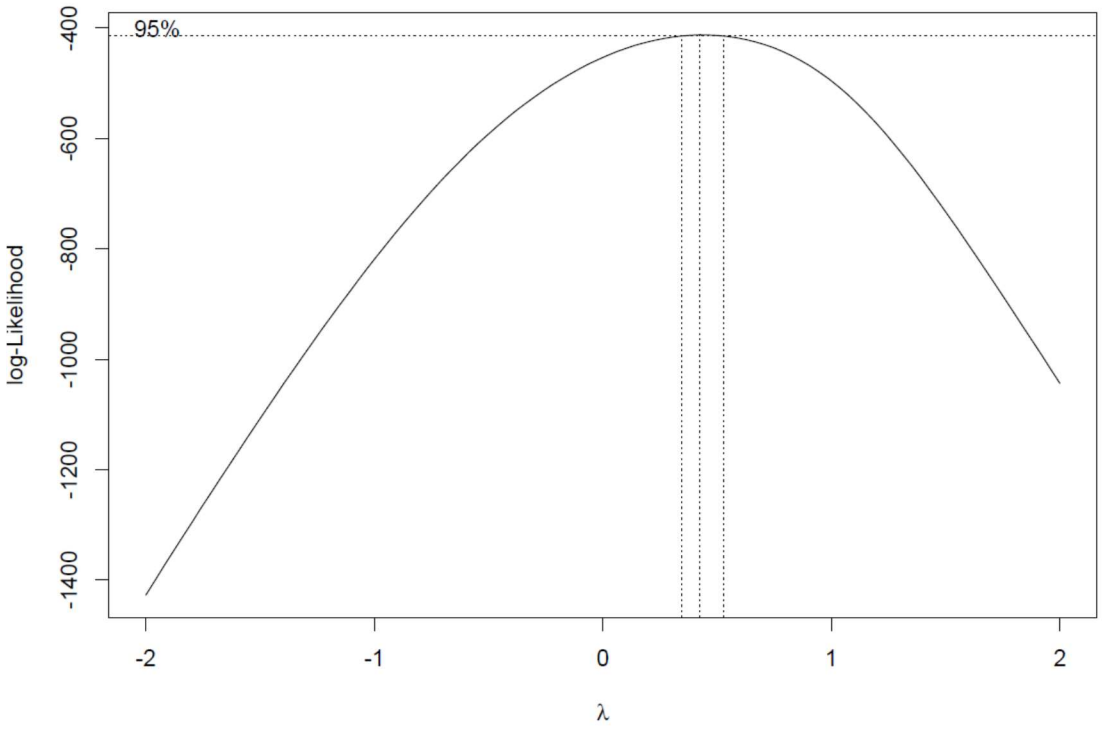

Figure 22: Box-Cox Graphical Analysis of the Full Regression Model

The transformed model now has the form of **Equation 38**:

$$\ln(\Delta p_{FCD}) = \beta_1^* ln(v) + \beta_2^* ln(v^2) + \beta_3^* ln(\rho) + \beta_4^* ln(\mu) + \beta_5^* ln(T) + \beta_6^* ln(X) + \beta_0^* \quad \textbf{... (Eq. 38)}$$

However, significant redundancy does exist in the model, an obvious conclusion in a model that considers both velocity and velocity squared concurrently. Thus it becomes necessary to consider what subsets of predictor variables accurately predict pressure drop across the FCD without overfitting the model.

Using R software packages, all possible combinations of predictor variables were combined and fit against the experimental data to see what combination generates the most favorable adjusted R-squared value. **Figure 21** graphically lays out these results, showing

that no additional improvement in model fit occurs for subsets larger than four predictor variables, suggesting the best reduced model will only consider three or four predictors.

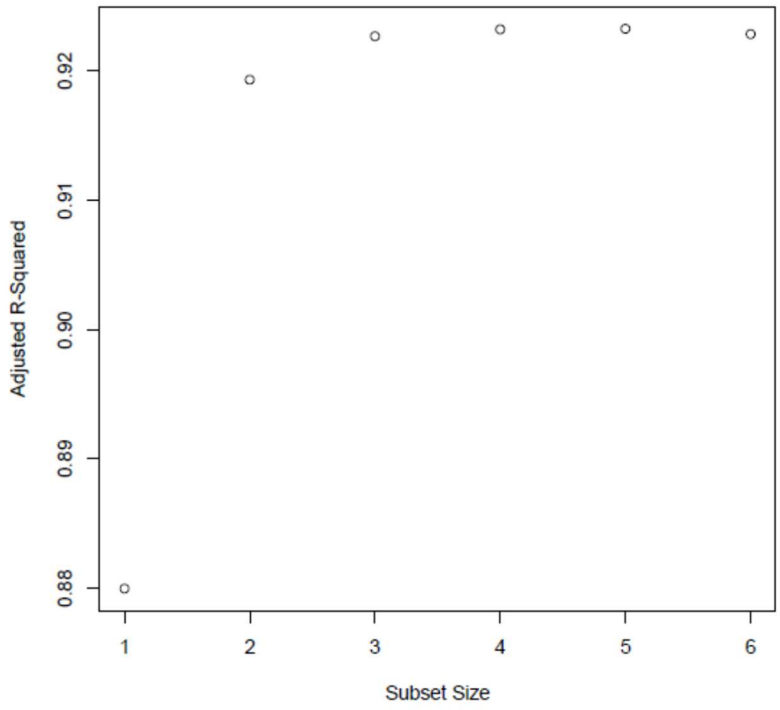

Figure 23: Adjusted R-square values for all possible subsets

Figure 22 plots the specific combination of predictor variables which optimizes the adjusted R-squared value. Here, a model that considers a combination of log(viscosity), log(velocity squared), and log(liquid mass fraction) or a model that combines log(Temperature), log(velocity), log(density), and log(liquid mass fraction) is suggested to be ideal.

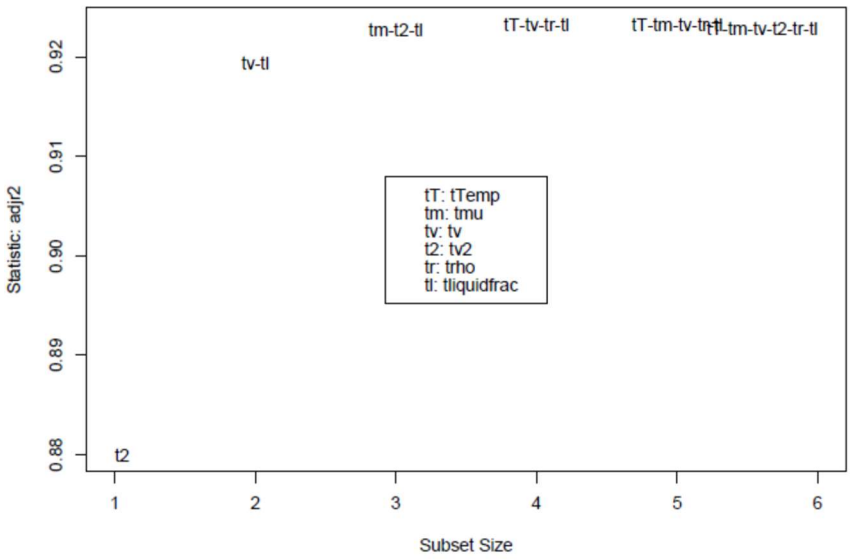

Figure 24: Ideal combination of predictor variables for each subset size

To pick between these two potential models, Baynesian Information Criteria (BIC), Akaike's Information Criteria (AIC), and and Akaike's Information Criteria – Corrected (AICc) were applied to each model. **Table 5** provides the results of these differing information criteria tests with the "best" value shown in bold. From this work, it is strongly suggested that a three predictor model is an excellent fit to experimental data.

Table 5: Information Criteria Testing of the Considered Subset Models

Subset Size	*Predictors*	*R^2 adj.*	*AIC*	*AICc*	*BIC*
3	log(Viscosity), log(Velocity Squared), log(Liquid Mass Fraction)	**0.9277**	-415.666	-415.343	**-402.636**
4	log(Temperature), log(Velocity), log(Density), Log(Liquid Mass Fraction)	0.9232	**-416.013**	**-415.558**	-399.725
5	log(Temperature), log(Viscosity), log(Velocity), log(Density), log(Liquid Mass Fraction)	0.9253	-415.159	-414.55	-395.614
6	log(Temperature), log(Viscosity), log(Viscosity Squared), log(Density), log(Liquid Mass Fraction)	0.9253	-413.159	-412.372	-390.356

However, the three predictors selected (viscosity, liquid mass fraction, and velocity squared) as being meaningful does generate some doubt in the model. Intuitively, density should be a likely component in any final model; as the liquid mass fraction does strongly influence the mixture density and mixture viscosity (by weighing the relative contribution of the much denser/viscous liquid phase), it is possible that the liquid mass fraction behaves as a variable substitution for the mixture density. A new analysis was considered against a model that did not consider liquid mass fraction at all. Again, a subset of three or four predictor variables was found to be optimum, but now use of information criteria suggests a reduced model that considers only viscosity, density, and velocity, which is more in line with previous analytical performance descriptions for FCDs. **Table 6** summarizes the results of the BIC, AIC, and AICc analysis on this new reduced model.

Table 6: Revised Information Criteria Testing of Considered Subset Models

Subset Size	*Predictors*	*R^2 adj.*	*AIC*	*AICc*	*BIC*
2	log(Density), log(Velocity)	0.915	-398.557	-398.343	-388.784
3	log(Density, log(Velocity), log(Viscosity)	0.9196	**-408.101**	**-407.779**	**-395.071**
4	log(Temperature), log(Density), log(Velocity), log(Viscosity)	**0.9199**	-408.042	-407.588	-391.754

Thus, the final optimized performance model has the form of **Equation 39**.

$$\ln(\Delta p_{FCD}) = \beta_1^* ln(v) + \beta_2^* ln(\rho) + \beta_3^* ln(\mu) + \beta_0^* \quad \textbf{...} \quad \textbf{(Eq. 39)}$$

Reversing the logarithmic transformation, and breaking mixture density and viscosity into individual liquid and vapor components, the final performance model has the form of **Equation 40**. In this equation, v is fluid mixture velocity [m/s], ρ is the density of the indicated gas or liquid phase [kg/m^3], μ is the viscosity of the indicated gas or liquid phase [cP], X is the liquid quality [fraction], and T is the mixture temperature [°C]. Standard error for each variable term, as well as t-test results to establish predictor significance, is provided in **Table 7**. This prediction model was compared against the empirical FCD data, and though it demonstrates a reasonable good fit to the laboratory data (R-squared=0.84), the presence of steam flashing in an experimental trial consistently shows a higher deviation from predicted values (**Figure 25**).

$$\Delta p_{FCD} = 6.77\nu + 0.0092\rho_{liquid} + 0.105\rho_{gas} - 0.0223\mu_{liquid} + 509.54\mu_{gas} + 509.53X + 7.43 * 10^{-5}T \quad \textbf{... (Eq. 40)}$$

Table 7: Regression Coefficient Values and t-test Significance for FCD Performance (Model 1/Eq. 40)

Term	Estimate	Std. Error	t Ratio	Prob > |t|
Intercept	-525.685	43.97187	-11.96	<.0001
Temperature	7.43E-05	0.013588	0.01	0.9956
Velocity	6.770588	0.23771	28.48	<.0001
Liquid Density	0.009161	0.014764	0.62	0.5357
Gas Density	0.104757	0.094727	1.11	0.2702
Gas Viscosity	130.7607	138.9323	0.94	0.3478
Liquid Cut	509.5434	42.69058	11.94	<.0001
Liquid Viscosity	-0.02233	0.044328	-0.5	0.615

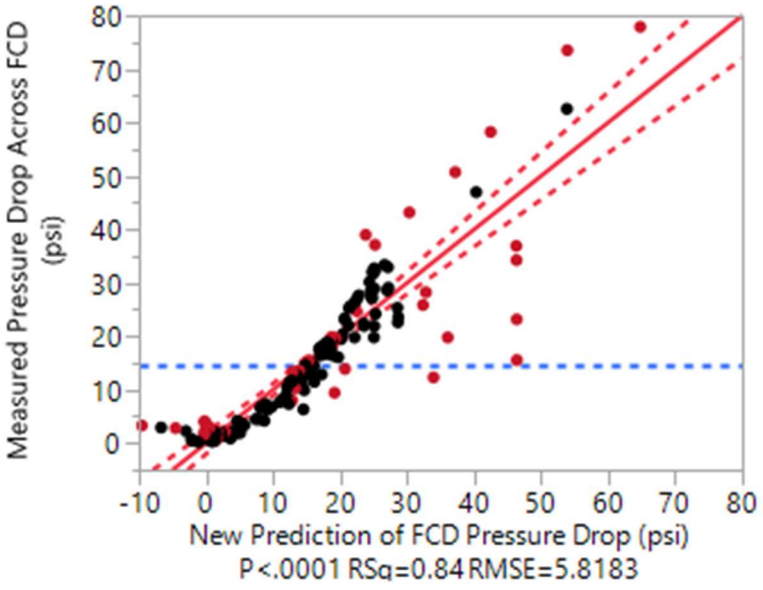

Figure 25: Comparison of Predicted FCD Pressure Drop (Eq. 40) versus Measured Pressure Drop. Red dots indicate a trial with steam flashing within the FCD.

A limitation of this linear fit model is that it does not capture the analytical causes of the pressure drop response. If understanding the autonomous hybrid FCD analytically were the end goal of this research, the performance description would likely have a non-linear regression expression closer to what has been presented in the past, such as **Equation 32** and **Equation 33**. However, an analytical description is not the goal of this research; instead, the goal is a statistically-significant and accurate prediction model of pressure drop. By simplifying the prediction model to a linear form, not only is it easier to validate the model and incorporate it into a reservoir simulator but some insight is gained into what predictors are most influential to FCD performance. These insights are useful not for understanding how this particular FCD geometry functions but in looking to a SAGD-specific FCD geometry for future study, one that can be designed to be sensitive to those predictors with the greatest distinction between steam and non-steam flow. To determine if the linear regression fit might be improved, the predictive model was split into two components: cases with no expectation of steam flashing and cases where steam flashing was expected. Fitting a linear regression to only data where no steam flash occurred, **Equation 41** was generated. This linear description demonstrates a strong goodness-of-fit to experimental data with an R-squared value of 0.94 (**Figure 26**) and keeps all predictors statistically significant with large absolute values to their respective t-test ratio (**Table 8**).

$$\Delta p_{FCD} = 7.38\nu - 0.0045\rho_{liquid} + 0.127\rho_{gas} - 0.0274\mu_{liquid} - 12571\mu_{gas} - 293.78 + 0.49T \quad \textbf{... (Eq. 41)}$$

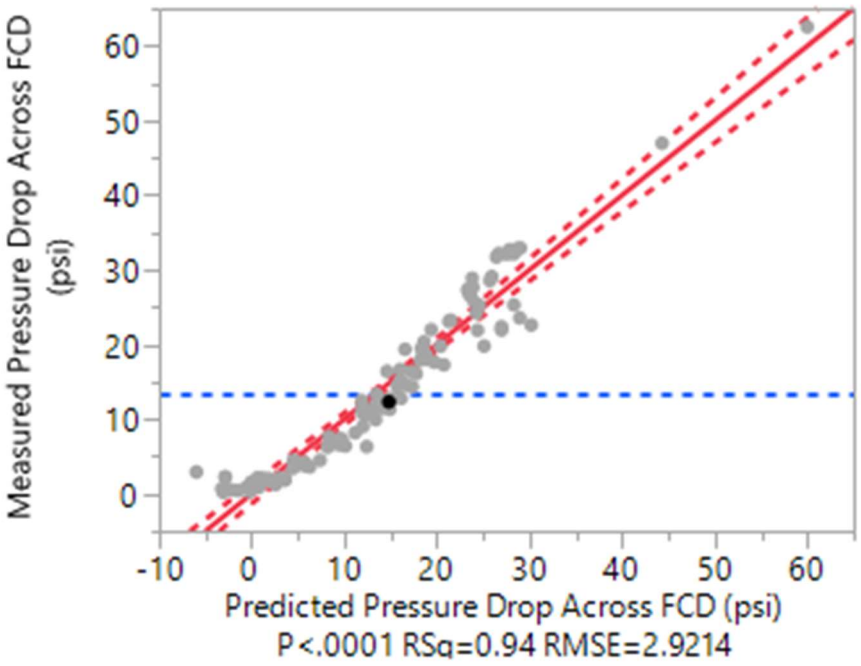

Figure 26: Comparison of Predicted FCD Pressure Drop (Model 2/Eq. 41) to Measured Pressure Drop for Non-Steam Flash Cases

Table 8: Regression Coefficient Values and t-test Significance for FCD Performance (Model 2/Eq. 41)

Term	Estimate	Std. Error	t Ratio	Prob > |t|
Intercept	**-293.778**	**55.54641**	**-5.29**	**<.0001**
Velocity	**7.38358**	**0.171434**	**43.07**	**<.0001**
Temperature	**0.493853**	**0.113211**	**4.36**	**<.0001**
Liquid Density	-0.00452	0.008881	-0.51	0.6113
Gas Density	0.127186	0.066928	1.9	0.0596
Gas Viscosity	**-12571.3**	**2845.708**	**-4.42**	**<.0001**
Liquid Cut	**506.5231**	**29.98839**	**16.89**	**<.0001**
Liquid Viscosity	-0.02748	0.02357	-1.17	0.2457

Finally, instances where steam flashing is likely to occur were considered. For this data set, a corrective step was taken: rather than considering fluid properties at inlet conditions, the velocity and liquid quality considered were established at the FCD outlet. Using this correction, a linear pressure drop correlation could be developed for steam flash cases (**Equation 42**). Contrasted against measured data, this new model for steam flash cases demonstrated a high R-squared value of 0.96 (**Figure 27**).

$$\Delta p_{FCD} = \nu - 0.154\rho_{liquid} - 1.59\rho_{gas} - 7.74\mu_{liquid} + 1867.22\mu_{gas} - 296 + 0.78T \quad \text{... (42)}$$

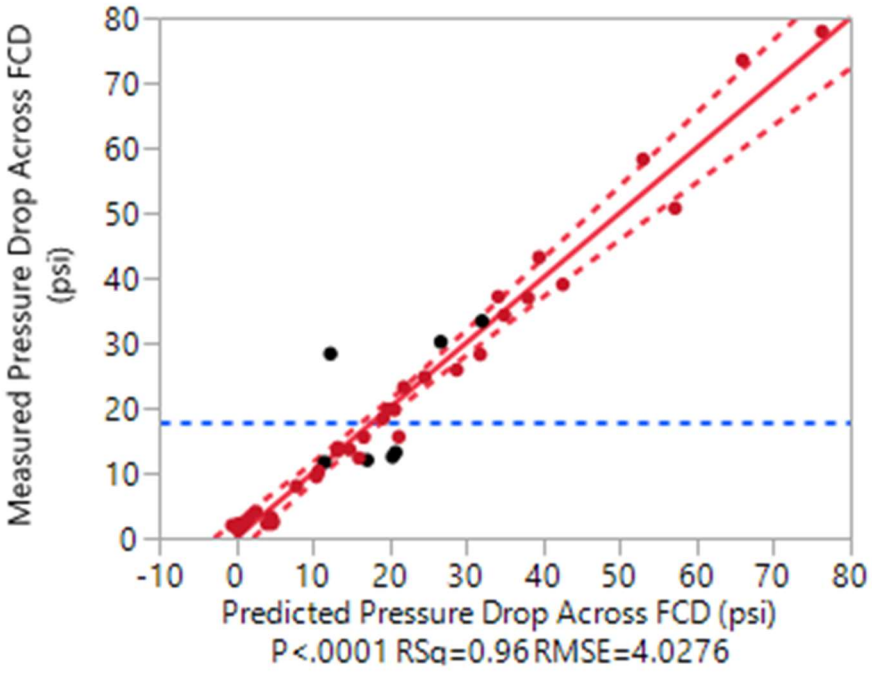

Figure 27: Comparison of Predicted FCD Pressure Drop (Model 3/Eq. 42) to Measured Pressure Drop for Steam Flash Cases

To effectively incorporate the linear model for non-steam flash cases (**Equation 41/Model 2**) and steam flash cases (**Equation 42/Model 3**) into a reservoir simulator, it became necessary to develop a recursive script to compute the fluid qualities at the FCD at each time step. This script calculated the pressure drop across the FCD at each time step according to **Equation 41**. Using this new downstream pressure, the mass fraction of the fluid that might flash to steam is calculated using the previously referenced **Equation 34** and look-up tables of steam properties. If no or minimal fractions change phase within the FCD, the script is complete. However, if more than 0.1% of the fluid stream within the FCD is expected to flash to a vapor state, the average mixture velocity is revised to consider the volumetric change due to the creation of steam and the liquid cut is revised downwards to reflect outlet conditions. The script is then re-run with these new values until no change in the gas fraction occurs within the FCD.

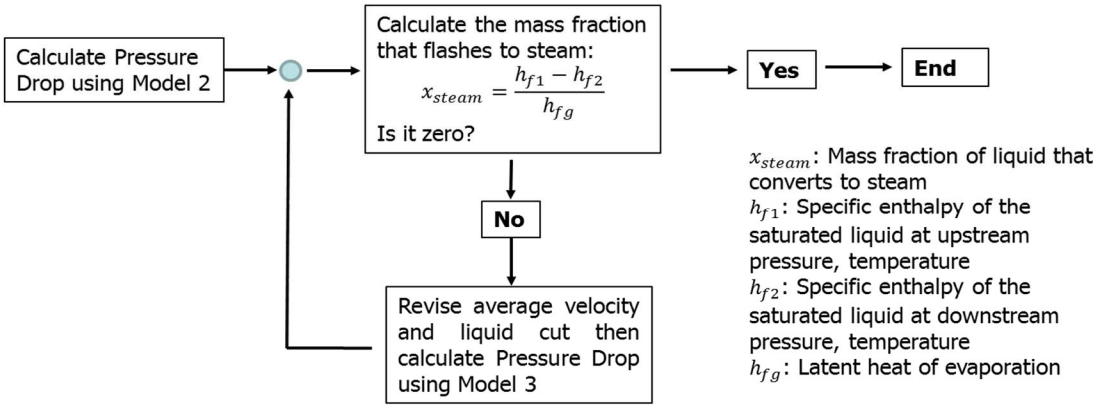

Figure 28: Flowchart Illustrating the Calculation of FCD Pressure Drop with the Reservoir Simulator

4.2 Numerical Simulation

With assurance that the generated FCD performance models now accurate represent the pressure drop experience by multiphase flow in SAGD conditions, the previously described correlations models (Model 2 & Model 3) were introduced into the REVEAL™ software platform in order to forecast the effect of FCD introduction into a SAGD injector and production lateral. Multiple simulations were run using representative geological models of different Albertan heavy oil fields in order to contrast a conventional SAGD completion design against the potential benefits of an FCD inclusive design.

Surmont Reservoir: Case 1

For this case, a geological model was built in PETREL using publically available log and core data from a 9 well pad area. This geological model was then imported into Petroleum Expert's REVEAL™ software for all SAGD simulations. Within the model the top five layers are set as an impermeable overburden layer with the remainder of the model containing an original oil-in-place volume of $9.24*10^5$ sm^3 ($5.8*10^6$ bbls). Both producer and injector laterals exhibited a 900-m length in contact and communication with the reservoir. Initially, there was no mobile water saturation. **Figure 29** provides a qualitative illustration of the varying permeability within the geospatial model, with blue representing the lowest permeability (75 mD) and red the highest permeability (11 D). **Figure 30** likewise illustrates varying porosity within the geospatial model.

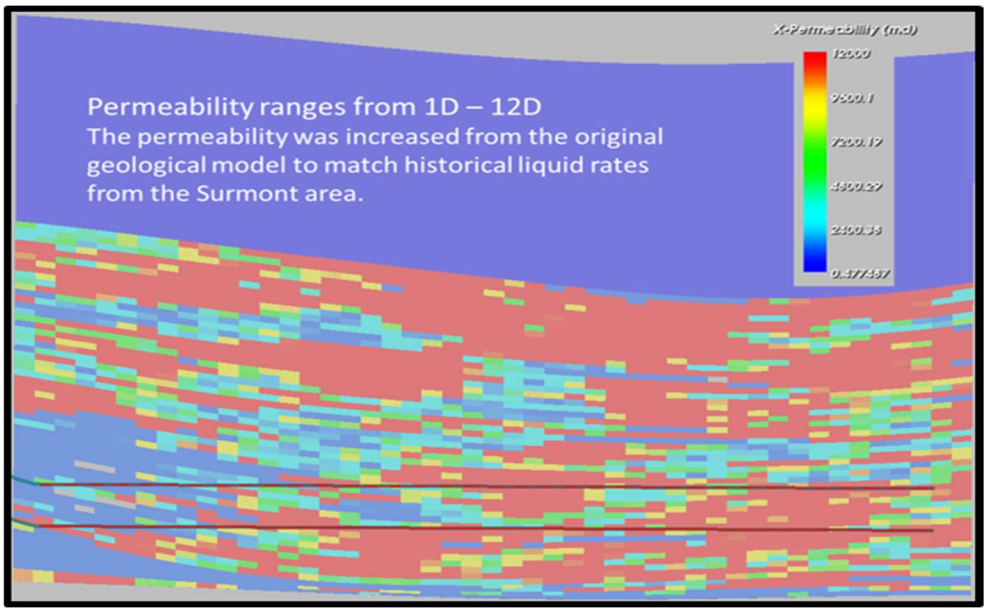

Figure 29: Permeability Variation in the Geospatial Model

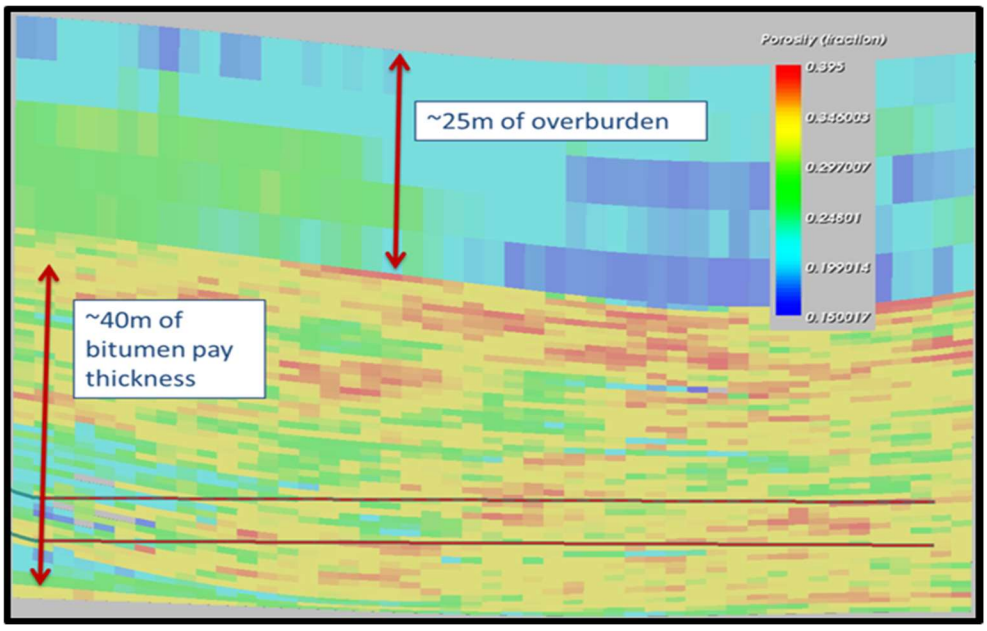

Figure 30: Porosity Variations in the Geospatial Model

Four operational cases were considered within the simulator. The first was a control case where no FCD was used in either the producer or injector lateral to establish how conventional well designs might perform in this geological strata. A 20°C subcool was the operational target for this case. The second case considered 0.4 fluid resistance rating (FRR) FCDs in every other joint of the injector and 1.6 FRR FCDs on every joint of the producer. Again, a 20°C subcool was the operational target for this second case. Simulation case three was identical to case two with one alteration, a significantly more aggressive subcool of 5 °C. Finally, case four considered the effects of retrofitting a well with FCDs; identical to case one initially, FCDs were inserted into the simulation 1 year and 9 months after commencing SAGD operations.

Examining a 4-year period of SAGD operations for cases 1-3, it is observed that the FCDs served to restrict the production of live steam. **Figure 31** plots the oil production rate over time and marks steam breakthrough events that occur in the non-FCD case that were avoided through FCD steam management. **Figure 32** considers the retrofit case and likewise demonstrates steam breakthrough events that are avoided by the introduction of FCDs.

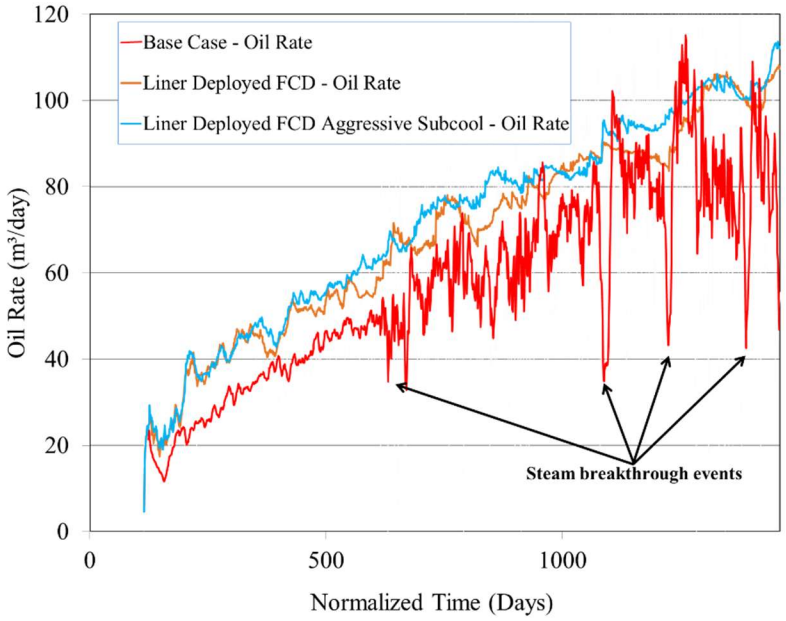

Figure 31: Oil Production for Simulated Case 1-3 vs. Time. Steam breakthrough events in the control case are highlighted and do not occur for the FCD cases.

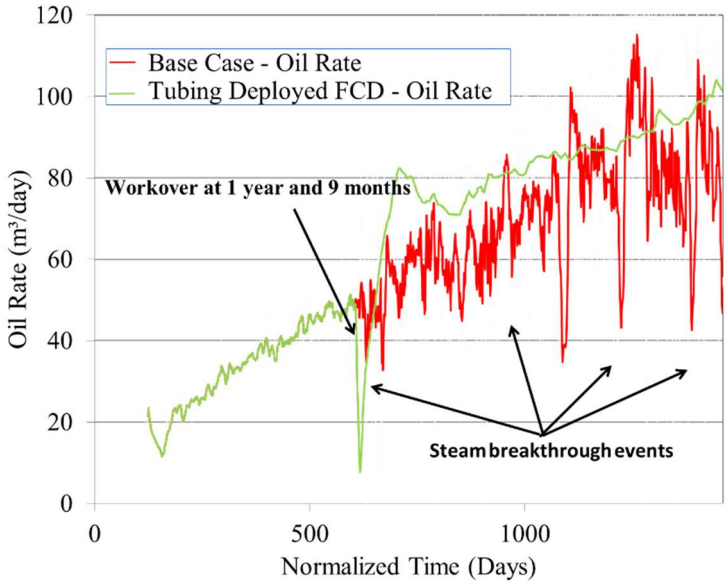

Figure 32: A Comparison of Oil Production over Time for the Base Case (Case 1) Against a Retrofit FCD Installation (Case 4). Steam breakthrough events for the Base Case are highlighted and did not occur for the FCD Retrofit.

Qualitatively, improved conformance can be shown in the FCD cases by examining the two-dimensional heating profiles along the length of the laterals. **Figure 33** provides cross-sectional views of heating profiles at select points near the heel of the wells (the far left of **Figure 33**) to the toe of the well (the far right of **Figure 33**). The profiles in the upper row represent the base case while the lower row represents the FCD usage case. It is apparent that near the middle of the laterals, in a zone that contains very poor quality, low permeability rock, that the heating of the in-situ bitumen is ineffectual in a conventional SAGD case. However, with the use of FCDs, this same position sees significantly better development of the steam chamber and heating more in line with other points along the wellbore. In contrast, zones that grow rapidly in the base case (e.g., zones near the toe of the wellbores, where rock quality is best) do not grow as rapidly in the FCD case and instead are more in line with the rest of the completion system.

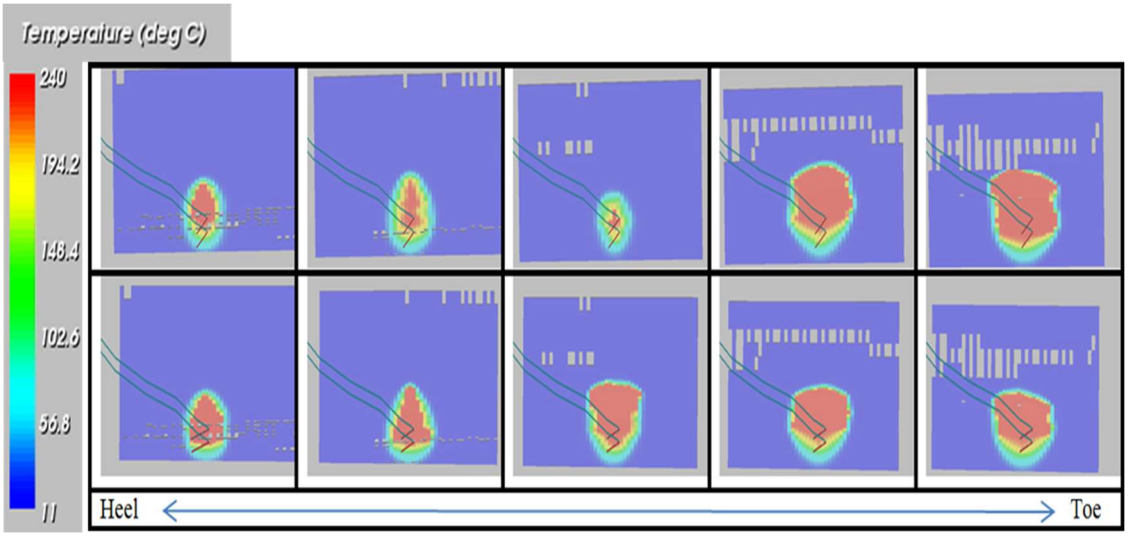

Figure 33: 2D Cross-Sections of Wellbore Heating Along the Lateral Length.
(Top) Cross-sections for a Non-FCD Case
(Bottom) Cross-Sections at Identical Points for an FCD Case.

More quantitatively, **Figure 34** provides a plot of cumulative oil production over time for each of the simulated cases. In all scenarios, the use of FCDs outperforms a conventional SAGD design. In **Figure 35**, cumulative steam-oil ratio is compared over time for each of the four simulated cases. Again, FCDs outperform a conventional SAGD well design by requiring less steam usage for each barrel of oil produced.

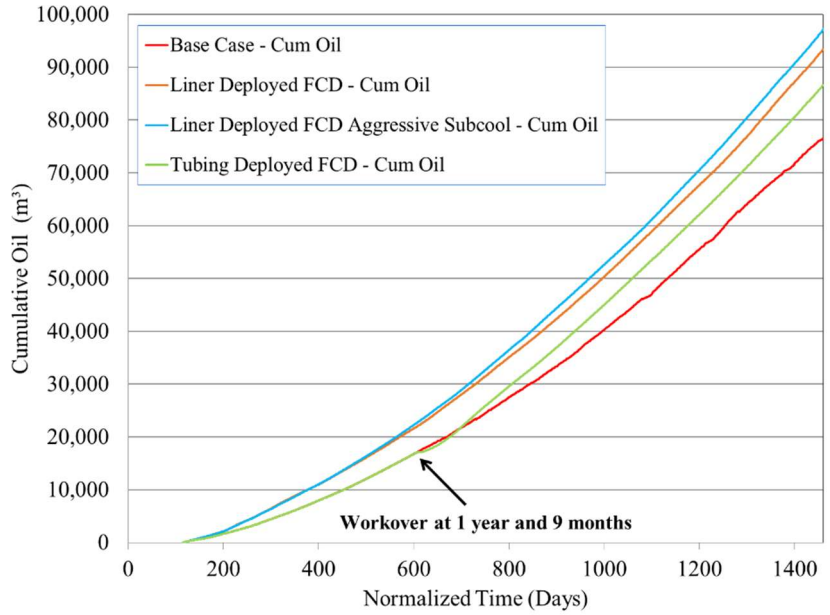

Figure 34: Cumulative Oil Production vs. Time for Each Simulated Case

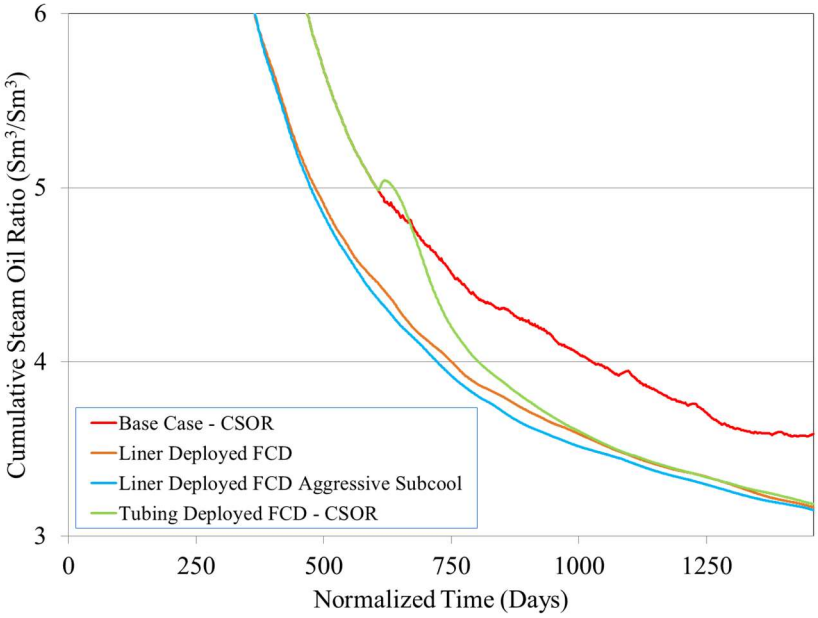

Figure 35: CSOR vs. Time for Each Simulated Case

In quantifying the benefit of FCD use in these simulated cases, calculations were performed to determine the effect of additional bitumen production and lower cSOR upon the Net Present Value (NPV) of the SAGD well pair. Figure 36 contrasts the results of these calculations assuming a one million USD investment in FCDs in both the injector and producer laterals. The result of this economic analysis is that the improvements of thermal efficiency that accompanies FCD usage increases the NPV over a four year period by over two million dollars with no operational changes. By running a more aggressive subcool and taking advantage of the additional conformance that comes with an autonomous FCD, this benefit may be increased by over an additional half million dollars to a total improvement of over three million USD over a conventional SAGD design. By considering also a retrofit case, where FCDs are introduced one year and nine months into SAGD production, it can be seen that improving SAGD conformance later in the life of the well also provides significant value to the investor. Here, correcting thermal inefficiencies results in nearly a 1.25 million dollar improvement in NPV.

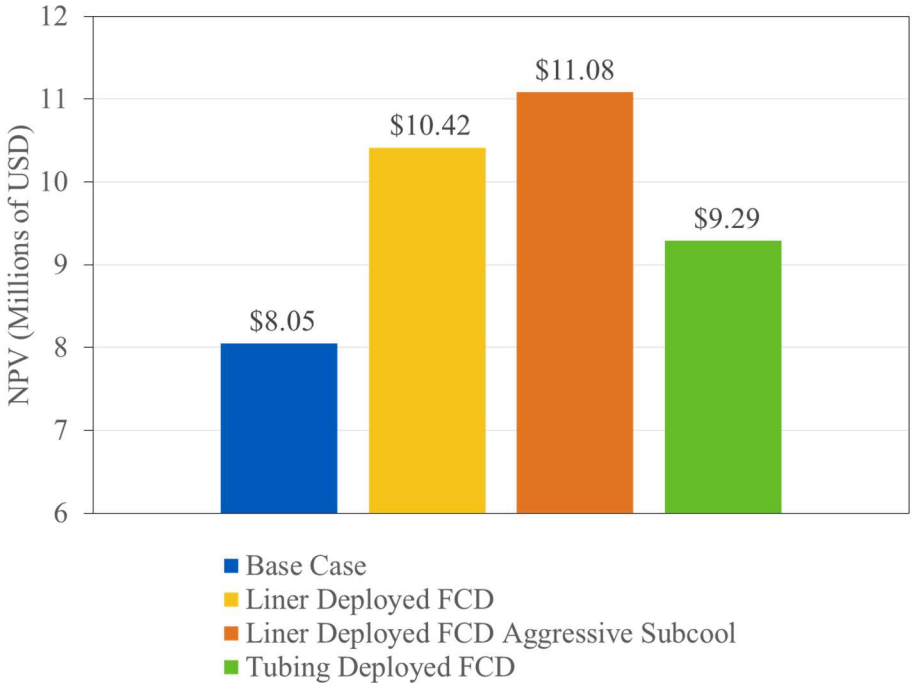

Figure 36: 4-Year NPV Analysis for the Scenarios of Surmont Simulation 1

Surmont Reservoir: Case 2

Unlike the previous simulation, which relied upon a reservoir model taken from available well data, Surmont Case 2 uses a randomly generated geological model based on expected values of permeability, porosity, and shale distribution for the Surmont field. **Figure 36** illustrates the geospatial distribution of horizontal permeability for the created Case 2 reservoir control volume. This model, unlike Surmont Case 1, is of lower quality with permeability largely in the range of 1-2 Darcies. Resulting, the preheat period was extended to 153 days and the rate of steam circulation in the injector and producer well were increased to 167 Sm3/day in order to achieve thermal communication between the

two laterals. **Figure 37** illustrates the corresponding porosity distribution for this geological model. For this simulation, lateral length was increased to 1500 meters from the previous 900 meters of Surmont Case 1.

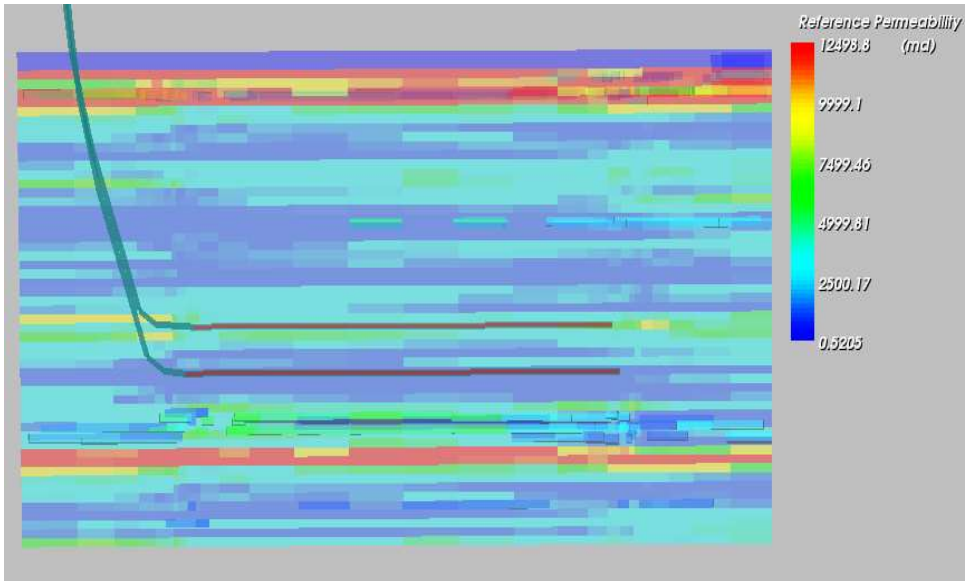

Figure 37: Permeability Variation for Surmont Simulation Case 2

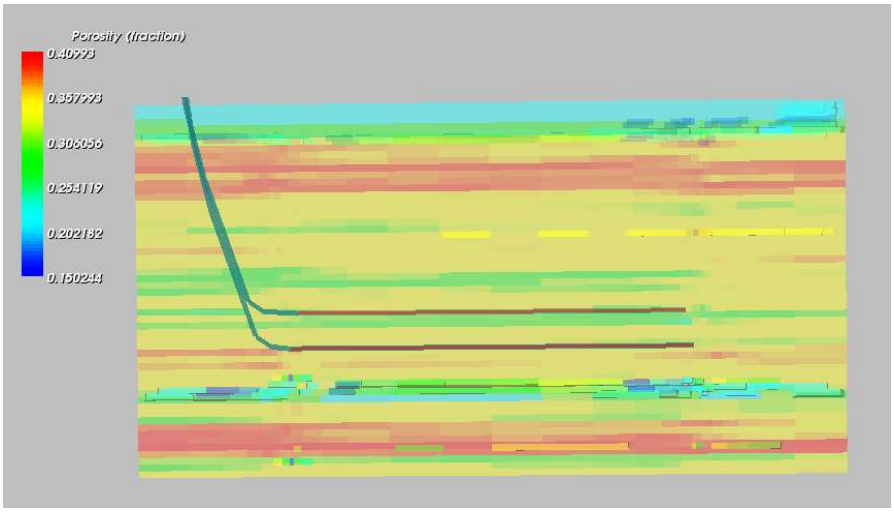

Figure 38: Porosity Variation for Surmont Simulation Case 2

Here three operational cases were considered within the simulator. The first was a control case where no FCD was used in either the producer or injector lateral to establish how conventional well designs might perform in this geological strata. A 20°C subcool was the operational target for this case. The second case considered 0.8 fluid resistance rating (FRR) FCDs in every other joint of the injector and 1.6 FRR FCDs on every joint of the producer. Again, a 20°C subcool was the operational target for this second case. Simulation case three was identical to case two with one alteration, a significantly more aggressive subcool of 5 °C.

Figure 38 plots the cumulative oil production for each simulated case for normalized time. A direct comparison of cumulative oil production at the end of four years is provided in **Figure 39** which illustrates a 109% improvement over the base case in Scenario 1 and a 186% improvement over the base case in scenario 2.

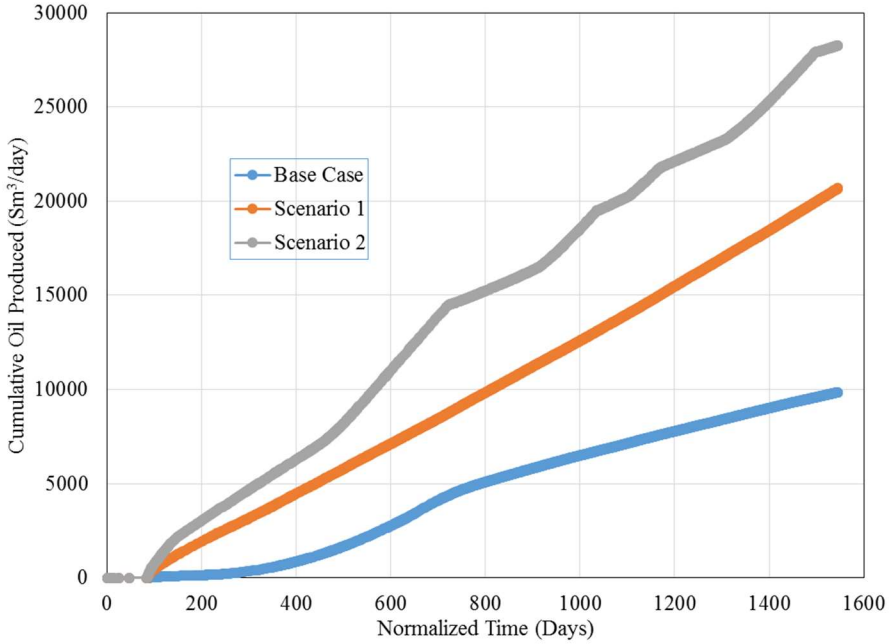

Figure 39: Cumulative Oil Production vs. Time for Each Simulated Scenario (Surmont Simulation 2)

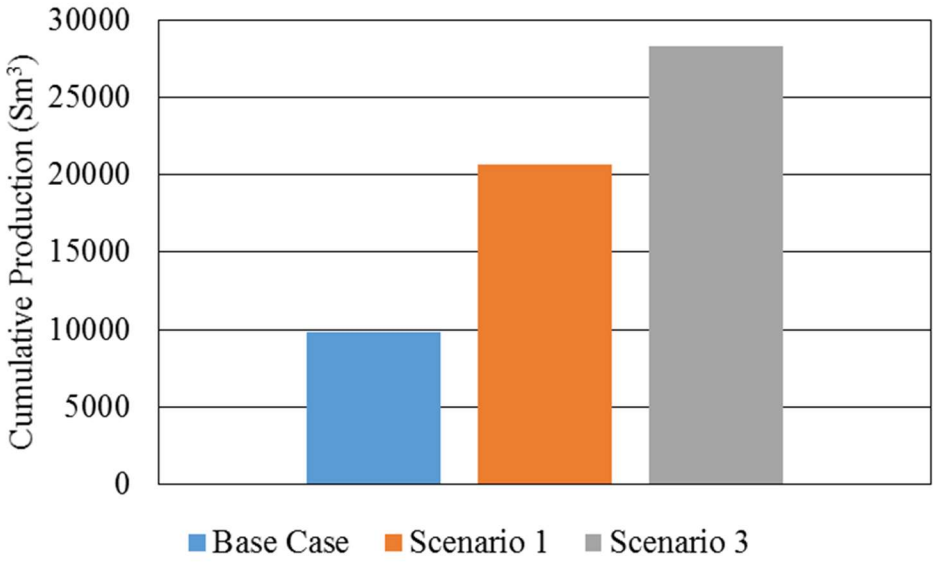

Figure 40: Comparison of Total Cumulative Oil Production for Each Scenario (Surmont Simulation 2)

Comparing cumulative Steam-Oil ratios (cSOR) for each scenario over time shows major improvement for both the FCD cases over the base case simulation, though minimal changes between the two FCD scenarios. These trends can be seen in **Figure 40** which plots cSOR versus time for each simulated scenario.

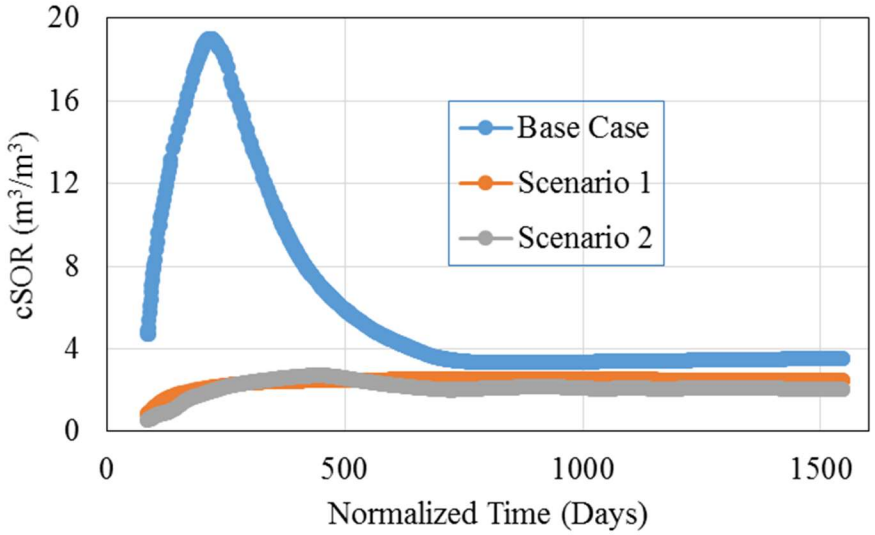

Figure 41: cSOR vs. Time for Each Simulated Scenario

Surmont Reservoir: Case 3

Surmont Case 3 uses a randomly generated geological model based on expected values of permeability, porosity, and shale distribution for the Surmont field. Unlike the previously generated reservoir, this simulation case is notable for minimal presence of shale and a higher average permeability that is more typical of the Surmont field. Where Surmont Case 2 had an average permeability of 2500 mD, Surmont Case 3 uses a

geological model where most of the reservoir varies between 4000 and 11000 mD. **Figure 41** depicts the porosity distribution used in this simulation model while **Figure 42** depicts the geospatial permeability distribution.

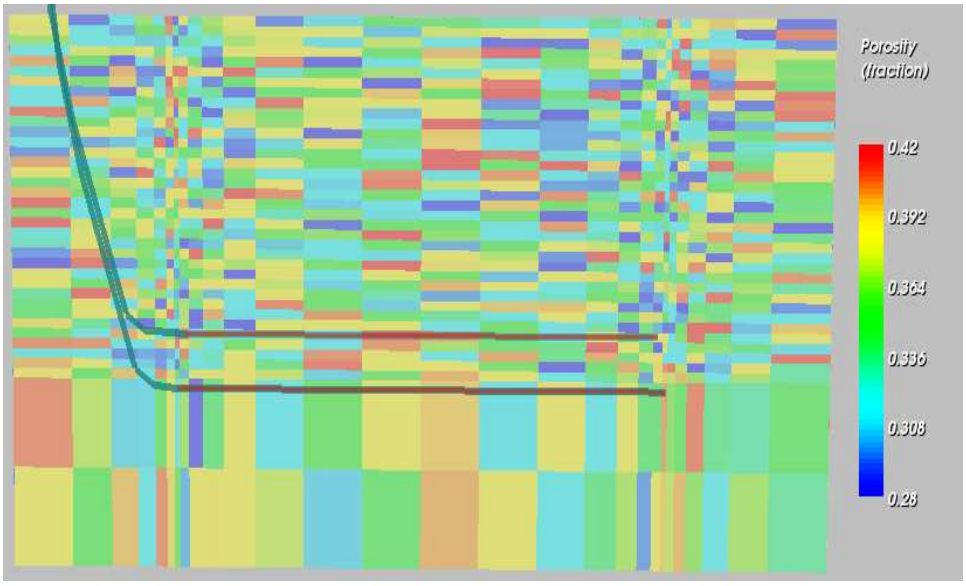

Figure 42: Geospatial Distribution of Porosity in Surmont Case 3

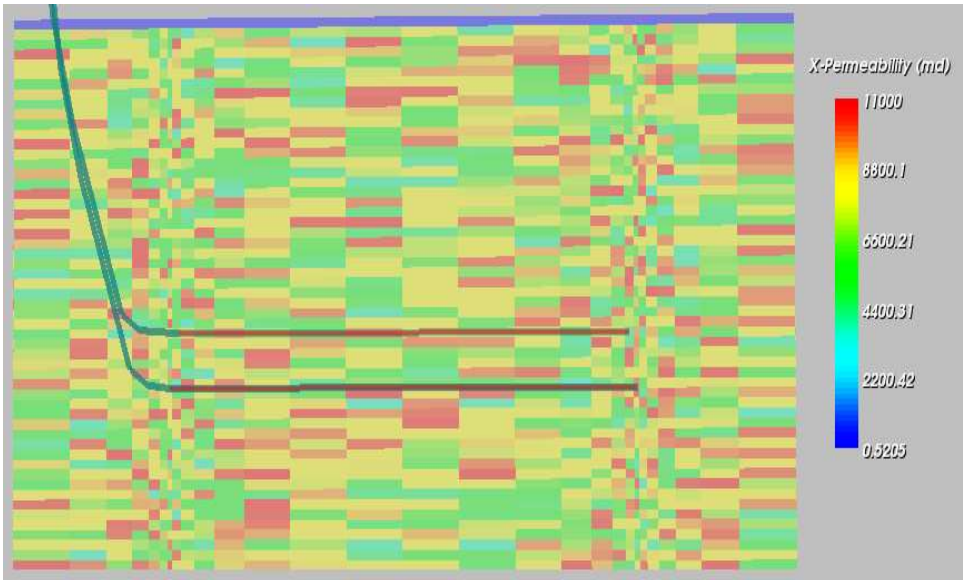

Figure 43: Geospatial Distribution of Permeability in Surmont Case 3

Comparing cumulative oil recovery over time in **Figure 43**, a distinct difference can be seen between the base case and a SAGD well pair with FCDs included in the completion. Over the course of four years, the FCD case with a similar subcool to the base case significantly outperforms the conventional SAGD well pair, with bitumen recovery increasing 148% over the base line. With an aggressive subcool, the FCDs are produces 168% of the bitumen that the base case is capable of producing, as depicted in **Figure 44**. Not only do both FCD cases outperform the base case in terms of bitumen production, they do so at consistently lower cumulative Steam-to-Oil ratio (cSOR). Where the base case maintains an average cSOR of 2.76, the FCD case of scenario 1 maintains an average cSOR of 1.65 while the FCD case of scenario 2 further reduces the cSOR to 1.61. **Figure 45** illustrates the changing cSOR of the simulated scenarios over time.

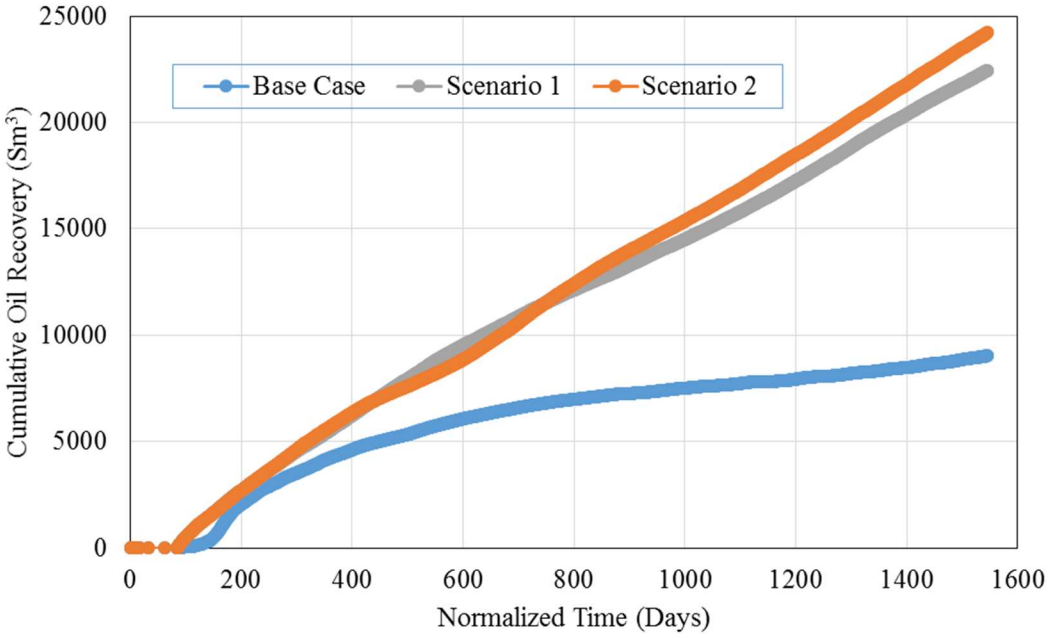

Figure 44: Cumulative Bitumen Recovery over Time for Each Simulated Case (Surmont Simulation 3)

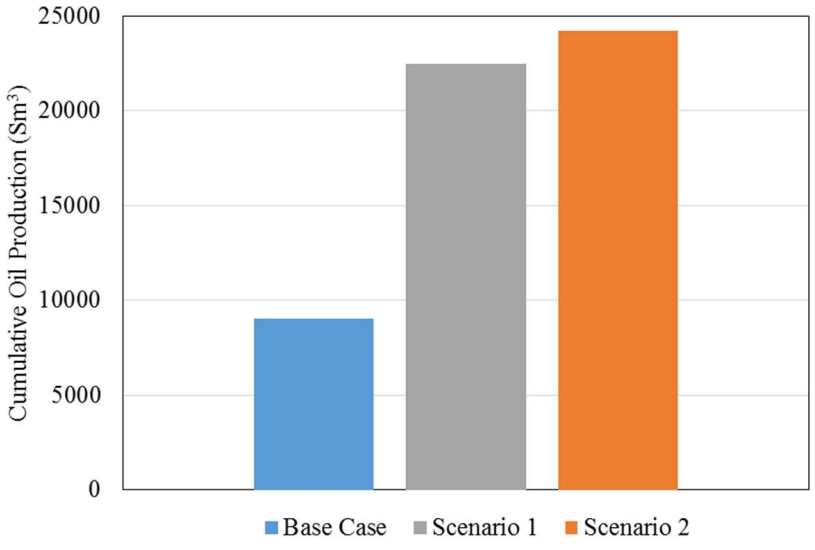

Figure 45: A Comparison of Total Cumulative Bitumen Recovery for Each Simulated Case (Surmont Simulation 3)

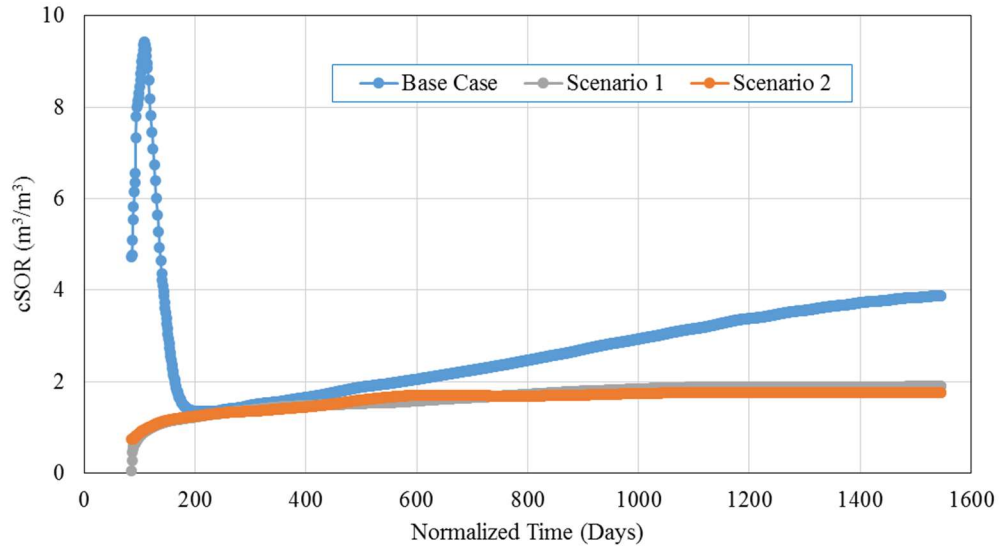

Figure 46: cSOR versus Time for Each Simulated Case

Consider again how these improvements in bitumen recovery and reductions in cSOR affect the investment value of a SAGD well pair. Performing a NPV analysis on Surmont simulation set 2 and Surmont simulation set 3 (**Figure 47**), it is apparently that the improvements in conformance that come with FCD usage improve the 4-year NPV analysis as well. For both simulated reservoirs, mere introduction of FCDs improves the net present value of the SAGD well pair by over a million dollars in a four year period. Changes in operational constraints, to better take advantage of the presence of FCDs and their improvements on wellbore fluid conformance, further improves the economic value of the SAGD well pair. This improvement is tied to how easily steam is diverted within the reservoir itself; for the Surmont 3 simulated reservoir, with its higher permeability, a more aggressive subcool and drawdown proves less benefit than it does in the Surmont 2 simulated case where the relative permeability of oil and steam is considerably lower.

This highlights a potential limitation in FCD usage in SAGD design; if heterogeneity is not present, there is no problem for an FCD to solve, and its benefits are constricted. Another concern is that improved conformance from FCD usage may work against thermal efficiencies; all simulated cases consider shales and other barriers to vertical or horizontal reservoir flow to be discontinuous. When these flow barriers are extensive and continuous, the conforming flow profiles of FCDs will be a detriment to the operator, heating non-production rock needlessly and forcing steam into zones where its thermal energy is trapped and non-productive.

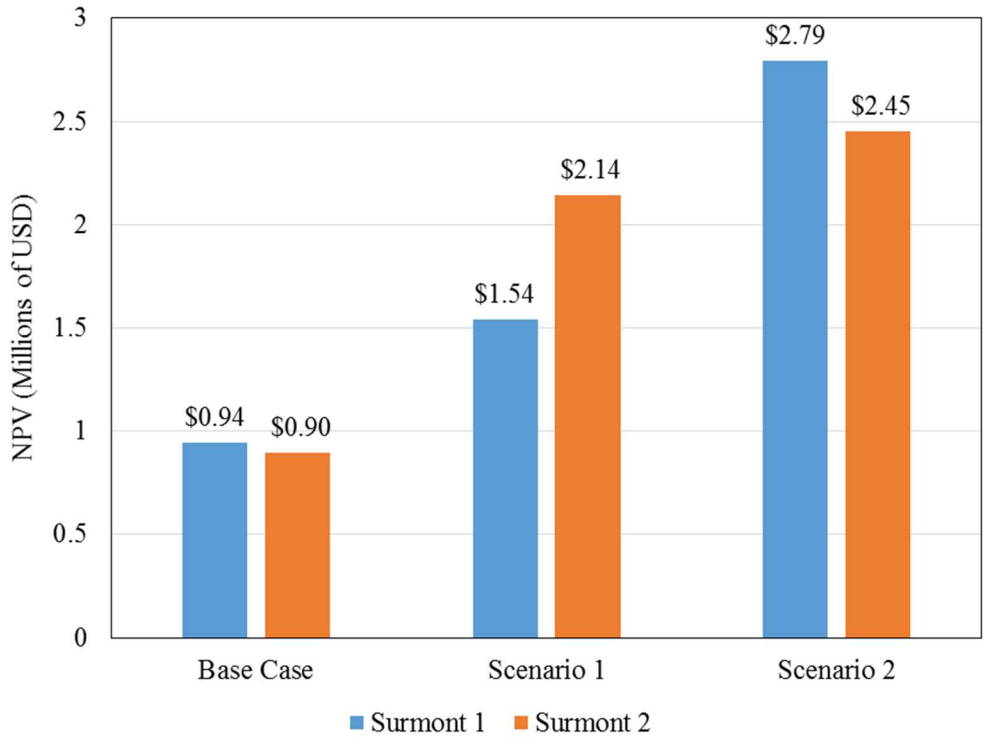

Figure 47: 4-Year NPV Analysis on Surmont 2 and Surmont 3 Simulation Cases

5. CONCLUSIONS

This dissertation addressed the role of steam flow and steam flashing in effective flow control device (FCD) performance descriptions, highlighting the inherent weaknesses in currently published data/correlations on FCD multiphase performance. Focusing on an autonomous hybrid FCD design, an empirical investigation on how this FCD geometry performs under SAGD conditions was conducted and regression upon the empirical data generated a more accurate FCD pressure drop model. From these tests, it was conclusively shown that published multiphase pressure drop equations for the autonomous hybrid FCD consistently underestimated the pressure drop of multiphase flow through the device in the absence of steam/steam flashing. However, errors in this predictive model were most egregious when the pressure loss within the FCD caused a saturated fluid to flash to a vapor phase within the FCD geometry itself. To correct these issues, ANOVA regression was used to develop a general multiphase pressure drop model (**Equation 41**) and a multiphase pressure drop model based on FCD outlet conditions to capture phase-change effects on FCD performance (**Equation 42**). These two equations were introduced into the REVEAL™ reservoir simulator by incorporating **Equation 41** into a new selectable FCD option within the REVEAL™ well builder control panel and by using a script that allowed for a regression calculation to capture phase change within the FCD and modification of the calculated pressure drop via **Equation 42**.

Having now updated a reservoir simulator to accurately model the effects of FCD completion tools upon the well performance, multiple simulation cases were performed to capture and quantify the benefits of FCDs upon SAGD completion design in a stochastic

manner. In this analysis, a definite trends emerged: with no change other than FCD improvement to conformance of the steam chamber and steam trap, an improvement in bitumen production and a reduction in cSOR was observed. In all simulated cases, bitumen production increased by a minimum of 50% and cumulative steam-oil ratio was reduced to under two, even when conventional SAGD well designs were operating under cSOR ranging from 3.5 to 4. In economic terms, this was contrasted in the changed Net-Present Value of the different simulated cases; use of FCDs improved NPV by a minimum of 64% and had, with a more aggressive operating style made possibly by FCD usage, the potential to increase NPV by 300% from the base case over a 4-year period. These benefits were obtained with the fundamental assumption that completion costs were increased by one million USD through use of FCDs.

However, given the substantial increases to recovery factor, reductions to cSOR, and improvements to NPV, a solid argument has been made by this research to consider FCDs in the default SAGD well design. Some possibilities for future research focus on topics not covered within the scope of this research; performance qualification has focused on a single autonomous FCD geometry, and other geometries must be qualified in a similar manner in order to contrast geometric effects on FCD performance. Furthermore, assumptions have been made about the long-term operational reliability of the tested FCD geometry, assumptions that must eventually be verified by extensive erosional testing of the autonomous hybrid FCD device and other competing geometries. Yet as SAGD projects become more common and more prominent, and as these projects expand into more challenging and heterogeneous reservoirs, one certain conclusion is that the use of

flow control devices to improve thermal efficiency of SAGD wells will be a topic of great important and immediacy for industry leaders.

REFERENCES

Abdelfattah, T.A., Banerjee, S., Garcia, G.A. et al. 2012. Effective Use of Passive Inflow Control Devices to Improve the Field Development Plan. Proc., SPE Deepwater Drilling and Completions Conference, Galveston, Texas. http://dx.doi.org/10.2118/146521-MS.

Achong, I. 1961. Revised Bean Performance Formula for Lake Maracaibo Wells, Shell Oil Company, Houston, Texas, USA.

Ajienka, J.A., Enaibe, O.E., Owolabi, O.O. 1994. Multiphase Flow Metering - an Evaluation of Discharge Coefficients. *J Can Petrol Technol* **33** (8): 57-62. http://dx.doi.org/10.2118/94-08-07.

Akin, S. 2013. Mathematical Modeling of Steam Assisted Gravity Drainage. *SPE Res Eval & Eng* **8** (05): 372-376. SPE-86963-PA. http://dx.doi.org/10.2118/86963-pa.

Al-Attar, H.H. 2013. New Correlations for Critical and Subcritical Two-Phase Flow Through Surface Chokes in High-Rate Oil Wells. *SPE Projects, Facilities & Construction* **5** (01): 31-37. SPE-120788-PA. http://dx.doi.org/10.2118/120788-pa.

Al-Khelaiwi, F.T., Birchenko, V.M., Konopczynski, M.R. et al. 2010. Advanced Wells: A Comprehensive Approach to the Selection Between Passive and Active Inflow-Control Completions. *SPE Prod & Oper* **25** (3): 305-326. SPE-132976-PA. http://dx.doi.org/10.2118/132976-PA.

Al-Khelaiwi, F.T., Davies, D.R. 2007. Inflow Control Devices: Application and Value Quantification of a Developing Technology. Proc., International Oil Conference and Exhibition, Veracruz, Mexico. http://dx.doi.org/10.2118/108700-MS.

Al-Murayri, M.T., Harding, T.G., Maini, B.B. 2011. Impact of Noncondensable Gas on Performance of Steam-Assisted Gravity Drainage. *J Can Petrol Technol* **50** (7-8): 46-54. http://dx.doi.org/10.2118/148943-PA.

Alimonti, C., Falcone, G., Bello, O. 2010. Two-Phase Flow Characteristics in Multiple Orifice Valves. *Experimental Thermal and Fluid Science* **34** (8): 1324-1333. http://dx.doi.org/10.1016/j.expthermflusci.2010.06.004.

Almeida, A.R. 2013. A Model To Calculate the Theoretical Critical Flow Rate Through Venturi Gas Lift Valves (includes Addendum). *SPE J* **16** (01): 134-147. SPE-126184-PA. http://dx.doi.org/10.2118/126184-pa.

Alsafran, E.M., Kelkar, M.G. 2013. Predictions of Two-Phase Critical-Flow Boundary and Mass-Flow Rate Across Chokes. *SPE Prod & Oper* **24** (02): 249-256. SPE-109243-PA. http://dx.doi.org/10.2118/109243-pa.

Anklam, E.G., Wiggins, M.L. 2005. A Review of Horizontal-Wellbore Pressure Equations. Proc., SPE Production Operations Symposium, Oklahoma City, Oklahoma, USA. http://dx.doi.org/10.2118/94314-MS.

Archer, R.A., Agbongiator, E.O. 2005. Correcting for Frictional Pressure Drop in Horizontal-Well Inflow-Performance Relationships. *SPE Prod & Fac* **20** (1): 21-25. SPE-80528-PA. http://dx.doi.org/10.2118/80528-PA.

Ashford, F.E., Pierce, P.E. 1975. Determining Multiphase Pressure Drops and Flow Capacities in Down-Hole Safety Valves. *JPT* **27** (9): 1145-1152. SPE-5161-PA. http://dx.doi.org/10.2118/5161-PA.

ASME MFC-3M-2004, Measurement of Fluid Flow in Pipes Using Orifice, Nozzle, and Venturi. 2006. New York, New York, USA: American Society of Mechanical Engineers.

Atkinson, C., Monmont, F., Zazovsky, A.F. 2004. Flow Performance of Horizontal Wells with Inflow Control Devices. *European Journal of Applied Mathematics* **15** (04): 409-450. http://dx.doi.org/10.1017/S0956792504005546.

Babu, D.K., Odeh, A.S. 1989. Productivity of a Horizontal Well (includes associated papers 20306, 20307, 20394, 20403, 20799, 21307, 21610, 21611, 21623, 21624, 25295, 25408, 26262, 26281, 31025, and 31035). *SPE Res Eng* **4** (4): 417-421. SPE-18298-PA. http://dx.doi.org/10.2118/18298-PA.

Baker, R., Fong, C., Bowes, C. et al. 2010. Understanding Volumetric Sweep Efficiency in SAGD Projects. *J Can Petrol Technol* **49** (1): 30-37. http://dx.doi.org/10.2118/132639-PA.

Baker, R.O., Fong, C., Li, T. et al. 2008. Practical Considerations of Reservoir Heterogeneities on SAGD Projects. Proc., SPE International Thermal Operations and Heavy Oil Symposium, Calgary, Alberta, Canada. http://dx.doi.org/10.2118/117525-MS.

Banerjee, S., Abdelfattah, T.A., Nguyen, H.T. 2013a. Benefits of Passive Inflow Control Devices in a SAGD Completion. Proc., SPE Heavy Oil Conference, Calgary, Alberta, Canada. http://dx.doi.org/10.2118/165478-MS.

Banerjee, S., Hascakir, B. 2015. Management of Steam Flashing in SAGD Completion Design via the Implementation of Flow Control Devices. Proc., SPE Thermal

Well Integrity and Design Symposium, Banff, Alberta, Canada. http://dx.doi.org/10.2118/178459-MS.

Banerjee, S., Jobling, R., Abdelfattah, T.A. et al. 2013b. The Role of Autonomous Flow Control in SAGD Well Design. Proc., SPE Annual Technical Conference and Exhibition, New Orleans, Louisiana, USA. http://dx.doi.org/10.2118/166266-MS.

Bitto, R. 2013. Passive Inflow Control Devices: Enhance Horizontal Well Productivity (White Paper), Baker Hughes Inc., Houston, Texas, USA (2013/4/1).

Bois, A.-P., Mainguy, M. 2011. Importance of Thermal Consolidation of Shale During SAGD Process. Proc., SPE Heavy Oil Conference and Exhibition, Kuwait City, Kuwait. http://dx.doi.org/10.2118/150420-MS.

Box, G.E.P., Cox, D.R. 1964. An Analysis of Transformations. *Journal of the Royal Statistical Society. Series B (Methodological)* **26** (2): 211-252.

Brandt, A.R. 2012. Variability and Uncertainty in Life Cycle Assessment Models for Greenhouse Gas Emissions from Canadian Oil Sands Production. *Environmental Science & Technology* **46** (2): 1253-1261. http://dx.doi.org/10.1021/es202312p.

Butler, R.M. 1985. A New Approach to the Modeling of Steam-Assisted Gravity Drainage. *J Can Petrol Technol* **24** (3): 42-51. http://dx.doi.org/10.2118/85-03-01.

Butler, R.M. 1987. Rise of Interfering Steam Chambers. *J Can Petrol Technol* **26** (3): 70-75. http://dx.doi.org/10.2118/87-03-07.

Butler, R.M., Kanakia, V. 1994. Recovery of Heavy and Conventional Oils from Pressure-Depleted Reservoirs Using Horizontal Wells. *J Can Petrol Technol* **33** (10): 27-33. http://dx.doi.org/10.2118/94-10-03.

Butler, R.M., Mcnab, G.S., Lo, H.Y. 1981. Theoretical Studies on the Gravity Drainage of Heavy Oil during In-Situ Steam Heating. *The Canadian Journal of Chemical Engineering* **59** (4): 455-460. http://dx.doi.org/10.1002/cjce.5450590407.

Butler, R.M., Stephens, D.J. 1981. The Gravity Drainage of Steam-Heated Heavy Oil to Parallel Horizontal Wells. *J Can Petrol Technol* **20** (2): 90-96. http://dx.doi.org/10.2118/81-02-07.

Butler, R.M., Yee, C.T. 2002. Progress in the In Situ Recovery of Heavy Oils and Bitumen. *J Can Petrol Technol* **41** (1): 31-40. http://dx.doi.org/10.2118/02-01-02.

Bybee, K. 2008. Production Operations: Inflow-Control Devices. *JPT* **60** (3): 81-83. SPE-0308-0081-JPT. http://dx.doi.org/10.2118/0308-0081-JPT.

Campos, S.R.V., Balino, J.L., Slobodcicov, I. et al. 2014. Orifice Plate Meter Field Performance: Formulation and Validation in Multiphase Flow Conditions. *Experimental Thermal and Fluid Science* **58**: 93-104. http://dx.doi.org/10.1016/j.expthermflusci.2014.06.018.

Carpenter, C. 2015. The Role of Autonomous Flow Control in SAGD Well Design. *J Pet Technol* **66** (03): 136-139. SPE-0314-0136-JPT. http://dx.doi.org/10.2118/0314-0136-jpt.

Chen, Q., Gerritsen, M.G., Kovscek, A.R. 2008. Effects of Reservoir Heterogeneities on the Steam-Assisted Gravity-Drainage Process. *SPE Res Eval & Eng* **11** (5): 921-932. http://dx.doi.org/Doi 10.2118/109873-Pa.

Chien, S.F., Schrodt, J.L.G. 1995. Determination of Steam Quality and Flow-Rate Using Pressure Data from an Orifice Meter and a Critical Flowmeter. *SPE Prod & Fac* **10** (2): 76-81. http://dx.doi.org/10.2118/24832-PA.

Chisholm, D. 1983. *Two-phase flow in pipelines and heat exchangers*. London ;, G. Godwin in association with Institution of Chemical Engineers (Reprint).

Chow, L., Butler, R.M. 1996. Numerical Simulation of the Steam-Assisted Gravity Drainage Process (SAGD). *J Can Petrol Technol* **35** (6): 55-62. http://dx.doi.org/10.2118/96-06-06.

Chung, K.H., Butler, R.M. 1988. Geometrical Effect Of Steam Injection On The Formation Of Emulsions On The Steam-Assisted Gravity Drainage Process. *J Can Petrol Technol* **27** (01). PETSOC-88-01-02. http://dx.doi.org/10.2118/88-01-02.

Churchill, S.W. 1977. Friction-Factor Equation Spans All Fluid-Flow Regimes. *Chemical Engineering* **84** (24): 91-92.

Coronado, M.P., Garcia, L., Russell, R. et al. 2009. New Inflow Control Device Reduces Fluid Viscosity Sensitivity and Maintains Erosion Resistance. Proc., Offshore Technology Conference, Houston, Texas, USA. http://dx.doi.org/10.4043/19811-MS.

Darby, R. 2001. *Chemical Engineering Fluid Mechanics*, 2nd edition. New York, Marcel Dekker (Reprint).

Denney, D. 2015. Analysis of Inflow-Control Devices. *J Pet Technol* **62** (05): 52-54. SPE-0510-0052-JPT. http://dx.doi.org/10.2118/0510-0052-jpt.

Dikken, B.J. 1990. Pressure Drop in Horizontal Wells and Its Effect on Production Performance. *J Pet Technol* **42** (11): 1426-1433. SPE-19824-PA. http://dx.doi.org/10.2118/19824-pa.

Economides, M.J. 2013. *Petroleum Production Systems*, 2nd edition. Upper Saddle River, NJ, Prentice Hall (Reprint).

Edmunds, N. 2013. Investigation of SAGD Steam Trap Control in Two and Three Dimensions. *J Can Petrol Technol* **39** (01). PETSOC-00-01-02. http://dx.doi.org/10.2118/00-01-02.

Edmunds, N., Chhina, H. 2001. Economic Optimum Operating Pressure for SAGD Projects in Alberta. *J Can Petrol Technol* **40** (12): 13-17. http://dx.doi.org/10.2118/01-12-DAS.

Edmunds, N.R., Gittins, S.D. 1993. Effective Application of Steam Assisted Gravity Drainage of Bitumen to Long Horizontal Well Pairs. *J Can Petrol Technol* **32** (6): 49-55. http://dx.doi.org/10.2118/93-06-05.

Elgibaly, A.A.M., Nashawi, I.S. 1998. New Correlations for Critical and Subcritical Two-Phase Flow through Wellhead Chokes. *J Can Petrol Technol* **37** (6): 36-43. http://dx.doi.org/10.2118/98-06-04.

Ezeuko, C.C., Wang, J., Gates, I.D. 2013. Investigation of Emulsion Flow in Steam-Assisted Gravity Drainage. *SPE J* **18** (3): 440-447. http://dx.doi.org/10.2118/157830-PA.

Fortunati, F. 1972. Two-Phase Flow through Wellhead Chokes. Proc., SPE European Spring Meeting, Amsterdam, Netherlands. http://dx.doi.org/10.2118/3742-MS.

Fossa, M., Guglielmini, G. 2002. Pressure Drop and Void Fraction Profiles During Horizontal Flow Through Thin and Thick Orifices. *Experimental Thermal and Fluid Science* **26** (5): 513-523. http://dx.doi.org/10.1016/s0894-1777(02)00156-5.

Foster, J.H., Beson, J., Boyle, W.G. 1987. Wellhead Equipment and Flow Control Devices (1987 PEH Chapter 3). In *Petroleum Engineering Handbook*, ed. Howard B. Bradley, Chap. 3. Richardson, Texas, USA, Society of Petroleum Engineers.

Fripp, M., Zhao, L., Least, B. 2013. The Theory of a Fluidic Diode Autonomous Inflow Control Device. Proc., SPE Middle East Intelligent Energy Conference and Exhibition, Manama, Bahrain. http://dx.doi.org/10.2118/167415-MS.

Fripp, M.L., Dykstra, J.D. 2013. Method and Apparatus for Controlling Fluid Flow in an Autonomous Valve Using a Sticky Switch. United States Patent No. US2012032044.

Fripp, M.L., Gano, J.C., Murphree, Z.R. 2015. Flow Control Device for Controlling Flow Based on Fluid Phase. United States Patent No. US20150053420 A1.

Furui, K., Zhu, D., Hill, A.D. 2003. A Rigorous Formation Damage Skin Factor and Reservoir Inflow Model for a Horizontal Well (includes associated papers 88817 and 88818). *SPE Prod & Fac* **18** (3): 151-157. SPE-84964-PA. http://dx.doi.org/10.2118/84964-PA.

Furui, K., Zhu, D., Hill, A.D. 2005. A Comprehensive Model of Horizontal Well Completion Performance. *SPE Prod & Fac* **20** (3): 207-220. SPE-84401-PA. http://dx.doi.org/10.2118/84401-PA.

Garcia, L.A., Coronado, M.P., Peterson, E.R. et al. 2009. Adjustable Flow Control Devices For Use In Hydrocarbon Production. United States Patent No. US20090205834 A1.

Gates, I.D., Adams, J., Larter, S. 2008. The Impact of Oil Viscosity Heterogeneity on the Production Characteristics of Tar Sand and Heavy Oil Reservoirs. Part II: Intelligent, Geotailored Recovery Processes in Compositionally Graded Reservoirs. *J Can Petrol Technol* **47** (9): 40-49. PETSOC-08-09-40. http://dx.doi.org/10.2118/08-09-40.

Gates, I.D., Chakrabarty, N. 2006. Optimization of Steam Assisted Gravity Drainage in McMurray Reservoir. *J Can Petrol Technol* **45** (9). PETSOC-06-09-05. http://dx.doi.org/10.2118/06-09-05.

Gates, I.D., Leskiw, C. 2010. Impact of Steam Trap Control on Performance of Steam-Assisted Gravity Drainage. *Journal of Petroleum Science and Engineering* **75** (1–2): 215-222. http://dx.doi.org/10.1016/j.petrol.2010.11.014.

Gelman, A., Hill, J. 2007. *Data Analysis Using Regression and Multilevel/Hierarchical Models*. New York, NY: Analytical methods for social research, Cambridge University Press (Reprint).

Ghesmat, K., Zhao, L. 2015. SAGD Well-Pair Completion Optimization Using Scab Liner and Steam Splitters. *J Can Petrol Technol* **54** (6): 387-393. http://dx.doi.org/10.2118/170076-PA.

Gilbert, W.E. 1954. Flowing and Gas-lift Well Performance. *Drilling and Production Practice* **13**: 126. API-54-126.

Gotawala, D.R., Gates, I.D. 2012. A Basis for Automated Control of Steam Trap Subcool in SAGD. *SPE J* **17** (3): 680-686. http://dx.doi.org/10.2118/159170-PA.

Green, D.W., Willhite, G.P. 1998. *Enhanced Oil Recovery*, Vol. 6. Richardson, Texas: SPE textbook series, Henry L. Doherty Memorial Fund of AIME, Society of Petroleum Engineers (Reprint).

Griston, S., Cire, F.L. 1989. Evaluation of Two-Phase Steam Flow Through an Orifice. Proc., SPE Annual Meeting, San Antonio, Texas, USA. http://dx.doi.org/10.2118/19700-MS.

Grose, R.D. 1985. Orifice Contraction Coefficient for Inviscid Incompressible Flow. *Journal of Fluids Engineering* **107** (1): 36-43. http://dx.doi.org/10.1115/1.3242437.

Halvorsen, M., Elseth, G., Naevdal, O.M. 2012. Increased Oil Production at Troll by Autonomous Inflow Control with RCP Valves. Proc., SPE Annual Technical Conference and Exhibition, San Antonio, Texas, USA. http://dx.doi.org/10.2118/159634-MS.

Henriksen, K.H., Gule, E.I., Augustine, J.R. 2006. Case Study: The Application of Inflow Control Devices in the Troll Field. Proc., SPE Europec/EAGE Annual Conference and Exhibition, Vienna, Austria. http://dx.doi.org/10.2118/100308-MS.

Hill, A.D., Zhu, D. 2008. The Relative Importance of Wellbore Pressure Drop and Formation Damage in Horizontal Wells. *SPE Prod & Oper* **23** (2): 232-240. http://dx.doi.org/Doi 10.2118/100207-Pa.

Ihara, M., Yanai, K., Takao, S. 2013. Two-Phase Flow in Horizontal Wells. *SPE Prod & Fac* **10** (04): 249-256. SPE-24493-PA. http://dx.doi.org/10.2118/24493-pa.

Ipek, G., Frauenfeld, T., Yuan, J.Y. 2008. Numerical Study of Shale Issues in SAGD. Proc., Canadian International Petroleum Conference, Calgary, Alberta, Canada. http://dx.doi.org/10.2118/2008-150.

Irani, M. 2013. Understanding the Steam-Hammer Mechanism in Steam-Assisted-Gravity-Drainage Wells. *SPE J* **18** (6): 1181-1201. http://dx.doi.org/10.2118/165456-PA.

Irani, M., Cokar, M. 2016. Discussion on the Effects of Temperature on Thermal Properties in the Steam-Assisted-Gravity-Drainage (SAGD) Process. Part 1: Thermal Conductivity. *SPE J* **21** (2): 334-352.

Irani, M., Ghannadi, S. 2013. Understanding the Heat-Transfer Mechanism in the Steam-Assisted Gravity-Drainage (SAGD) Process and Comparing the Conduction and Convection Flux in Bitumen Reservoirs. *SPE J* **18** (1): 134-145. SPE-163079-PA. http://dx.doi.org/10.2118/163079-PA.

Jain, R., Long, T.A., Dickson, J. et al. 2014. Experimental Investigation of Pressure-Drop/Flow-Rate Relationship for Small-Aperture Holes for High-Viscosity Fluids. *SPE Prod & Oper* **29** (2): 114-121. http://dx.doi.org/10.2118/159735-PA.

Jain, R., Syal, S., Long, T. et al. 2013. An Integrated Approach To Design Completions for Horizontal Wells for Unconventional Reservoirs. *SPE J* **18** (6): 1026-1032. SPE-147120-PA. http://dx.doi.org/10.2118/147120-PA.

James, R. 1965. Metering of Steam-Water Two-Phase Flow by Sharp-Edged Orifices. *Proceedings of the Institution of Mechanical Engineers* **180** (1): 549-572. http://dx.doi.org/10.1243/pime_proc_1965_180_038_02.

Janssen, E. 1966. Two-Phase Pressure Loss Across Abrupt Contractions and Expansions, Steam-Water at 600 to 1400 PSIA. *Chicago, Illinois*, Vol. V, 13-23. New York, New York: General Electric Co.

Joshi, S.D. 2003. Cost/Benefits of Horizontal Wells. Proc., SPE Western Regional Meeting, Long Beach, California, USA. http://dx.doi.org/10.2118/83621-MS.

Karim, R.A., Goh, K.F.G., Nuriyadi, M.A. et al. 2010. Horizontal Well Optimization With Inflow Control Devices (ICDs) Application in Heterogeneous and Dipping Gas-Capped Oil Reservoirs. Proc., SPE Annual Technical Conference and Exhibition, Florence, Italy. http://dx.doi.org/10.2118/133336-MS.

Kiljański, T. 1993. Discharge Coefficient for Free Jets From Orifices at Low Reynolds Number. *Journal of Fluids Engineering* **115** (4): 778-781. http://dx.doi.org/10.1115/1.2910212.

Kojasoy, G., Landis, F., Kwame-Mensah, P. et al. 1997. Two-phase pressure drop in multiple thick- and thin-orifice plates. *Experimental Thermal and Fluid Science* **15** (4): 347-358. http://dx.doi.org/10.1016/S0894-1777(97)00003-4.

Kovscek, A.R. 2012. Emerging challenges and potential futures for thermally enhanced oil recovery. *Journal of Petroleum Science and Engineering* **98–99**: 130-143. http://dx.doi.org/10.1016/j.petrol.2012.08.004.

Kumar, D., Hampton, T., Azom, P. et al. 2013. Analysis of Impact of Thermal and Permeability Heterogeneity on SAGD Performance Using a Semi-Analytical Approach. Proc., SPE Heavy Oil Conference-Canada, Calgary, Alberta, Canada. http://dx.doi.org/10.2118/165565-MS.

Kyanpour, M., Chen, Z. 2013. A New Approach for Designing Steam Splitters and Inflow Control Devices in Steam Assisted Gravity Drainage. Proc., SPE Heavy Oil Conference-Canada, Calgary, Alberta, Canada. http://dx.doi.org/10.2118/165487-MS.

Larter, S., Adams, J., Gates, I.D. et al. 2008. The Origin, Prediction and Impact of Oil Viscosity Heterogeneity on the Production Characteristics of Tar Sand and Heavy Oil Reservoirs. *J Can Petrol Technol* **47** (1): 52-61. PETSOC-08-01-52. http://dx.doi.org/10.2118/08-01-52.

Lauritzen, J.E., Martiniussen, I.B. 2011. Single and Multi-phase Flow Loop Testing Results for Industry Standard Inflow Control Devices. Proc., SPE Offshore Europe Oil and Gas Conference and Exhibition, Aberdeen, UK. http://dx.doi.org/10.2118/146347-MS.

Lauritzen, J.E., Shahreyar, N., Jacob, S. 2011. Selection Methodology for Passive, Active, and Hybrid Inflow Control Completions. Proc., Offshore Technology Conference, Houston, Texas, USA. http://dx.doi.org/10.4043/21910-MS.

Le Ravalec, M., Morlot, C., Marmier, R. et al. 2009. Impact des hétérogénéités sur la production d'huiles lourdes mobiles par SAGD. *Oil & Gas Science and Technology - Rev. IFP* **64** (4): 469-476.

Least, B., Greci, S., Burkey, R.C. et al. 2012. Autonomous ICD Single Phase Testing. Proc., SPE Annual Technical Conference and Exhibition, San Antonio, Texas, USA. http://dx.doi.org/10.2118/160165-MS.

Least, B., Greci, S., Huffer, R. et al. 2014. Steam Flow Tests for Comparing Performance of Nozzle, Tube, and Fluidic Diode Autonomous ICDs in SAGD Wells. Proc., SPE Heavy Oil Conference-Canada, Calgary, Alberta, Canada. http://dx.doi.org/10.2118/170083-MS.

Least, B., Greci, S., Wilemon, A. et al. 2013. Autonomous ICD Range 3B Single-Phase Testing. Proc., SPE Annual Technical Conference and Exhibition, New Orleans, Louisiana, USA. http://dx.doi.org/10.2118/166285-MS.

Lee, B.O., Rabeh, M.N., Vicario, R. et al. 2013. Multi-Phase (Oil-Water) Loop Flow Test for Helical and Hybrid Passive Inflow Control Devices. Proc., International Petroleum Technology Conference, Beijing, China. http://dx.doi.org/10.2523/IPTC-17125-MS.

Li, Z., Fernandes, P.X., Zhu, D. 2013. Understanding the Roles of Inflow-Control Devices in Optimizing Horizontal-Well Performance. *SPE Drilling & Compl* **26** (03): 376-385. SPE-124677-PA. http://dx.doi.org/10.2118/124677-pa.

Li, Z.Y., Zhu, D. 2010. Predicting Flow Profile of Horizontal Well by Downhole Pressure and Distributed-Temperature Data for Waterdrive Reservoir. *SPE Prod & Oper* **25** (3): 296-304. http://dx.doi.org/10.2118/124873-PA.

Lin, Z.H. 1982. Two-phase flow measurements with sharp-edged orifices. *International Journal of Multiphase Flow* **8** (6): 683-693. http://dx.doi.org/10.1016/0301-9322(82)90071-4.

Llaguno, P.E., Moreno, F., Garcia, R. et al. 2002. A Reservoir Screening Methodology for SAGD Applications. Proc., Canadian International Petroleum Conference, Calgary, Alberta, Canada. http://dx.doi.org/10.2118/2002-124.

Loretz, I., Hosatte, P. 2007. Flow Control Device. United States Patent No. US20070169942.

Mayer, C.S.J., Spiecker, M., Shuchart, C.E. et al. 2014. Multiphase Flow Performance of Inflow Control Devices - Characterizing Downhole Flow Behavior in Lab Experiments. Proc., Abu Dhabi International Petroleum Exhibition and Conference, Abu Dhabi, UAE. http://dx.doi.org/10.2118/171890-MS.

Medina, M. 2015. Design and Field Evaluation of Tubing-Deployed Passive Outflow-Control Devices in Steam-Assisted-Gravity-Drainage Injection Wells. *SPE Prod & Oper* **30** (4): 283-292. http://dx.doi.org/10.2118/165563-PA.

Mikkelsen, J.K., Norheim, T., Sagatun, S.I. 2005. The Troll Story. Proc., Offshore Technology Conference, Houston, Texas, USA. http://dx.doi.org/10.4043/17108-MS.

Miller, R.W. 1996. *Flow Measurement Engineering Handbook*, 3rd edition. New York, McGraw-Hill (Reprint).

Moen, T., Asheim, H.A. 2008. Inflow Control Device and Near-Wellbore Interaction. Proc., SPE International Symposium and Exhibition on Formation Damage Control, Lafayette, Louisiana, USA. http://dx.doi.org/10.2118/112471-MS.

Morris, G.K., Garimella, S.V. 1998. Orifice and Impingement Flow Fields in Confined Jet Impingement. *Journal of Electronic Packaging* **120** (1): 68-72. http://dx.doi.org/10.1115/1.2792288.

Morrison, G.L. 2003. Euler Number Based Orifice Discharge Coefficient Relationship. *Journal of Fluids Engineering* **125** (1): 189-191. http://dx.doi.org/10.1115/1.1521955.

Morrow, A.W., Mukhametshina, A., Aleksandrov, D. et al. 2014. Environmental Impact of Bitumen Extraction with Thermal Recovery. Proc., SPE Heavy Oil Conference - Canada, Calgary, Alberta, Canada. http://dx.doi.org/10.2118/170066-MS.

Nasr, T.N., Law, D.H.S., Golbeck, H. et al. 2000. Counter-current Aspect of the SAGD Process. *J Can Petrol Technol* **39** (1). PETSOC-00-01-03. http://dx.doi.org/10.2118/00-01-03.

National Energy Board. 2016. Canada's Energy Future 2016: Energy Supply and Demand Projections to 2040, Canada National Energy Board, Ottawa, Canada.

Novy, R.A. 1995. Pressure Drops in Horizontal Wells: When Can They Be Ignored? *SPE Res Eng* **10** (01): 29-35. SPE-24941-PA. http://dx.doi.org/10.2118/24941-pa.

Osman, M.E., Dokla, M.E. 1992. Correlations Predict Gas-Condensate Flow through Chokes. *Oil & Gas Journal* **90** (11): 43-46.

Oyeka, O., Felten, F., Least, B. 2014. Screen-Inflow-Design Considerations with Inflow Control Devices in Heavy Oil. Proc., SPE Heavy Oil Conference-Canada, Calgary, Alberta, Canada. http://dx.doi.org/10.2118/170097-MS.

Ozkan, E., Sarica, C., Haciislamoglu, M. et al. 1995. Effect of Conductivity on Horizontal Well Pressure Behavior. *SPE Advanced Technology Series* **3** (1): 85-94. SPE-24683-PA. http://dx.doi.org/10.2118/24683-PA.

Penmatcha, V.R., Arbabi, S., Aziz, K. 1999. Effects of Pressure Drop in Horizontal Wells and Optimum Well Length. *SPE J* **4** (03): 215-223. SPE-57193-PA. http://dx.doi.org/10.2118/57193-pa.

Penmatcha, V.R., Aziz, K. 1999. Comprehensive Reservoir/Wellbore Model for Horizontal Wells. *SPE J* **4** (3): 224-234. SPE-57194-PA. http://dx.doi.org/10.2118/57194-PA.

Perkins, T.K. 1993. Critical and Subcritical Flow of Multiphase Mixtures Through Chokes. *SPE Drilling & Completion* **8** (04): 271-276. SPE-20633-PA. http://dx.doi.org/10.2118/20633-PA.

Peterson, E.R., Coronado, M.P., Garcia, L. et al. 2010. Well Completion Applications for the Latest-Generation Low-Viscosity-Sensitive Passive Inflow-Control Device. Proc., IADC/SPE Drilling Conference and Exhibition, New Orleans, Louisiana, USA. http://dx.doi.org/10.2118/128481-MS.

Pooladi-Darvish, M., Mattar, L. 2002. SAGD Operations in the Presence of Overlying Gas Cap and Water Layer - Effect of Shale Layers. *J Can Petrol Technol* **41** (6): 40-51. http://dx.doi.org/10.2118/02-06-04.

Qudaihy, D.S., Faraj, O.A., Alnughaimish, F.N. et al. 2005. Improving Horizontal Well Productivity Using Novel Technology and Optimization of Drilling Fluids. *SPE Drilling & Completion* **20** (3): 205-208. SPE-85332-PA. http://dx.doi.org/10.2118/85332-PA.

Rahman, M., Biswas, R., Mahfuz, W. 2009. Effects of Beta Ratio and Reynolds Number on Coefficient of Discharge of Orifice Meter. *Journal of Agriculture & Rural Development* **7** (1): 151-156.

Ramamurthi, K., Nandakumar, K. 1999. Characteristics of Flow Through Small Sharp-Edged Cylindrical Orifices. *Flow Measurement and Instrumentation* **10** (3): 133-143. http://dx.doi.org/http://dx.doi.org/10.1016/S0955-5986(99)00005-9.

Reis, J.C. 1992. A Steam-Assisted Gravity Drainage Model For Tar Sands: Linear Geometry. *J Can Petrol Technol* **31** (10): 14-20. PETSOC-92-10-01. http://dx.doi.org/10.2118/92-10-01.

Riel, A., Burton, R.C., Wheeler, T.J. et al. 2014. An Innovative Modeling Approach to Unveil Flow Control Devices Potential in SAGD Application. Proc., SPE Heavy Oil Conference-Canada, Calgary, Alberta, Canada. http://dx.doi.org/10.2118/170045-MS.

Ros, N.C.J. 1960. An Analysis of Critical Simultaneous Gas/Liquid Flow Through a Restriction and Its Application to Flowmetering. *Applied Scientific Research* **9** (1): 374-388. http://dx.doi.org/10.1007/bf00382215.

Roul, M.K., Dash, S.K. 2012. Single-Phase and Two-Phase Flow Through Thin and Thick Orifices in Horizontal Pipes. *Journal of Fluids Engineering-Transactions of the Asme* **134** (9). J Fluid Eng-T Asme. http://dx.doi.org/10.1115/1.4007267.

Russell, R.D., Garcia, L.A., Garcia, G.A. et al. 2013a. Flow Control Device that Substantially Decreases Flow of a Fluid when a Property of the Fluid is in a Selected Range. United States Patent No. US8403038 B2.

Russell, R.D., Garcia, L.A., Garcia, G.A. et al. 2013b. Method of Making a Flow Control Device that Reduces Flow of the Fluid when a Selected Property of the Fluid is in Selected Range. United States Patent No. US8403061 B2.

Sachdeva, R., Schmidt, Z., Brill, J.P. et al. 1986. Two-Phase Flow through Chokes. Proc., SPE Annual Technical Conference and Exhibition, New Orleans, Louisiana, USA. http://dx.doi.org/10.2118/15657-MS.

Sagatun, S.I. 2010. Boundary Control of a Horizontal Oil Reservoir. *SPE J* **15** (4): 1026-1033. SPE-135534-PA. http://dx.doi.org/10.2118/135534-PA.

Sahin, B., Ceyhan, H. 1996. Numerical and Experimental Analysis of Laminar Flow through Square-Edged Orifice with Variable Thickness. *Transactions of the Institute of Measurement and Control* **18** (4): 166-174. http://dx.doi.org/10.1177/014233129601800401.

Sasaki, K., Akibayashi, S., Yazawa, N. et al. 2001. Numerical and Experimental Modelling of the Steam Assisted Gravity Drainage (SAGD) Process. *J Can Petrol Technol* **40** (1): 44-50. http://dx.doi.org/10.2118/01-01-04.

Schüller, R.B., Solbakken, T., Selmer-Olsen, S. 2003. Evaluation of Multiphase Flow Rate Models for Chokes Under Subcritical Oil/Gas/Water Flow Conditions. *SPE Prod & Fac* **18** (03): 170-181. SPE-84961-PA. http://dx.doi.org/10.2118/84961-pa.

Sharma, J., Gates, I.D. 2011. Convection at the Edge of a Steam-Assisted-Gravity-Drainage Steam Chamber. *SPE J* **16** (3): 503-512. http://dx.doi.org/10.2118/142432-PA.

Sheather, S.J. 2008. *A Modern Approach to Regression with R*. New York, New York: Springer Texts in Statistics, Springer (Reprint).

Simpson, H., Grattan, E., Rooney, D. 1981. Two-phase Flow through Gate Valves and Orifice Plates. *Proceedings of the International Conference on Physical Modelling of Multi-Phase Flow* **82** (1).

Stalder, J.L. 2013. Test of SAGD Flow-Distribution-Control Liner System in the Surmont Field, Alberta, Canada. *J Can Petrol Technol* **52** (2): 95-100. http://dx.doi.org/10.2118/153706-pa.

Stapleton, J.H. 2009. *Linear Statistical Models*, 2nd edition. Hoboken, NJ: Wiley Series in Probability and Statistics, Wiley Publishing (Reprint).

Steven, R., Hall, A. 2009. Orifice Plate Meter Wet Gas Flow Performance. *Flow Measurement and Instrumentation* **20** (4–5): 141-151. http://dx.doi.org/http://dx.doi.org/10.1016/j.flowmeasinst.2009.07.001.

Stone, H.L. 1973. Estimation of Three-Phase Relative Permeability and Residual Oil Data. *J Can Petrol Technol* **12** (4): 53-61. PETSOC-73-04-06. http://dx.doi.org/10.2118/73-04-06.

Surbey, D.W., Kelkar, B.G., Brill, J.P. 2013. Study of Subcritical Flow through Multiple-Orifice Valves. *SPE Prod Eng* **3** (01): 103-108. SPE-14285-PA. http://dx.doi.org/10.2118/14285-pa.

Tabatabaei, M., Ghalambor, A. 2011. A New Method to Predict Performance of Horizontal and Multilateral Wells. *SPE Prod & Oper* **26** (1): 75-87. SPE-141164-PA. http://dx.doi.org/10.2118/141164-PA.

Tam, E.S., Modien, R.M., Best, D.A. 2013. The Effect of Production Well Open Interval on Steamflood Performance. *J Can Petrol Technol* **27** (03). PETSOC-88-03-07. http://dx.doi.org/10.2118/88-03-07.

Urner, G. 1997. Pressure Loss of Orifice Plates According to ISO 5167-1. *Flow Measurement and Instrumentation* **8** (1): 39-41. Flow Meas Instrum. http://dx.doi.org/10.1016/S0955-5986(97)00014-9.

Vachon, G.P., Klaczek, W., Erickson, P.J. et al. 2015. Use of Flow Control Devices (FCDs) to Enforce Conformance in Steam Assisted Gravity Drainage (SAGD) Completions. Proc., SPE Canada Heavy Oil Technical Conference, Calgary, Alberta, Canada. http://dx.doi.org/10.2118/174416-MS.

Van Ness, H.C., Abbott, M.M. 2008. *Perry's Chemical Engineers' Handbook*, Vol. 8th ed. [New York]: Perry's Chemical Engineers' Handbook, McGraw-Hill Professional (Reprint).

Vander Valk, P.A., Yang, P. 2007. Investigation of Key Parameters in SAGD Wellbore Design and Operation. *J Can Petrol Technol* **46** (06): 49-56. PETSOC-07-06-02. http://dx.doi.org/10.2118/07-06-02.

Visosky, J.M., Clem, N.J., Coronado, M.P. et al. 2007. Examining Erosion Potential of Various Inflow Control Devices to Determine Duration of Performance. Proc., SPE Annual Technical Conference and Exhibition, Anaheim, California, USA. http://dx.doi.org/10.2118/110667-MS.

Wang, C., Leung, J.Y. 2015. Characterizing the Effects of Lean Zones and Shale Distribution in Steam-Assisted-Gravity-Drainage Recovery Performance. *SPE Res Eval & Eng* **18** (3): 329-345. http://dx.doi.org/10.2118/170101-PA.

Welch, M. 2011. Greener EOR: Employing Cogeneration to Improve the Energy Efficiency of Thermal EOR projects. Proc., SPE Asia Pacific Oil and Gas Conference and Exhibition, Jakarta, Indonesia. http://dx.doi.org/10.2118/144224-MS.

Wileman, A., Least, B., Greci, S. et al. 2013. Fluidic Diode Autonomous Inflow Control Device Range 3B - Oil, Water, and Gas Flow Performance Testing. Proc., SPE Kuwait Oil and Gas Show and Conference, Mishref, Kuwait. http://dx.doi.org/10.2118/167379-MS.

Wilson, A. 2015. Simulation of Flow-Control Devices with Feedback Control for Thermal Operations. *JPT* **66** (01): 69-72. SPE-0114-0069-JPT. http://dx.doi.org/10.2118/0114-0069-JPT.

Wu, Z., Vasantharajan, S., El-Mandouh, M. et al. 2011. Inflow Performance of a Cyclic-Steam-Stimulated Horizontal Well Under the Influence of Gravity Drainage. *SPE J* **16** (13): 494-502. SPE-127518-PA. http://dx.doi.org/10.2118/127518-PA.

Yang, C., Card, C., Nghiem, L. 2009. Economic Optimization and Uncertainty Assessment of Commercial SAGD Operations. *J Can Petrol Technol* **48** (9): 33-40. http://dx.doi.org/10.2118/09-09-33.

Yang, G.H., Butler, R.M. 1992. Effects of Reservoir Heterogeneities on Heavy Oil Recovery By Steam-Assisted Gravity Drainage. *J Can Petrol Technol* **31** (08). PETSOC-92-08-03. http://dx.doi.org/10.2118/92-08-03.

Yuan, J.Y., Nugent, D. 2013. Subcool, Fluid Productivity, and Liquid Level Above a SAGD Producer. *J Can Petrol Technol* **52** (5): 360-367. http://dx.doi.org/10.2118/157899-PA.

Zhang, Z.J., Cai, J.M. 1999. Compromise Orifice Geometry to Minimize Pressure Drop. *Journal of Hydraulic Engineering* **125** (11): 1150-1153. http://dx.doi.org/10.1061/(Asce)0733-9429(1999)125:11(1150).

Zhao, L., Least, B., Greci, S. et al. 2014. Fluidic Diode Autonomous ICD Range 2A Single-Phase Testing. Proc., SPE Oilfield Water Management Conference and Exhibition, Kuwait City, Kuwait. http://dx.doi.org/10.2118/170993-MS.

APPENDIX A

EXAMPLE OF REVEAL™ CONTROL SCRIPT FOR SAGD SIMULATION

```
'Note everything is in internal field units
SetUnits(99)
fNAN = 3.4e35 'To remove values by OpenServer (constraints)

'Preheating time (first schedule)
tPreheat = eval(DoGet("Reveal.Script.Schedule[0].Exit[0].Value"))

'Last schedule in well results
iSchedule = eval(DoGet("Reveal.Script.Well[(Chung and Butler)].WellSched.Count")) - 1

'Injection Control
injMode = 0 '0-Rate 1-Pressure
iStarted = 0

QHeat = eval(DoGet("Reveal.Script.Well[(Chung and Butler)].WellSched["+Cstr(iSchedule)+"].Heat"))
'BTU/lb
DualInjection = eval(DoGet("Reveal.Script.Well[(Chung and Butler)].SecondTubing"))
InjSplit = 0 'Heal fraction (assumed to be Second Tubing)
ICVsetting = 1 'Initially open

InjMin = eval(DoGet("Reveal.Script.Well[(Chung and Butler)].WellSched["+Cstr(iSchedule)+"].Q"))
'STB/d
If (DualInjection = 1) Then
        InjDual = eval(DoGet("Reveal.Script.Well[(Chung and
        Butler)].WellSched["+Cstr(iSchedule)+"].Sources[0].LiqRate")) 'STB/d
        InjMin = InjMin + InjDual
        InjSplit = InjDual / InjMin
End If

InjStep = InjMin / 10 'STB/d/d
QLiqInj = InjMin
ThpStep = 10

injResMD = -1 'ft (center of completion for negative value)
injResPipe = -1

PWFcontrol = eval(DoGet("Reveal.Script.EqlRegion[{EqlRegion1}].InitialPressure")) 'psig (-1 set to
initial injection pressure)
THPcontrol = -1 'psig (target injector THP)
PWFrange = 50 'psi

'Production Control
subCoolMD = -1 'ft (last tubing or just below pump for negative value)
subCoolPipe = -1
prodResPipe = -1
Tcontrol = 41 'Degrees F – Varied depending on desired subcool constraint
Trange = Tcontrol * 1.0'F
```

```
ProdMin = eval(DoGet("Reveal.Script.Well[{producer}].WellSched["+Cstr(iSchedule)+"].Q")) 'STB/d
ProdStep = ProdMin / 5 'STB/d/d
QLiqProd = ProdMin

'SubCool PID
derivControlSC = 0
intControlSC = 0
SubCool = -1
SubCoolLast = -1
SubCoolDeiv = -1
SubCoolInt = -1

'Pressure PID
derivControlPWF = 0
intControlPWF = 0
PWF = -1
PWFLast = -1
PWFDeiv = -1
PWFInt = -1

SetUnits(0)

Sub SetUp()

'Calculate center of injector completion
If (injResMD < 0) Then
	nPipe = eval(DoGet("Reveal.XflowRes[{injector}][1].Count"))
	iStep = eval(DoGet("Reveal.XflowRes[{injector}].Count")) - 1
	injFirstMD = -1
	injLastMD = -1
	For iPipe = 0 To nPipe-1
		'Injector
		resInj =
		eval(DoGet("Reveal.XflowRes[{injector}]["+CStr(iStep)+"]["+CStr(iPipe)+"].Annulus
		WellIndex")) 'RB/d/psi/ft
		MD =
		eval(DoGet("Reveal.XflowRes[{injector}][1]["+CStr(iPipe)+"].AnnulusMeasuredDepth
		")) 'ft
		If (Not(IsEmpty(resInj)) And Not(IsEmpty(MD)) And resInj > 0) Then
			If (injFirstMD < 0) Then
				injFirstMD = MD
			End If
			injLastMD = MD
		End If
	Next
		injResMD = (injFirstMD + injLastMD) / 2.0 'Middle of injector
	End If
	For iPipe = 0 To nPipe-1
		'Injector
		MD =
		eval(DoGet("Reveal.XflowRes[{injector}][1]["+CStr(iPipe)+"].AnnulusMeasuredDepth
		")) 'ft
		If (injResPipe < 0 And MD > injResMD) Then
```

```
                injResPipe = iPipe + 1 '+1 is the way these are indexed (0 is parent tree total
                unused for pipes)
        End If
Next

'Find Subcool Pipe at required MD in producer
nPipe = eval(DoGet("Reveal.XflowRes[{producer}][1].Count"))
nPump =
eval(DoGet("Reveal.Script.Well[{producer}].WellSched["+Cstr(iSchedule)+"].Pumps.Count"))
If (subCoolMD < 0 And nPump > 0) Then
        subCoolMD =
        eval(DoGet("Reveal.Script.Well[{producer}].WellSched["+Cstr(iSchedule)+"].Pumps[0
        ].MD")) 'ft
End If
For iPipe = 0 To nPipe-1
        'Producer
        MD =
        eval(DoGet("Reveal.XflowRes[{producer}][1]["+CStr(iPipe)+"].TubingMeasuredDepth
        ")) 'ft
        If (Not(IsEmpty(MD))) Then 'Last tubing (default)
                lastPipe = iPipe + 1
        End If
        If (subCoolPipe < 0 And MD >= subCoolMD) Then
                subCoolPipe = iPipe + 1 '+1 is the way these are indexed (0 is parent tree total
                unused for pipes)
                'Try pipe upstream from pump
                MD =
                eval(DoGet("Reveal.XflowRes[{producer}][1]["+CStr(subCoolPipe)+"].Annul
                usMeasuredDepth")) 'ft
                If (Not(IsEmpty(MD))) Then
                        subCoolPipe = subCoolPipe+1
                End If
        End If
Next
'Unset from depth, use last tubing pipe
If (subCoolPipe < 0 And lastPipe > 0) Then
        subCoolPipe = lastPipe
End If

'Center of producer completion (below injector at the same X)
iStep = eval(DoGet("Reveal.XflowRes[{injector}].Count")) - 1
XInjPos = eval(DoGet("Reveal.XflowRes[{injector}]["+Cstr(iStep)+"]["+Cstr(injResPipe -
1)+"].AnnulusXCoord")) 'ft
iStep = eval(DoGet("Reveal.XflowRes[{producer}].Count")) - 1
For iPipe = 0 To nPipe-1
        'Producer
        XPos =
        eval(DoGet("Reveal.XflowRes[{producer}]["+Cstr(iStep)+"]["+Cstr(iPipe)+"].Annulus
        XCoord")) 'ft
        If (prodResPipe < 0 And XPos >= XInjPos) Then
                prodResPipe = iPipe+1
        End If
Next
```

```
'Add addition SAGD-specific default plots
Call DoCmd(""Reveal.REMOVE_PLOT_STORE(""Rates"")")
Call DoCmd(""Reveal.SET_PLOT_STORE(""Rates"",""Current Run"",""Current
Run"",""Date"",""WaterInjected"",0)")
Call DoCmd(""Reveal.SET_PLOT_STORE(""Rates"",""Current Run"",""Current
Run"",""Date"",""LiquidProduced"",0)")
Call DoCmd(""Reveal.SET_PLOT_STORE(""Rates"",""Current Run"",""Current
Run"",""Date"",""OilProduced"",0)")
Call DoCmd(""Reveal.SET_PLOT_STORE(""Rates"",""Current Run"",""Current
Run"",""Date"",""WaterProduced"",0)")

Call DoCmd(""Reveal.REMOVE_PLOT_STORE(""SubCool"")")
Call
DoCmd(""Reveal.SET_PLOT_STORE(""SubCool"",""producer"","""+Cstr(subCoolPipe)+""","""Date"","""
AnnulusTemperature"",0)")
Call
DoCmd(""Reveal.SET_PLOT_STORE(""SubCool"",""producer"","""+Cstr(subCoolPipe)+""","""Date"","""
AnnulusSteamSatTemp"",0)")

Call DoCmd(""Reveal.REMOVE_PLOT_STORE(""ResPres"")")
Call
DoCmd(""Reveal.SET_PLOT_STORE(""ResPres"",""injector"","""+Cstr(injResPipe)+""","""Date"","""Anul
lusReservoirPressure"",0)")
Call
DoCmd(""Reveal.SET_PLOT_STORE(""ResPres"",""producer"","""+Cstr(prodResPipe)+""","""Date"","""A
nnulusReservoirPressure"",0)")

If (DualInjection = 1) Then
        Call DoCmd(""Reveal.REMOVE_PLOT_STORE(""ICV_Control"")")
        Call DoCmd(""Reveal.SET_PLOT_STORE(""ICV_Control"",""Current
        Run"",""injector"",""Date"",""ICV1Setting"",0)")
        Call
        DoCmd(""Reveal.SET_PLOT_STORE(""ICV_Control"",""injector"",""5"",""Date"",""TubingWa
        terRate"",1)")
        Call
        DoCmd(""Reveal.SET_PLOT_STORE(""ICV_Control"",""injector"",""5"",""Date"",""SecondTu
        bingWaterRate"",1)")
End If
End Sub

Sub SetUnits(value)
        Call DoSet("Reveal.DOUNITCONV",value) 'Strictly always internal Field Units
        Call DoCmd("Reveal.RUN_DOUNITCONV("+Cstr(value)+")") 'For Run Commands
End Sub

'End of (Declarations)

Sub Reveal_RunPreTimestep()

SetUnits(99)
If (Reveal.Step    > 1) Then 'We have some results
'Check we have finished preheating
        If (Reveal.Time >= tPreheat) Then
```

```
'Resolve run - GAP constraints through RESOLVE
iResolve = eval(DoGet("Reveal.Run.LRESOLVE"))

        If (iStarted = 0) Then
                'Prevent GAP results from being applied (ignore them)
                'Well 1 Is producer And 3 Is injector
                If (iResolve < 0) Then
                        Call DoSet("Reveal.Run.IRESOLVECONTROL[1]",1)
                        Call DoSet("Reveal.Run.IRESOLVECONTROL[3]",1)
                End If

                'Initial schedule rates for first time step
                Call
                DoCmd("Reveal.RUN_WELL_PRODUCE_LIQUIDRATE(""producer"","+Cs
                tr(QLiqProd)+")")
                Call
                DoCmd("Reveal.RUN_WELL_INJECT_WATERRATE(""injector"","+Cstr(Q
                LiqInj)+")")
                iStarted = 1
        Else

                If (subCoolPipe < 0) Then
                        Call SetUp()
                End If

                'Treat Resolve controls as constraints after first Resolve solve
                If (iResolve < 0) Then
                        ResolveDT = eval(DoGet("Reveal.Run.RESOLVEDT")) 'days
                        'Set control from GAP to be treated as constraints only
                        If (Reveal.Time - tPreheat > ResolveDT) Then
                                Call DoSet("Reveal.Run.IRESOLVECONTROL[1]",2)
                                Call DoSet("Reveal.Run.IRESOLVECONTROL[3]",2)
                        End If
                End If

                'Get TimeStep size - to try to keep things time step neutral
                DT = Reveal.TimestepSize

                'Get Injection Reservoir pressure (Field units)
                iStep =
                eval(DoGet("Reveal.XflowPipeRes[{injector}]["+Cstr(injResPipe)+"].Count"))
                - 1
                Pinj =
                eval(DoGet("Reveal.XflowPipeRes[{injector}]["+Cstr(injResPipe)+"]["+CStr(i
                Step)+"].AnnulusReservoirPressure")) 'F

                'Calculate Subcool (Field units)
                iStep =
                eval(DoGet("Reveal.XflowPipeRes[{producer}]["+Cstr(subCoolPipe)+"].Coun
                t")) - 1
                Tprod =
                eval(DoGet("Reveal.XflowPipeRes[{producer}]["+Cstr(subCoolPipe)+"]["+CS
```

```
tr(iStep)+"].AnnulusTemperature")) 'F – Critical that this be
.AnnulusTemperature for FCD case and .TubingTemperature for conventional
Tsat =
eval(DoGet("Reveal.XflowPipeRes[{producer}]["+Cstr(subCoolPipe)+"]["+CS
tr(iStep)+"].AnnulusSteamSatTemp")) 'F – Critical that this be
.AnnulusTemperature for FCD case and .TubingTemperature for conventional
Pprod =
eval(DoGet("Reveal.XflowPipeRes[{producer}]["+Cstr(prodResPipe)+"]["+CS
tr(iStep)+"].AnnulusReservoirPressure")) 'F

'Get Injection THP (Pwf in Reveal here)
iStep = eval(DoGet("Reveal.WellRes[{Current Run}][{injector}].Count")) -
1THP = eval(DoGet("Reveal.WellRes[{Current
Run}][{injector}]["+Cstr(iStep)+"].BottomHolePressure")) 'psig

'Get Last step rates - could be constrained by GAP
If (iResolve < 0) Then
        QLiqInj = eval(DoGet("Reveal.WellRes[{Current
        Run}][{injector}]["+Cstr(iStep)+"].LiquidInjected")) 'STB/d
        QLiqProd = eval(DoGet("Reveal.WellRes[{Current
        Run}][{producer}]["+Cstr(iStep)+"].LiquidProduced")) 'STB/d
End If

'Injector Rates
iStep = eval(DoGet("Reveal.XflowPipeRes[{injector}][5].Count")) - 1
QToe =
abs(eval(DoGet("Reveal.XflowPipeRes[{Injector}][5]["+Cstr(iStep)+"].Annul
usWaterRate"))) 'STB/d

If (DualInjection = 1) Then
        QHeal =
        abs(eval(DoGet("Reveal.XflowPipeRes[{Injector}][5]["+Cstr(iStep)+
        "].SecondTubingWaterRate"))) 'STB/d
End If

SubCool = Tsat - Tprod 'F
PWF = Pinj 'psig

'Target pressure is initial (if unset)
If (PWFcontrol < 0) Then
        PWFcontrol = Pinj
End If

'Initial values for previous step values
If (PWFLast < 0) Then
        SubCoolLast = SubCool
        SubCoolInt = SubCool
        PWFLast = PWF
        PWFInt = PWF
End If

SubCoolDeriv = (SubCool - SubCoolLast) / DT 'A smoothed rate of change
```

```
SubCoolInt = 0.95*SubCoolInt + 0.05*SubCool 'A smoothed rolling average

PID_SC = (1-intControlSC)*SubCool + intControlSC*SubCoolInt +
derivControlSC * SubCoolDeriv*DT

PWFDeriv = (PWF - PWFLast) / DT 'A smoothed rate of change
PWFInt = 0.99*PWFInt + 0.01*PWF 'A smoothed rolling average

PID_PWF = (1-intControlPWF)*PWF + intControlPWF*PWFInt +
derivControlPWF * PWFDeriv*DT

'Update last step values
SubCoolLast = SubCool
PWFLast = PWF

'Modify step rates
If (iResolve = 0 And Pprod > Pinj + 1 And SubCool > Tcontrol + Trange) Then
        'Super stable production
        DT = DT*(Pprod-Pinj)
End If

'Update Production rate based on SubCool
scale = (PID_SC - Tcontrol) / Trange
If (Pprod < Pinj-1) Then 'Unstable production
        scale = -1
End If

If (scale < -1) Then
        scale = -1
Elseif (scale > 1) Then
        scale = 1
Else
        'scale = scale*scale*scale 'Large damping near setpoint
End If

QLiqProd = QLiqProd + scale * ProdStep * DT


'Update injection rate to achieve injection pressure target
scale = (PWFcontrol - PID_PWF) / PWFrange
If (scale < -1) Then
        scale = -1
Elseif (scale > 1) Then
        scale = 1
Else
        'scale = scale*scale*scale 'Large damping near setpoint
End If

QLiqInj = QLiqInj + scale * InjStep * DT

'Injector ICV
If (DualInjection = 1 And QToe > 0 And QHeal > 0) Then
        ICVsetting = ICVsetting * (1 + QToe/QHeal * InjSplit/(1-InjSplit)) / 2.0
```

```
                If (ICVsetting < 0.001) Then ICVsetting = 0.001
                End If

                If (ICVsetting > 1) Then ICVsetting = 1
                End If
        End If

        'Use maximum for estimated THP - limit to ThpStep psi increases
        If (PWFcontrol - PWF + THP > THPcontrol) Then
                If (PWFcontrol - PWF + THP > THPcontrol + ThpStep) Then
                        THPcontrol = THPcontrol + ThpStep
                        Else
                        THPcontrol = PWFcontrol - PWF + THP
                End If
        End If

'Hard input limits
If (QLiqProd < ProdMin) Then
        QLiqProd = ProdMin
End If

If (QLiqInj < InjMin) Then
        QLiqInj = InjMin
End If

'GAP constraints through RESOLVE
If (iResolve < 0) Then 'Logicals are -1 for true
        'Network constraints from GAP will be handled as constrains rather set points
        'Constraints for GAP (current + a bit) - HEAT is over-written by Resolve from GAP
                        Call
        DoSet("Reveal.Script.Well[{producer}].WellSched[0].QMax",QLiqProd+ProdStep*Res
        olveDT) 'Extra for producer to prevent GAP constraining unnecessarily

        If (injMode = 0) Then
                Call
                DoSet("Reveal.Script.Well[{injector}].WellSched[0].QMax",QLiqInj+InjStep)
                'Limited extra for injector since it is returning control to Reveal
                Call DoSet("Reveal.Script.Well[{injector}].WellSched[0].BHPMax",fNAN)
                'Remove constraint
        Else
                Call DoSet("Reveal.Script.Well[{injector}].WellSched[0].QMax",fNAN)
                'Remove constraint
                Call
                DoSet("Reveal.Script.Well[{injector}].WellSched[0].BHPMax",THPcontrol+T
                hpStep) 'Limited extra for injector since it is returning control to Reveal
        End If
End If

'Injector partitioning
QToe = (1-InjSplit) * QLiqInj
QHeal = InjSplit * QLiqInj

'Set Controls
```

```
        Call
        DoCmd("Reveal.RUN_WELL_PRODUCE_LIQUIDRATE(""producer"","+Cstr(QLiqProd)+")")
        Call DoCmd("Reveal.RUN_WELL_RESET_CONSTRAINTS(""injector"")")

        If (DualInjection = 1) Then
                Call DoCmd("Reveal.RUN_SET_SOURCE(""injector"",0,0,0,"+Cstr(QHeat)+")")
                'Controlled by ICV
                Call DoCmd("Reveal.RUN_SETICV(""injector"",0,"+Cstr(ICVsetting)+")")
        End If

If (injMode = 0) Then
        Call DoCmd("Reveal.RUN_WELL_INJECT_WATERRATE(""injector"","+Cstr(QLiqInj)+")")
Else
        Call
        DoCmd("Reveal.RUN_WELL_INJECT_WATERPWF(""injector"","+Cstr(THPcontrol)+")")
End If

'Log to Debug Results
logmsg("SubCool is "+Cstr(SubCool)+" F")
'logmsg("SubCool Derivative is "+Cstr(SubCoolDeriv*DT)+" dF")
'logmsg("SubCool Integral is "+Cstr(SubCoolInt)+" F")
'logmsg("SubCool PID is "+Cstr(PID_SC)+" F")
logmsg("Injection Reservoir Pressure is "+Cstr(Pinj)+" psig")
logmsg("Production Reservoir Pressure is "+Cstr(Pprod)+" psig")
'logmsg("Pwf Derivative is "+Cstr(PWFDeriv*DT)+" dpsi")
'logmsg("Pwf Integral is "+Cstr(PWFInt)+" psig")
'logmsg("Pwf PID is "+Cstr(PID_PWF)+" psig")
logmsg("Target Injection Rate is "+Cstr(QLiqInj)+" STB/d")
If (injMode = 1) Then
        logmsg("Target Injection WHP is "+Cstr(THPcontrol)+" psig")
End If
logmsg("Target Production Rate is "+Cstr(QLiqProd)+" STB/d")

'Control Mode change For Next timestep if not a Resolve coupled run
                        If (iResolve = 0 And injMode = 0 And PWF < PWFcontrol And SubCool <
                        Tcontrol + Trange And SubCool > Tcontrol) Then
                                injMode = 1
                                THPcontrol = THP
                        End If
                End If
        End If
End If

SetUnits(0)

End Sub
```